# Process Optimization for Machining of Hardened Steels

A Dissertation

Presented to

The Academic Faculty

By

JingYing Zhang

In Partial Fulfillment

Of the Requirements for the Degree

Doctor of Philosophy in Mechanical Engineering

Georgia Institute of Technology

August, 2005

Process Optimization for Machining of Hardened Steels

Approved by:

Dr. Steven Y. Liang, Advisor
School of Mechanical Engineering
*Georgia Institute of Technology*

Dr. Paul M. Griffin
Industrial System Engineering
*Georgia Institute of Technology*

Dr. Thomas R. Kurfess
School of Mechanical Engineering
*Georgia Institute of Technology*

Dr. Chen Zhou
Industrial System Engineering
*Georgia Institute of Technology*

Dr. Shreyes N. Melkote
School of Mechanical Engineering
*Georgia Institute of Technology*

*Date Approved: July 11 2005*

# DEDICATION

This work is dedicated to my family, for everything.

# ACKNOWLEDGEMENT

I would like to take this opportunity to thank many people who helped to make this thesis possible. My deepest gratitude goes to my advisor, Dr. Steven Y. Liang. Without his constant inspiration, guidance, encouragement and support, this thesis is nearly impossible. I am thankful for his mentoring over those four years which has shaped me in more ways than I'll ever know.

I would also like to thank my committee members, Dr. Thomas R. Kurfess, Dr. Shreyes N. Melkote, Dr. Paul M. Griffin and Dr. Chen Zhou for their knowledgeable advice and valuable input for my thesis development.

I am also grateful to Dr. David Yen of Delphi Corporation, Dr. Taylan Altan of Ohio State University, Dr. Ed Oles of Kennameta Inc. and Dr. Troy Marusich of Third Wave Systems (TWS) Inc. for their valuable comments and suggestions.

I would also like to express my sincere appreciation to many friends and colleagues, Kuan-Ming Lee, Sangil Han, Dr. Yong Huang, Dr. Rogelio Hecker, Michael Swinson at Georiga Tech, Guowei Zhang and Eugene Yen at Delphi Corporation for their creative discussion and enormous help. I am also thankful for the help from Steven Sheffield, John Morehouse, Jiann-cherng Su, Kai Liu**,** Mike Lazarakis, Sathyan Subbiah of the Precision Machining Research Consortium (PMRC), to name a few.

My thanks also go to the Georgia W. Woodruff School of Mechanical Engineering faculty and staff for their support during my study at Georgia Tech. In

particular I would like to thank Dr. William Wepfer, Pamela D. Rountree, Cosetta Williams and Dr. Jeffrey Donnell for their professional help.

I am in debt to my parents, Jinniao Zhang and Yagui Hu, and parents-in-law, Jizhou Li and Yanfang Chen, for what they have done for me. Most of all, I am thankful to my husband, Qiang Li, for his love and support; and my daughter, Emma Z. Li, for her sweet smiles.

# TABLE OF CONTENTS

# LIST OF TABLES

# LIST OF FIGURES

LIST OF SYMBOLS

## Chapter 2

| Symbol | Definition |
|---|---|
| $a$ | Depth of cut (mm) |
| $a_d$ | Dressing depth ( $\mu$m ) |
| $a_f$ | Depth of cut in finishing (mm) |
| $a_r$ | Depth of cut in roughing (mm) |
| $a_t$ | Truing depth ( $\mu$m ) |
| $b$ | A system parameter used in non-mutation operator |
| $b_e$ | Extra cross travel (mm) |
| $b_s$ | Wheel width (mm) |
| $b_w$ | Width of workpiece (mm) |
| $C$ | Grinding cost ($/pc) |
| $C_3$ | Constant for condition of the continuous chip formation |
| $C_d$ | Cost of wheel dresser ($) |
| $C_s$ | Cost of grinding wheel per unit usable volume ($/mm$^3$) |
| $d$ | Depth of cut |

| | |
|---|---|
| $d_c$ | Maximum depth with compressive residual stress |
| $d_{given}$ | Upper limit on $d_c$ |
| $d_s$ | Wheel diameter (mm) |
| $f$ | Feed rate |
| $f(X)$, $F$ | Objective function |
| $G$ | G-ratio |
| $G^*$ | Minimum G-ratio to maintain |
| $g_j(X)$ | The inequality constraints |
| $h_{given}$ | Upper limit on $h_{\max}$ |
| $h_j(X)$ | The equality constraints |
| $h_{\max}$ | Peak to valley surface roughness |
| $i$ | Sorted individual index |
| $L_1$ | Flank wear rate caused by adhesion |
| $L_2$ | Flank wear rate caused by diffusion |
| $L_e$ | Extra length of table travel (mm) |
| $L_i$, $LB$ | Lower bound |
| $LI$ | Linear inequality constraints |
| $L_w$ | Length of workpiece (mm) |
| $M$ | Cost per hour of labor and administration ($/h) |

| | |
|---|---|
| $n$ | Constant = 0.3 |
| $n_f$ | Number of grinding passes in finishing |
| $n_r$ | Number of grinding passes in roughing |
| $N_{td}$ | Total number of dressings during the life of a dresser |
| $NE$ | Nonlinear equality constraints |
| $NI$ | Nonlinear inequality constraints |
| $P$ | Grinding power (W) |
| $P^*$ | Maximum grinding power allowed (W) |
| $p_i$ | Selection probability |
| $q$ | Tournament size |
| $r[0,1],\ r_1,\ r_2$ | Uniform random number between $[0,\ 1]$ |
| $R$ | Nose Radius |
| $R_a$ | Surface roughness ( $\mu$m ) |
| $R_a^*$ | Maximum surface roughness allowed ( $\mu$m ) |
| $s_t$ | Cross feed (mm) |
| $t$ | The current generation number |
| $T$ | The generation size |
| $T_a$ | Total thickness of cut (mm) |
| $T_C$ | Crater wear Temperature |
| $t_d$ | Time to true and dress the wheel (min) |

| | |
|---|---|
| $T_{\max}$ | Upper limit on the tool plastic deformation temperature |
| $T_{\text{pz}}$ | Plastic deformation temperature of the tool |
| $T_{softening}$ | Softening temperature of tool material |
| $U_i$, $UB$ | Upper bound |
| $V$ | Cutting speed |
| $X$ | N-dimensional design vector (Design variables) |
| $X^c$ | Continuous design variables |
| $X^d$ | Discrete design variables |
| $X^i$ | Integer design variables |
| $\alpha$ | The number of solutions forced to be feasible in initial population |
| $\delta$ | Dimensional accuracy (static deflection of the machined part) |
| $\delta_{given}$ | Upper limit on $\delta$ |
| $\varepsilon$ | infinitesimal number |
| $\mu$ | Population size |
| $\rho$ | The ratio between the feasible space and the search space |
| $\sigma_{\text{l}}$ | Tool tensile stress |
| $\sigma_c$ | Compressive residual stress |
| $\sigma_{given}$ | Upper limit on $\sigma_c$ |
| $\sigma_{\max}$ | Upper limit on tool tensile stress |
| $\sigma_r$ | Maximum Residual stress (MPa) |

| | |
|---|---|
| $\sigma_r^*$ | Maximum residual stress allowed (MPa) |
| $\mathcal{F}$ | Feasible space |
| $\mathcal{F}^c$ | Infeasible space |
| $\mathcal{S}$ | Search/Legal space |
| $\mathcal{S}^c$ | Illegal space |
| $\mathbb{R}^n$ | N-dimensional space |

## Chapter 3

| Symbol | Definition |
|---|---|
| $a$ | Hardness constants (Wear coefficient) |
| $a_j^q$ | Output from neuron j at qth layer |
| $a^*$ | Equivalent depth of cut |
| $A,\ B,\ C,\ m,\ n$ | The constants of the Johnson-Cook equation |
| $C$ | Chip specific heat |
| $C_s^*$ | The equivalent side cutting edge angle |
| $doc$ | Depth of cut |
| $E$ | The error function of BPNN |
| $f$ | Feed rate |
| $F$ | Frictional force at tool-chip interface |
| $F_C$ , $F_Q$ | Cutting and thrust force component due to chip formation |

| | |
|---|---|
| $F_{CW}$ , $F_{QW}$ | Cutting and thrust force component due to tool flank wear |
| $F_{C\_t}$ , $F_{Q\_t}$ | Total cutting force and thrust force |
| $F_s$ | Shear force |
| $h$ | Tool chip contact length |
| $H_a$ | Hardness of abrasive particle |
| $H_t$ | Tool hardness |
| $i^*$ | The equivalent inclination angle |
| $K_{abrasion}$ | Abrasive wear coefficient |
| $K_{adhesion}$ | Adhesion wear coefficient |
| $K_{diff}$ | Diffusion wear coefficient |
| $K_Q$ | Constant related with activation energy for diffusion |
| $K$ , $n$ | Constants |
| $l_c$ | Cutting edge contact length |
| $n_j^q$ | Potential from jth neuron at qth layer |
| $P$ | Cutting power (W) |
| $P_c$ , $P_a$ , $P_r$ | Cutting forces in cutting, axial and radial directions |
| $P_{c\_t}$ , $P_{a\_t}$ , $P_{r\_t}$ | Total cutting forces in cutting, axial and radial directions |
| $q_r$ | Heat intensity of the rubbing heat source due to flank wear |
| $R$ | Tool nose radius |

| | |
|---|---|
| $Ra$ | Surface roughness |
| $R_T$ | Non-dimensional thermal number |
| $t^*$ | Equivalent undeformed chip thickness |
| $t_2$ | Chip thickness |
| $\bar{T}_f$ | Average temperature along flank face |
| $T_k$ | The target/desired output pattern |
| $T_m$ | Workpiece melting point temperature |
| $\bar{T}_{ra}$ | Average temperature along rake face |
| $T_r$ | Reference Temperature |
| $V_c$ | Cutting velocity |
| $V_{chip}$ | Chip velocity |
| $V_s$ | Shear velocity |
| $VB$ | Flank wear length |
| $w_{i,j}^q$ | The connection weights between neuron i and j at qth layer |
| $WL$ | White layer thickness |
| $X_k$ | The input pattern |
| $\alpha$ | Tool rake angle |
| $\alpha_{\mathrm{n}}^*$ | The equivalent cutting edge normal rake angle |
| $\beta$ | Proportion of primary heat conducted into the workpiece |

| | |
|---|---|
| $\gamma$ | Tool clearance angle |
| $\Gamma$ | Proportion of rubbing heat transported by chip |
| $\delta$ | Ratio of tool-chip interface plastic zone thickness to chip Thickness |
| $\Delta T_c$ | Average temperature rise due to the secondary heat source |
| $\Delta T_M$ | Maximum temperature rise in chip |
| $\Delta T_{sz}$ | Average temperature rise due to the primary heat source |
| $\Delta T_{VB}$ | Average temperature rise due to the third heat source |
| $\varepsilon$ | Effective strain |
| $\dot{\varepsilon}$ | Strain rate |
| $\dot{\varepsilon}_o$ | Reference Strain rate |
| $\eta_c^*$ | Equivalent chip flow angle |
| $\lambda$ | The learning rate in BPNN |
| $\rho$ | Chip density |
| $\bar{\sigma}$ | Average normal stress along the tool/workpiece interface |
| $\sigma_C$ | Circumferential residual stress |
| $\sigma_L$ | Longitudinal residual stress |
| $\varphi$ | Tool chamfer angle |
| $\psi$ | Tool-chip interface temperature factor ($\psi$ = 0.7 is used) |
| $\psi_j^q$ | The error signal from jth neuron at qth layer |
| $\Upsilon$ | The ratio of average flank face temperature to average rake face |

temperature (in Kelvin)

## Chapter 4

| Symbol | Definition |
|---|---|
| $C_m^{'}$ | Machine related cost ($/min) |
| $C_p$ | Cost per part ($/pc) |
| $C_p^*$ | Target cost per part ($/pc) |
| $C_t$ | Cost of a single cutting edge ($/edge) |
| $C_w^{'}$ | Labor related cost ($/min) |
| $f$ | Feed rate\ |
| $f_{mach}$ | Fraction of active machining time once loaded (%) |
| $MRR$ | Material removal rate |
| $MRR^t$ | The target material removal rate |
| $N$ | The number of part cut per insert |
| $P$ | Cutting power (W) |
| $P^*$ | Maximum available power (W) |
| $R$ | Nose radius |
| $R_a$ | Surface roughness ( $\mu m$ ) |
| $R_a^*$ | Maximum surface roughness allowed ( $\mu m$ ) |
| $R_a^t$ | The target surface roughness ( $\mu m$ ) |

| | |
|---|---|
| $t_{ct}$ | Tool change time (min) |
| $t_{load}$ | Loading time (min/part) |
| $t_{mach}$ | The actual machining time |
| $t_t$ | Cycle time per part |
| $t_t^*$ | Target cycle time per part (min/pc) |
| $V_c$ | Cutting speed |
| $VB$ | Flank wear length ( $\mu m$ ) |
| $VB^*$ | Maximum flank wear length allowed ( $\mu m$ ) |
| $VB^t$ | The target flank wear length ( $\mu m$ ) |
| $w_1, w_2, w_3$ | Weight factors |
| $WL$ | White layer thickness ( $\mu m$ ) |
| $WL^*$ | Maximum white layer thickness allowed ( $\mu m$ ) |
| $\alpha$ | Back rake angle |
| $\gamma$ | Clearance angle |
| $\sigma_{C\max}$ | Maximum circumferential residual stress |
| $\sigma_C^*$ | Maximum circumferential residual stress allowed (Mpa) |
| $\sigma_{L\max}$ | Maximum longitudinal residual stress |
| $\sigma_L^*$ | Maximum longitudinal residual stress allowed (Mpa) |
| $\varphi$ | Chamfer angle |

# SUMMARY

Finish machining of hardened steel is receiving increasing attention as an alternative to the grinding process, because it offers comparable part finish, lower production cost, shorter cycle time, fewer process steps, higher flexibility and the elimination of environmentally hazardous cutting fluids. In order to demonstrate its economic viability, it is of particular importance to enable critical hard turning processes to run in optimal conditions based on specified objectives and practical constraints.

In this dissertation, a scientific and systematic methodology to design the optimal tool geometry and cutting conditions is developed. First, a systematic evolutionary algorithm is elaborated as its optimization block in the areas of: problem representation; selection scheme; genetic operators for integer, discrete, and continuous variables; constraint handling and population initialization. Secondly, models to predict process thermal, forces/stresses, tool wear and surface integrity are addressed. And then hard turning process planning and optimization are implemented and experimentally validated. Finally, an intelligent advisory system for hard turning technology by integrating experimental, numerical and analytical knowledge into one system with user friendly interface is presented. The work of this dissertation improves the state of the art in making tooling solution and process planning decisions for hard turning processes.

# CHAPTER I

# INTRODUCTION AND LITERATURE REVIEW

## 1.1 Introduction and Objective

Machined parts of hardened steel are high performance components with critical functions, which are often loaded near their physical limits (Tonshoff 2000). Therefore, geometrical tolerance and surface integrity are critically important for those steel components, such as bearings, gears, shafts, dies and molds. They have to be thermally hardened to the desired mechanical properties and must be finished in the hardened state in order to maintain surface integrity, dimensional accuracy, and shape. Such finishing process is usually undertaken by grinding. However, with the advent of Polycrystalline Cubic Boron Nitride (PCBN) cutting tools, hard turning has the potential to replace the grinding process, as it provides lower production cost, shorter cycle time, fewer process steps, and higher flexibility in machining the complex workpiece geometry. It can also be more environmentally friendly by eliminating hazardous cutting fluids while still offering the comparable surface integrity.

However, there are still several fundamental issues to be solved in order for hard turning to be a viable technology. Rapid tool wear remains an impediment to the process being economically viable due to high cost of CBN cutting tools and the tool change down time. Another issue is related with surface integrity. A hard and brittle white layer

will be generated at the machined surface under certain conditions which is detrimental to part performance. Additionally, tensile residual stress will tend to be present in the machined surface and subsurface, which will greatly reduce the part fatigue life. Therefore, it is vital to enable critical hard turning processes to run in optimal conditions to achieve longer tool life with satisfactory surface integrity.

Various experimental, numerical, and analytical studies of hard turning have been made available; however they are fragmented and uncorrelated pieces of information that cannot be used for process planning in an effective manner. A suitable modeling scheme that integrates existing experimental, numerical and analytical knowledge into process planning and optimization is desired.

Furthermore, optimization of the hard turning process remains very challenging in view of the following four issues. First, models of the hard turning process are very complex and some are highly non-linear, non-explicit and not analytically differentiable with the design variables, all of which renders traditional non-linear optimization methods difficult to apply (Rao 1996). For example, an explicit analytical expression relating tool wear to both cutting condition and tool geometry is not available. Tool flank wear length is calculated iteratively by numerical integration from the tool flank wear rate model which is a function of cutting condition, tool geometry and process information (cutting temperature, stress) while process information should be updated with the progress of the tool wear. Additionally, no comprehensive analytical models for white layer formation and residual stress distribution are readily available. They are predicted from the Back Propagation Neural Network constructed based on the

experimental data in this study. Secondly, some of the prediction models are computationally expensive, such as the 3-D cutting forces which are calculated based on the modified Oxley's predictive machining theory, in which shear angle has to be determined iteratively from $5^{\circ}$ to $45^{\circ}$ by a step size of $0.1^{\circ}$ for every cutting condition and tool geometry based on minimum force principle. An efficient and robust search strategy is needed in order to locate the optimal solution in such a computationally expensive problem. Thirdly, some design variables have to be chosen from integer/discrete values, such as tool geometry (rake angle, clearance angle, edge preparation, and nose radius). Generally, it is more economical to choose the standard design from the tool maker's catalog. Hence, integer programming is involved. Fourthly, hard turning process optimization is under constraints of surface quality and machine capability, which make the feasible space small and relatively sparse; extra care has to be taken in order to search for the feasible and optimal solution.

Despite the active research and progress in global optimization in recent years, it is fair to say that no efficient solution procedure is in sight for the general nonlinear problems. Instead a code that fits the problem we are solving should be selected/developed. Therefore a general optimization scheme which takes the characteristics of the hard turning process and general machining processes into consideration is desired.

The objective of this dissertation is to develop a scientific, systematic and reliable methodology to design optimal tool geometry (edge preparation, rake angle, clearance angle and tool nose radius, etc.) and cutting condition (cutting speed, feedrate, and depth

of cut) to achieve specified process performance goals under the satisfactory surface finish (surface roughness, white layer thickness and residual stress distribution) and any other practical constraints, such as tool wear, available horsepower, dynamic stability for the hard turning process. In achieving this goal, this study includes: (1) Development of a Mixed Integer Evolutionary Algorithm (MIEA). (2) Development of suitable models to integrate experimental, numerical, and analytical knowledge into hard turning process planning and optimization. (3) Development of an Intelligent Advisory System for hard turning technology.

This research offers a general solution for hard turning process planning and optimization and also a general solution for various machining processes, such as milling and grinding processes. It allows the industry to design the tool geometry and optimize cutting parameters over an extended range of tool designs and process configurations, thereby maximizing process agility and competitiveness, which are crucial for hard turning to be a viable technology.

## 1.2 Hard Turning Process

The hard turning process is to turn material whose hardness is higher than 45 HRC. Most hard turning applications involve turning of hardened steels (Konig, 1984). There are great demands for the application of the hardened steels in bearings, camshafts, gearshafts, cutting tools, dies, molds, etc due to their improved strength and wear resistance, which involve 30 - 35 billion US$ per year in the United States alone. Those

hardened steels are finished mostly by grinding nowadays. However, with the advent of new cutting tool technology and machine tool systems, finish cutting of hardened steel has become a reality and a topic of high interest for today's industrial production and scientific research.

Hard turning differs from conventional turning because of the workpiece material, the cutting tools required, the cutting conditions applied and the chip formation mechanism. The common characteristics of hard turning are summarized in the following.

*Cutting Tools:*

Due to hard material's characteristics, the applicable cutting tool should meet the following requirements: high indentation hardness, high hardness to modulus ratio, high thermal conductivity, high abrasive wear resistance and high thermal physical and chemical stability (Tonshoff 2000). The most often applied cutting tool materials for hard turning and face milling operations are Al2O3/TiC ceramics, polycrystalline cubic boron nitride (PCBN) and CBN composite tools. PCBN tools have higher fracture toughness, higher thermal conductivity and low thermal expansion coefficient, favorable in interrupted cutting operations, all of which have made PCBN the most widely used tool material for hard turning applications. Though polycrystalline cubic diamond (PCD) tools exhibit excellent wear resistance and higher hardness than PCBN tools, PCD tools diffuse rapidly to the steel workpiece due to the carbon composite, especially in high temperature hard turning process.

PCBN tools are formed by sintering CBN particles mixed with cobalt, TiC, TiN or other materials. In general there are two categories of PCBN tools: High CBN content tools which consist of 90% volume of CBN grains with metallic binders (e.g., cobalt); Low CBN content tools which consist of 50-70%volume of CBN grains with ceramic binders (e.g., TiC, TiN).

*Workpiece Material*

The hardness of workpiece materials is generally higher than 45 HRC with high indentation hardness, high abrasiveness, low ductility, high value of the hardness over E-modulus ratio (Nakayama 1998). Among them, hardened AISI 52100, 1053 and 1070 are studied. Hardened AISI 52100 is the most widely used bearing steel; its machinability has been extensively studied by numerous researchers. Hardened AISI 1070 and AISI 1053 have many applications in the automotive industry; however few efforts have been devoted to studying their machinability in the hardened state.

*Tool Geometry*

Cutting tool materials used for hard turning, such as PCBN tool inserts, have extremely high indentation hardness and high thermal stability. However they are also brittle and prone to fracture. Hence a large negative rake angle with special edge preparation is applied to strengthen the tool edge. Chamfered or honed edges are typical for edge preparation. A large nose radius is adopted to improve the surface roughness.

*Cutting Condition:*

The typical cutting conditions for finish turning of hardened steels with low CBN tool inserts are listed below; these will be used in most practical hard turning applications.

| | |
|---|---|
| Cutting Speed | 91.2 - 183 m/min (300 - 600 sfpm) |
| Feed Rate | 0.052 – 0.152 mm/rev (0.002 - 0.006 in/rev) |
| Depth of Cut | 0.101 – 0.305 mm (0.004 - 0.012 inch) |

*Chip formation mechanism:*

Segmental chips (also called saw-tooth chips) are formed during machining of hardened steel under certain cutting conditions, as shown in Figure 1-1 for hard turning of AISI 1053 (58 – 60 HRC) with Kennametal KB5625 low CBN tool inserts. The tool has a negative $20^{o}$ chamfer angle and 0.8 mm nose radius. For the left hand case, the cutting speed is 4.573 m/s, the depth of cut is 0.1270 mm and the feed rate is 0.2032 mm/rev and for the right hand case, the cutting speed is 2.541 m/s, the depth of cut is 0.1270 mm and the feed rate is 0.2032 mm/rev.

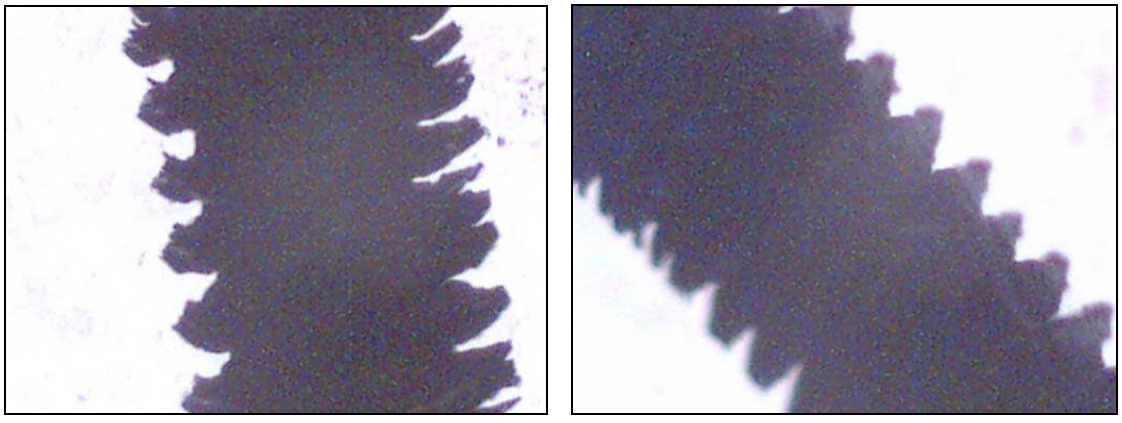

Figure 1-1 Chip morphology in hard turning of hardened AISI 1053

*Tool Wear*

Abrasion, adhesion, diffusion and the chemical reactions are dominant wear mechanisms in hard turning with the main wear pattern of: flank wear, crater wear, thermal shock, cracking, notching wear and chipping (Chou 1994, Huang 2002).

PCBN is the cutting tool material with the longest possible tool life. PCBN tool wear rate depends on three main factors: 1) Tool material composition: CBN particle size, CBN content, binder materials and applied coating material, coating thickness. 2) Tool geometry: rake angle, edge preparation (Chamfer length and angle for chamfer tools, hone radius for honed tool), and nose radius. 3) Cutting condition: feed rate, depth of cut, cutting velocity.

Documentation shows that for high stock removal rate operations (roughing), high CBN content tools give longer lives. For finish hard turning, low CBN tools will yield a longer tool life and consistently better surface finishes.

*Surface Integrity*

The hard turning process, an alternative to the grinding process, must provide acceptable dimensional tolerance, form accuracy and surface integrity. White layer formation and tensile residual stress profiles are two major undesired surface damages from the hard turning process.

*Surface Roughness*

Surface roughness is greatly affected by cutting conditions (feed rate, cutting speed and depth of cut), tool geometry (edge preparation, tool nose radius, tool orientation) and tool wear in finish hard turning process. Among them, feed rate and tool

nose radius are believed to be the most dominant control factors. In finish hard turning, feed rate applied is generally very small and is as the same scale as the tool nose radius or even smaller. The ploughing effect and material side-flow effect are pronounced at such cutting conditions, which pose difficulty in predicting machined surface roughness.

*White Layer*

A featureless, hard and brittle white layer will present at the machined surface under certain hard turning conditions. The white layer consists of 30% martensite and almost 70% austenite while bulk material was composed of approximately 75% martensite and 25% austenite (Tonshoff 1996). It is significantly harder than the bulk material. A dark "overtempered" layer was observed immediately below the white layer produced. A typical white layer from hard turning can be seen in Figure 1-2.

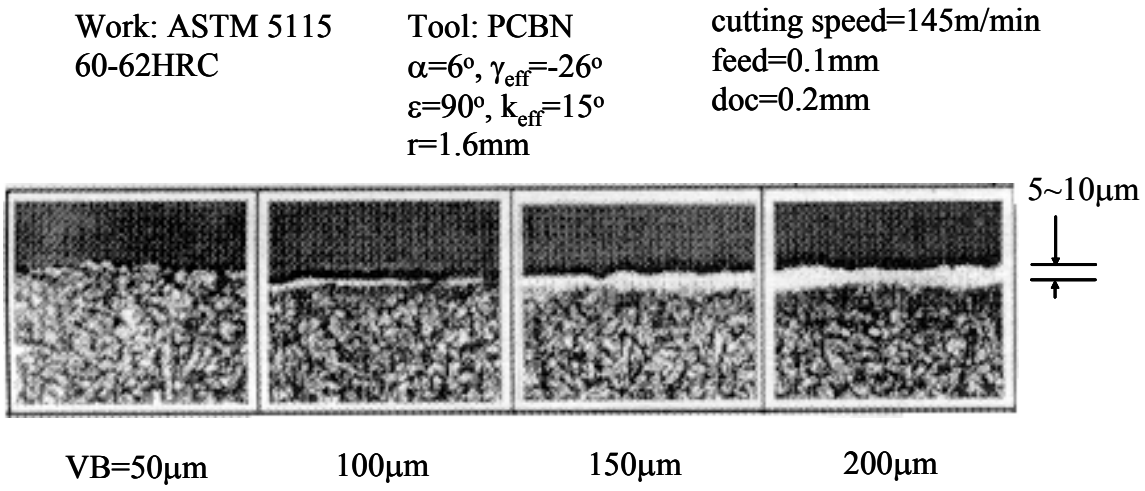


Figure 1-2 Typical white layer (Tonshoff *et al.* 1995)

White layer formation results from complex mechanical, thermal and metallurgical processes. Three main mechanisms responsible for white layer formation are suggested (Griffiths 1987, Ramesh 2002): (1) mechanical grain refinement arising from severe plastic deformation, (2) thermally-induced phase transformation due to high cutting temperature, (3) surface reaction with the environment.

White layer is believed to be detrimental to the part performance and can affect its tribological performance, corrosion resistance and fatigue life. Hence, it is vital to understand the white layer formation and to minimize its thickness during the hard turning process.

*Residue Stress*

The residual stress profile attributes, including both magnitude and direction along the depth below workpiece surface, are known to significantly affect component fatigue life. Generally, residual stress profiles are compressive at machined surfacew or subsurfacew with fresh tool and changes to tensile at certain flank wear. Figure 1-3 shows the trend of residual stress with increased tool wear. As can be seen, increased tool wear typically results in larger residual tensile stresses near the surface.

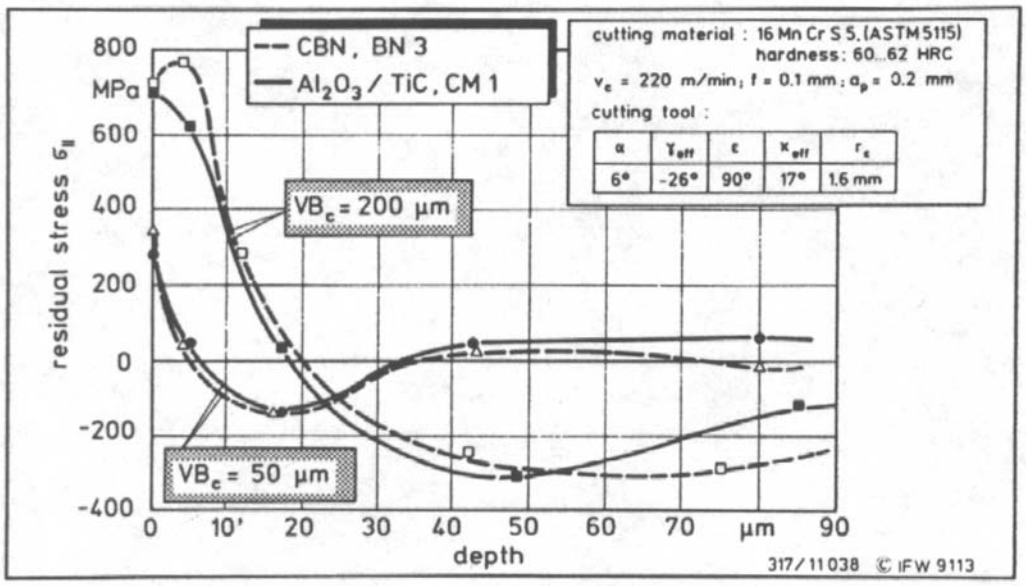


Figure 1-3 Residual stress patterns in hard turned components (Tonshoff et al. 1995)

There are five main factors that could drastically affect the residual stress distribution in finish hard turning: 1. insert grade, 2. tool geometry, including nose radius and edge preparation (chamfer angle and length, hone radius), 3. cutting parameters, including cutting speed, feed rate and depth of cut, 4. tool wear progression, 5. workpiece materials. Other factors that could also have a bearing include the type of cooling method, tool orientation, such as rake angle and clearance angle, etc.

## 1.3 Optimization Techniques in Machining Processes

In 1907, F. W. Taylor recognized the problem of economic (optimum) cutting conditions for metal-cutting in his pioneering work “On the Art of Cutting Metals.” Since then, optimization of machining processes remains an ongoing activity, as evidenced by

the optimization studies that were carried out over the last century (Ermer 1997). Several optimization techniques have been employed for the machining process optimization since the introduction of computers to machining systems.

### 1.3.1 Linear Programming

Linear programming was used in the early stage of machining process optimization (Ermer and Patel 1974, Milner 1976) in which objective functions and various constraints were expressed as empirical power equations and logarithms were used to linearize the key relationships. Goal programming as a special type of linear programming has been applied in machining process optimization (Sundaram 1978, Phillipson & Ravindran 1978, Fischer 1989). Goal programming seeks to minimize the deviations between the preset goals and the actual results to be obtained according to the assigned priorities. All the goals can be incorporated into the objective function by assigning different priorities for each of the goals to meet. It is a good technique to simplify the problem to a single objective linear programming problem that fulfills the multiple, conflicting objectives, which are subject to complex environment constraints. However, linear programming can only deal with the linear equations. All non-linear equations have to be able to transfer to linear equations.

### 1.3.2 Non-Linear Programming

Non-linear programming has been extensively applied for more general non-linear machining optimization problems. Geometric Programming (GP), one of the non-linear optimization techniques, has been extensively adopted (Walvekar 1970, Phillips

1970, Ermer 1972, Eskicioglu *et al.* 1985, Tsai 1986, Gopalakrishnan & Al-Khayyal 1991). In Geometric Programming (GP), the constrained models are converted into a dual geometry programming formulation and then into an unconstrained nonlinear programming formulation. The geometric programming approach furnished a unique insight into how the optimizing criterion is distributed among its components for a given set of input parameter values (Ermer 1997). The major disadvantage of the method is that it requires the objective function and the constraints in the form of polynomials (Rao 1996) and expressed in the general form of the GP and transformed to the corresponding dual objective function. Furthermore additional techniques are needed to solve the problem according to the degree of difficulty of the GP problem. The degree of difficulty increases with the number of constraints in GP. GP skill will meet difficulty in dealing with the flexible constraints in machining problems. Machining process optimization with very limited constraints has been studied by most of the researchers to keep the work down to one degree of difficulty.

Traditional non-linear optimization techniques have also been extensively used. Armarego *et al.* (1993 and 1994) developed computer-aided optimization analysis and strategies for single-pass peripheral milling and multipass rough peripheral and end-milling on NC/CNC and conventional machine tools. A combination of mathematical optimization analyses and limited numerical search techniques were used to arrive at the global optimal solution for nonlinear milling problems. Jang D. Y. (1992) developed a unified optimization approach for the selection of the machining parameters (cutting speed, feed, and depth of cut) to provide the maximum metal removal rate. Powell's

unconstrained method with the exterior penalty function was employed to solve the non-linear constrained optimization problem. The exterior penalty function needs lots of penalty parameters; it is very difficult to choose those parameters to suit the problem. Wen *et al.* (1992) adopted the successive quadratic programming method to solve the non-linear off-line optimization scheme for a surface grinding process. Xiao *et al.* (1992) applied an iterative Newton's method for a non-linear internal cylindrical plunge grinding process. Jha (1995) used the generalized reduced gradient method to optimize the tool geometry and cutting conditions in plain milling process. Jha's is one of the very few works where the cutter's tool geometry and the cutting conditions are optimized simultaneously.

The traditional non-linear optimization techniques are mostly gradient-based and possess many limitations in application to today's complex machining models. Secondly, they cannot deal with integer/discrete design variables directly; integer design variables have to be approximated from continuous values. This simple rounding procedure often fails completely, resulting in either a suboptimal design or in some cases, even generating an infeasible design. Furthermore, a judicious choice of an initial starting point in the design space is required; otherwise those methods are very likely to get trapped in a local optimum. This can be a severe drawback in optimization of machining processes whose models are highly non-linear. Yet, as the machining processes get more and more complex, the process models are possibly discontinuous, not analytically differentiable, or non-explicit. The gradient-based non-linear optimization techniques have difficulty in

solving those optimization problems; one must resort to non-systematic optimization techniques, i.e., Evolutionary Algorithm.

Groover (1975) used Monte Carlo simulation to study the machining economic problems considering tool wear and surface roughness. Monte Carlo simulation is one of the stochastic optimization methods. This method is nothing more than a simple random search method that keeps track of the best. Evolutionary Algorithm (EA) is a more "enhanced" version of the Classical Monte Carlo method, whose ability to get the optimal solutions is much more powerful than Monte Carlo method.

### 1.3.3 Evolutionary Algorithm

Evolutionary Algorithms (EAs) have received a great deal of attention regarding their potential as optimization techniques for highly non-linear, ill-behaved complex engineering problems. There are three different mainstream evolutionary algorithms (EA): Genetic Algorithms (GA), Evolutionary Strategies (ES) and Evolutionary Programming (EP). The biological background, the relation to artificial intelligence, the relation to global optimization and the computational complexity of the global optimization problem are the four important aspects of EA (Back 1996). Algorithms are formulated in a language obtained by mixing pseudo code and mathematical notations. These are: A population of individuals which is manipulated by genetic operators – especially mutation and recombination, but others may also be incorporated – and undergoes a fitness based selection process, where fitness of an individual depends on its quality with respect to the optimization task (Back 1996).

EAs have been applied successfully in the area of engineering optimization (Lin and Hajela 1992, Wu and Chow 1995, Back and Schutz 1995, Gen and Cheng 2000) and also in optimization problems of machining processes. Strenkowski *et al.* (1997) applied Genetic Algorithm (GA) for the optimal selection of cutting tools and operating conditions for end milling process. Lee C. W. (2000) used Evolutionary Strategies (ES) in selecting the optimal grinding and dressing conditions for grinding processes. However despite of their great potential for locating the global optimum in challenging problems, EAs have not found much application in optimization problems of machining processes.

EA has advantages over other conventional optimization methods due to the following features:

(1) EA is a population based algorithm. It starts with a population of search points instead of a single point. It gives more robustness in finding the global optimum. The performance of most traditional methods greatly depends on the judicious choice of an initial point and is easier to track to the local optimum.

(2) EA uses direct search technique. It does not need derivative information from the objective function and constraints for the search.

(3) EA is not a simple random and grid search method, it employs the principle of nature evolution to search stochastically and deterministically toward global optimum.

Genetic Algorithm (GA) is the most popular EA and has been actively used in various application areas, and shown successful results. GA is computationally suitable for integer (discrete) variables due to its inherent ability of binary representation. GA has higher flexibility to handle constraints and thus is especially suitable to solve constrained

manufacturing optimization problems. Hence, GA is chosen as the platform method in this research for hard turning process optimization and the general machining process optimization.

However other EAs also have their own unique advantages. For example the continuous design variables in ES can be represented by real-valued (floating point) variables. The conventional GA uses bit-string to represent problem domains. All design variables in each optimization problem have to be encoded into a long binary chromosome for binary genetic operators and decoded back to the real variables for function evaluations in each generation. An excessively long binary string is required for a high resolution, high dimension optimization problem, thereby lowering the efficiency and accuracy of the algorithm. The desirable components in the other EA should be incorporated into GA, making it possible for the GA to obtain the best solution for the general machining optimization problems.

A real-coded GA is proposed (Wright 1991, Eshelman & Schaffer 1992) and has been proven to ensure faster convergence than the traditional bit-string GA in numerical optimization (Michalewicz 1996). Unfortunately, a systematic method which is able to deal with mixed integer, discrete, and continuous design variables and with boundary, inequality and equality constraints, has not been formulated.

There also exist some other stumbling blocks before GA can be effectively applied to the machining process optimization.

First, the conventional GA lacks local fine-tuning capabilities. GA can reach the global optimal region very quickly but it needs a better scheme to improve GA's local

search ability after it converges to the global optimal region. One of the most common forms of genetic local search is the hybrid genetic algorithm. With the hybrid approach, local optimization is applied to each newly generated offspring to move it to a local optimum before injecting it into the population. The heavy computational load required to move each offspring to a local optimum is prohibitive for most machining problems due to their computationally expensive function evaluation.

Yet another stumbling block of conventional GA is its lack of any self-adaptation mechanism to solve its own parameterization problem, as well as the lack of theoretically confirmed knowledge about the choice of those parameters available (Back 1996). GA is a stochastic technique and its behavior is still, in many aspects, not well understood.

Hard turning process optimizations are constrained problems as well as a vast majority of machining processes. Another difficulty to overcome for GA is how to deal with those nonlinear constraints, though it is a common challenge to all optimization methods. Those constraints normally make the feasible space small and quite sparse in the whole search space, and it is difficult to make any pre-assumption about the feasible space while a genetic operator often yields infeasible offspring. An effective constraint handling method is required in order to prevent "premature" and "slow convergence" when GA is used for hard turning process planning and optimization.

Hence, further research on extension and implementation of the evolutionary algorithm based on GA is required for the complex hard turning process and other general machining process optimization.

### 1.3.4 Handling Constraints Using Genetic Algorithms

During the last two decades, several methods have been proposed for handling constraints in GAs. They can be roughly classified into the categories of rejecting methods, repairing methods, and penalty methods.

The rejecting method is the simplest method to deal with the constraints by discarding any solutions in the initial population and offspring that violate the constraints. The rejecting method has proven to be the least effective and the least stable even with time consuming rejection scheme from numerical experiment (Michalewicz 1996a). Some infeasible solutions in the population are helpful because they can drive the search across infeasible regions to arrive at the optimum point.

Both the repairing methods and the penalty methods keep a certain number of infeasible solutions in the population to facilitate the genetic search in both feasible and infeasible regions. Repairing methods convert infeasible solutions back to feasible solutions through a repair procedure. It can be ineffective to perform such conversions in highly constrained and computationally expansive problems with small and sparse feasible space. Penalty methods are perhaps the most common technique used in GA. This technique transforms a constrained problem into an unconstrained one by penalizing the infeasible solutions with a penalty function or by applying different evaluation schemes to feasible and infeasible solutions.

There are different methods where penalty functions differ in some important details. They can be classified as: "Problem dependent" or "Problem independent." A

"Problem dependent" method involves a number of penalty parameters. Careful tuning of those parameters for each problem is necessary in order to ensure convergence to correct answers. The problem dependent property of those methods remains a key disadvantage. "Feasible superior" (Powell and Skolnick 1993, Schoenauer and Xanthakis 1993) or "No feasible superior" (Homaifar et al. 1994, Joines and Houch 1994, Michalewicz and Attia 1994): the "Feasible superior" method makes every feasible solution better than every infeasible solution. A feasible "optimal" solution is guaranteed at the end of the search. The "No feasible superior" method will suffer when the "reward" of infeasible solution is higher than the "penalty". "Static" (Homaifar et al. 1994) or "dynamic" (Joines and Houch 1994, Michalewicz and Attia 1994): The penalty keeps constant from generation to generation for the static method, while the penalty changes with the generation for the dynamic one.

There are a number of other interesting methods which have been reported such as the adaptive method (Hadj-Alouane and Bean 1992), the co-evolutionary method (Paredis 1994) and the decoder-based method (Koziel and Michalewicz 1999). Unfortunately, those methods are either convoluted, involving lots of transformation, or are difficult to implement and are computationally expensive as far as complex machining processes are concerned. There is still a need for a systematic and efficient constraint handling method in GA to optimize the complex machining process by taking the characteristics of the specific problems under consideration.

## 1.4 Design of Cutting Condition and Tool Geometry

For a given tool and workpiece material combination, tool geometry and cutting conditions in hard turning can be optimized based on specified performance goals (such as minimum cost per part, maximum production rate, finest surface finish, etc). To solve this specification, many efforts have been devoted throughout the history of machining. Unfortunately most of the model-based machining process optimization studies seek only the optimal cutting conditions or only the optimal tool geometry based on laborious experiments and/or time-consuming FEM methodology (Mayer 1974, Shintani 1989, Dawson 1999, Bouzakis 2000). There is very little work done to optimize the tool geometry together with the cutting condition to assess the feasibility of the process and to achieve specified performance goals. Traditionally cutting tools are designed by empirical relationships, which is a very inefficient approach (Jha 1995). The tooling solution and process planning decision should be made in a systematic manner by computing all design parameters simultaneously so that interrelationships and interactions of all design parameters can be taken into account.

Furthermore, Taylor's tool life equation has been extensively used as a tool life governing equation to decide how many parts can be cut before the tool insert is changed. However, several factors may limit tool life and therefore affect machining cost. In finish hard turning, surface integrity (surface roughness, white layer thickness and residual stress distribution) is often of great concern because of its impact on product performance. Tool life is often limited by part surface integrity. Surface integrity together with tool wear (flank wear and crater wear) should be used as a tool life criterion.

In light of the discussed shortcomings in machining process optimization scheme, a scientific, systematic and reliable methodology to design optimal tool geometry and cutting conditions within permissible space for given tool-workpiece combination is needed.

## 1.5 Organization of This Dissertation

The major focus of this dissertation is model-based hard turning process planning and optimization. The finished research is arranged as in Figure 1-4. Chapter 1 is the introduction and literature review to give the background of the focused topic and point out the motivation and objective. Chapter 2 and Chapter 3 are the major foundation for the focused research. In Chapter 2, the proposed optimization algorithm, a Mixed Integer Evolutionary Algorithm, is described to address the underlying drawbacks when Genetic Algorithm is applied to the hard turning process optimization problems. In Chapter 3, the hard turning process models - including thermal model, force model, tool wear model and surface integrity models - are presented to provide the indispensable process information for hard turning process planning and optimization. Implementation and validation of the model-based hard turning process planning and optimization, using the proposed optimization algorithm in Chapter 2 and the developed hard turning process models in Chapter 3, are presented in Chapter 4. Chapter 5 is devoted to developing an intelligent advisory system of hard turning process with user friendly interface, which can be used to predict the process variables, design the tool geometry and optimize the cutting conditions to help critical hard turning processes run in the optimal conditions. Chapter 6

is the closure of this dissertation, in which the major contribution are summarized and future work is recommended.

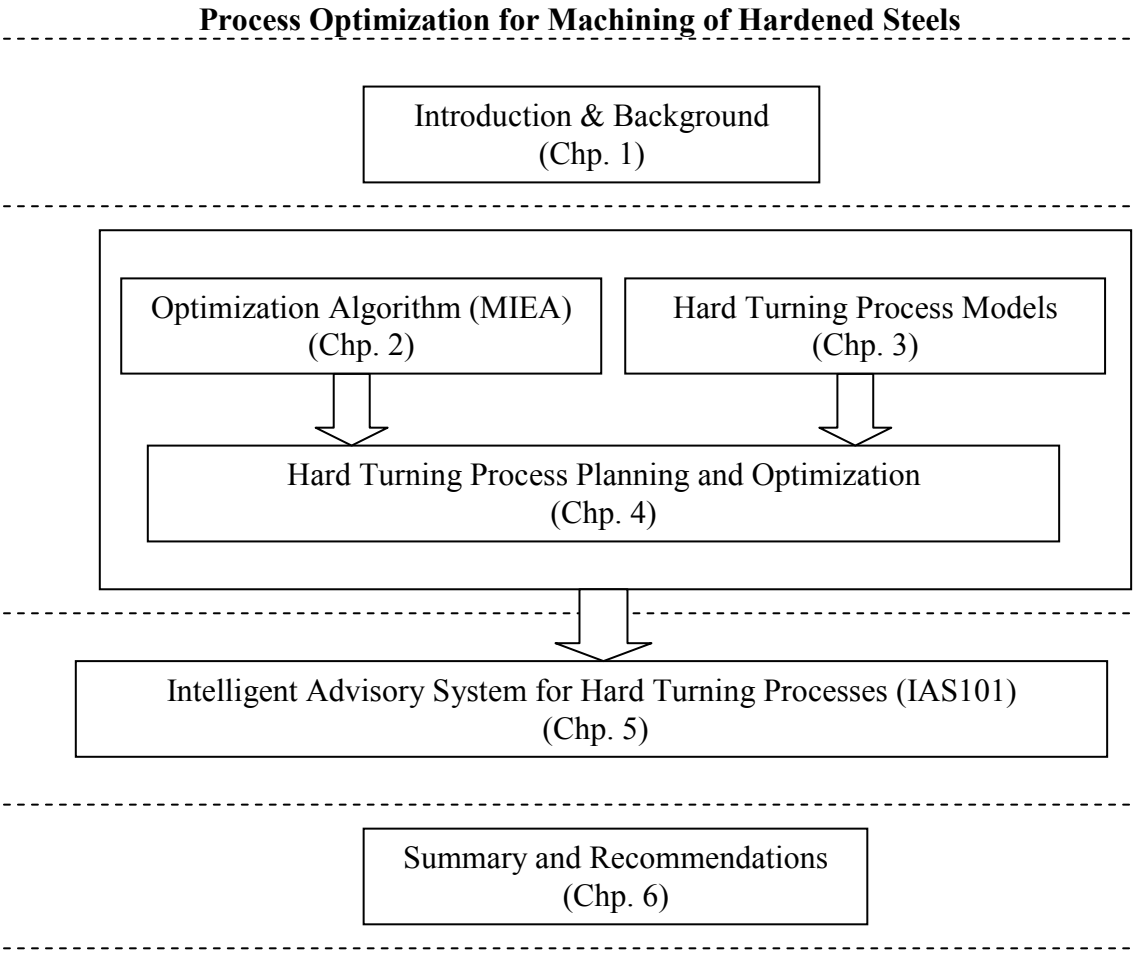


Figure 1-4 The structure of the dissertation

# CHAPTER II

# OPTIMIZATION ALGORITHM

## 2.1 Introduction

Machining process optimization not only remains an ongoing activity but also is becoming increasingly important in industry in the drive for reduced cycle time and agile manufacturing. Extensive literature exists on optimization of machining processes (Ermer 1997). Linear programming was used in the early stage of machining process optimization (Ermer and Patel 1974, Milner 1976), which can only deal with the linear equations. Non-linear programming has been extensively applied for more general non-linear machining optimization problems. Geometric Programming (GP), as one of the non-linear optimization techniques, has been widely adopted (Walvekar 1970, Phillips 1970, Ermer 1972, Eskicioglu et al. 1985, Tsai 1986, Gopalakrishnan and Al-Khayyal 1991). Its major disadvantage lies in its requirement that the objective function and constraints be in the form of polynomials. Traditional gradient-based optimization techniques have also been extensively used. For example, the successive quadratic programming method (Wen et al. 1992) and an iterative Newton's method (Xiao et al. 1992) were applied to optimize grinding processes; the generalized reduced gradient method (Jha 1995) was used to optimize tool geometry and cutting condition in plain milling processes.

However models of the hard turning process are very complex and some are highly non-linear, non-explicit and not analytically differentiable. The gradient-based non-linear optimization techniques have difficulty in solving this optimization problem; one must resort to non-systematic optimization techniques, i.e., Evolutionary Algorithms.

Currently, there are three different mainstreams in EA: Evolutionary Strategies (ES), Genetic Algorithms (GA) and Evolutionary Programmings (EP). GA has been applied to cutting tool and parameter selection for end milling (Strenkowski 1997). Another EA approach, evolutionary strategy, was investigated for optimization in grinding process optimization (Lee 2000).

Genetic Algorithm (GA) is selected as the platform method in this study due to its inherent nature in dealing with integer variables and its flexibility in handling constraints. However, GA still has its own drawbacks when it is applied to machining process optimization, including the lack of efficiency due to its binary representation scheme for continuous design variables, a lack of local fine-tuning capabilities, a lack of self-adaptation mechanism, and a lack of an effective constraint handling method.

The objective of this chapter is to develop a novel and systematic evolutionary algorithm based on Genetic Algorithm to address the above mentioned drawbacks when GA is applied to hard turning process planning and optimization. First, a general form of machining process optimization is mathematically formulated and its related terminologies are defined. Subsequently, the proposed Mixed Integer Evolutionary Algorithm (MIEA) is elaborated in the areas of problem representation; selection scheme; genetic operators for integer, discrete, and continuous design variables; constraint

handling method; and population initialization. Finally, the developed scheme is applied to twelve numerical cases and two machining problems to measure its performance.

## 2.2 Problem Formulation

A general machining process optimization problem can be characterized as a constrained, nonlinear programming problem with mixed-integer-discrete-continuous design variables. The general form of machining process optimization can be mathematically formulated as below:

***Minimize:***

$$f(X),\ X \in \mathcal{F} \subseteq \mathcal{S} \subseteq \mathbb{R}^n,$$

$$X = \{x_1, \ldots x_n\} = \{X^c, X^i, X^d\}$$

***Subject to (constraints):***

1) Boundary constraints:

$$L_i \le x_i \le U_i,\ \text{for } x_i \in X^c, X^i$$

$$x_i \in \{x_i^{(1)}, x_i^{(2)}, \ldots x_i^{(d_i)}\},\ \text{for } x_i \in X^d$$

2) Inequality and equality constraints:

$$g_j(X) \ge 0,\ j = 1, 2, \ldots k$$

$$h_j(X) = 0,\ j = k+1, k+2, \ldots m$$

$f(X)$ is the objective function, which can be cost per part, production rate, surface integrity, material removal rate, tool life, etc or any combination of them. $X$ : is the n-dimensional design vector to be optimized, including continuous design

variables $X^c$, such as feed rate, depth of cut, and cutting speed; integer design variables $X^i$, such as number of part cut per insert and grinding wheel diameter; and discrete design variables $X^d$, such as tool rake angle, tool clearance angle, and tool nose radius.

The problem usually is subject to boundary constraints for design variables and to inequality and equality constraints for process outputs. $g_j(X)$ is the inequality constraint, such as surface roughness, dimensional accuracy, cutting force and maximum available horsepower, $h_j(X)$ is the equality constraint, such as the desired part size and grinding power.

In general, the space $\mathbb{R}^n$ includes legal space and illegal space. Legal Space $\mathcal{S} \subseteq \mathbb{R}^n$ also refers to the search space, in which variables are restricted only by the boundary constraints. Any solution $X \in \mathcal{S}$ is a legal solution. Legal space includes feasible space and infeasible space. Illegal space $\mathcal{S}^c = \mathbb{R}^n - \mathcal{S}$ is the space out of the legal space. Any solution $X \in \mathcal{S}^c$ is an illegal solution. Feasible space $\mathcal{F} \subseteq \mathcal{S}$ is where design variables not only satisfy the boundary constraints but also satisfy all the inequality and equality constraints in the problem. Any solution $X \in \mathcal{F}$ is a feasible solution. Infeasible space $\mathcal{F}^c = \mathcal{S} - \mathcal{F}$ is the space inside the search space and outside the feasible space. Any solution $X \in \mathcal{F}^c$ is an infeasible solution.

Figure 2-1 illustrates all the related spaces and solutions in a two dimensional problem, where (x, a, b, c, d) are feasible solutions, (e, f, g, h, k) are legal but infeasible solutions, they are both in legal space (search space) while the optimum solution is ‘x’. (l, m) are illegal solutions.

Inasmuch as a maximization problem can be easily transformed to a minimization problem by minimizing $(-f(X))$, only minimization problems are discussed in this study.

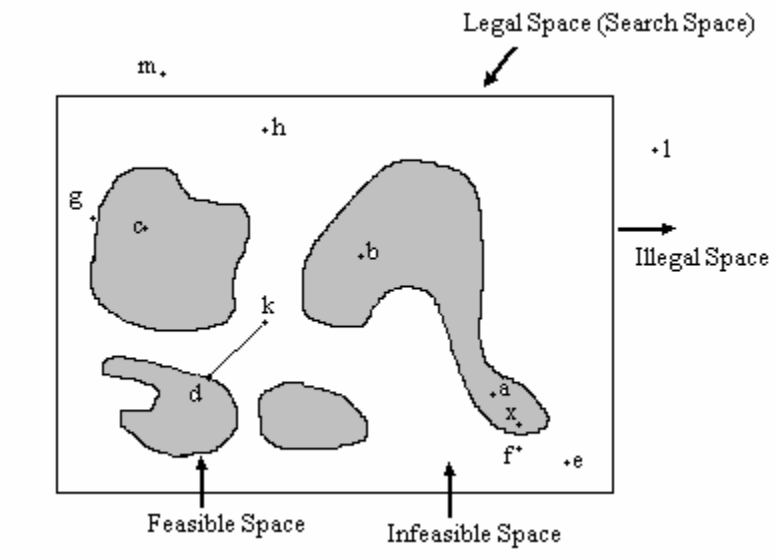


Figure 2-1 Legal space vs. illegal space and feasible space vs. infeasible space

## 2.3 Mixed-Integer Evolutionary Algorithm (MIEA)

A novel and systematic scheme of a Mixed-Integer Evolutionary Algorithm (MIEA) has been developed. The primary characteristics of this MIEA can be summarized as:

- The design variables are represented by the natural data types to implement one-gene-one-variable correspondence without additional encoding and decoding scheme. A gene corresponds to a real variable and a chromosome is a vector of

integer, discrete, and continuous variables. Hence, the genetype space is moved to be the same as the phenotype space, facilitating application to the general machining process optimization and increasing the algorithm's efficiency and effectiveness.

- Binary implementation is combined with the floating point implementation to deal with integer (discrete) and continuous design variables respectively and to take advantage of both bit representation of GA and real-valued representation of ES. Adaptive mutation and crossover is proposed for integer (discrete) variables, while non-uniform mutation with local tuning capability and uniform crossover is adopted for continuous variables.
- Tournament selection with elitism is used as the selection scheme to achieve a suitable balance between population diversity and selective pressure while tracking the best solution at each generation.
- A new integrated constraint handling method is proposed to propel search toward the feasible and optimal direction. It is computationally efficient, simple, and easy to implement. No additional penalty parameters are needed and a feasible solution is guaranteed.
- $(\alpha, \mu)-$population initialization is used to help distribute the initial population uniformly in the whole search space.

The new scheme of MIEA will be illustrated in detail in the areas of: selection scheme; problem representation; genetic operators for integer, discrete, and continuous variables; constraint handling method; and population initialization.

### 2.3.1 Selection Scheme

There are two important issues in the evolution process of the genetic search: population diversity and selective pressure. These two factors are strongly related and it is important to strive for a balance between them. A selection scheme attempts to achieve this goal (Back 1996, Michalewicz 1996). In this work, tournament selection as Equation (2-1) has been adopted:

$$p_i = \frac{1}{\mu^q}((\mu - i + 1)^q - (\mu - i)^q)$$
$$\sum_{i=1}^{u} p_i = 1,\ i \in \{1, ..., \mu\} \tag{2-1}$$

where $\mu$ is the population size, $i$ is the rank of a solution's fitness, and $q$ is the tournament size.

The whole selection scheme works as follows: All the solutions occurring in a population $P(t) = \{X_1(t), X_2(t)...X_\mu(t)\}$ are sorted with respect to their fitness values (calculated from the evaluation function). A probability value ($p_i$) is assigned to that individual based on Equation (2-1). This value maps to the area of the roulette wheel proportionally. Successive pairs of parents are drawn stochastically by spinning the marble of the roulette wheel.

Back (Back 1996) has systematically investigated the optimal selection scheme using a meta-evolutionary algorithm for problems with boundary constraints only.

Tournament selection with $q$=20 prevails over the other selection schemes. However when tournament selection is applied to the problem with boundary constraints together with inequality and equality constraints, tournament size $q$=20 imposes too high selection pressure to feasible solutions for some problems when a feasible superior scheme is also adopted in the algorithm. In MIEA, tournament size $q$=8 is selected as its default setting based on the preliminary numerical investigation of this study.

Elitist election**,** which always copies the most-fit solution into the next generation, has been used to enhance the performance of MIEA.

### 2.3.2 Problem Representation and Genetic Operators

The design variables are represented directly by the natural data types (such as "*int*" type for integer variables and "*float*" or "*double*" type for continuous variables in c/c++) to implement one-gene-one-variable correspondence. Hence, a gene corresponds to a real variable and a chromosome is a vector of integer, discrete, and continuous variables; This is represented by a *genotype* data structure in c++ as shown in Figure 2-2. The array *XI[I_SIZE]* represents the integer and discrete design variables and the array *XC[C_SIZE]* represents the continuous design variables, and *fit* represents the fitness of this design.

```
struct genotype
        {
                int XI[I_SIZE];
                float  XC[C_SIZE];
                float fit;
        };
```

Figure 2-2 Data structure to represent the design variables

This natural representation moves GA closer to the problem space in line with the principle of ES and EP. Crossover is applied to each design variable instead of one long binary string; hence crossover points automatically increase with increase in the problem's dimension.

The real-coded GA has been championed as opposed to the traditional binary-coded GA in numerical optimization (Goldberg 1990, Wright 1991, Eshelman 1993, Michalewicz 1996). However binary representation naturally deals with the integer variables. Hence, the binary implementation is kept for integer and discrete design variables while the floating point implementation is adopted for continuous design variables. In MIEA, the default mutation rate is set to 30% and the default crossover rate is 90% for all genetic operators based on the numerical experiments of this study.

Integer and discrete design variables

It is accepted by most researchers that discrete variables are mapped to the integer variables, so as to transfer discrete variables to integer variables. For example, if a discrete variable can take 10 discrete values as below, then the corresponding set of integer values will be:

$$\{0.90, 0.95, 1.04, 1.18, 1.28, 1.32, 1.40, 1.50, 1.62, 1.73\} \Rightarrow \{0, 1, 2, 3, 4, 5, 6, 7, 8, 9\}$$

Also, if an integer variable has lower and upper bounds such as 112 to 160; a mapping system from 0 to 47 is used.

Binary implementation is kept for integer and discrete design variables due to its inherent nature to represent the integer variables. A natural data type is used to represent each integer/discrete variable (such as "*int*" in c++ is used in this work which consists of 32 bits).

However, this scheme will lead to redundant bits in the gene. The valid number of bits needed to represent an integer can be calculated as $m$, which is the smallest number that satisfies $2^m \geq n+1$, $n = (X_U - X_L)$ for integer variables, n is the number of discrete values for discrete variables. The remaining $(32 - m)$ is the redundant bits in the gene. An example is shown in Figure 2-3 for integer variable [0, 47], where the valid number of bits is 6, and the remaining 26 bits are redundant bits.

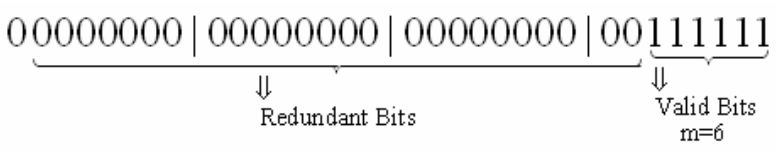


Figure 2-3 Integer representation for [0-47]

These redundant bits are not needed to represent that integer and will lead to undesired redundant mapping violating the "no redundancy principle". They will also introduce useless mutation and crossover operations when the mutation bit and crossover point are chosen within those redundant bits. Figure 2-4 illustrates an example of a useless crossover operation where the offspring remain the same as the parents after the crossover operation. Figure 2-5 demonstrates an example of useless mutation where an out-of-boundary integer is expected after the mutation operation. Those useless genetic operators will decrease the performance of the one-gene-one-variable scheme worse than the encoding and decoding method.

| | | |
|---|---|---|
| Parent1 (35): | 0000000000 | 00000000100011 |
| Parent2 (17): | 0000000000 | 00000000010001 |
| | | ↑ crossover point |
| Offspring1 (35): | 0000000000 | 00000000100011 |
| Offspring2 (17): | 0000000000 | 00000000010001 |

Figure 2-4 Demonstration of useless crossover

Befeore mutation (35): 000000000 0 00000000100011

↑ mutation bit

After mutation (16419) : 000000000 1 00000000100011

Figure 2-5 Demonstration of useless mutation

Mutation and crossover adapted to this valid number of bits ( $m$ ) are designed for integer/discrete variables. The mutation bit and crossover point are selected by: $\text{int}\left(r[0,1]*m\right)$ while leaving redundant bits unchanged as shown in Figures 2-6 and 2-7. The proposed method achieves the same working principle as the encoding and decoding method where the valid bits of all the integers are coded to one long binary string and at the same time makes the one-gene-one-variable scheme effective for mixed-integer problems. $r[0,1]$ is a uniform random number between $[0, 1]$ and it is assigned anew each time.

Parent1 (35): 00000000000000000010 | 0011

Parent2 (17): 00000000000000000001 | 0001

crossover point ↑

Offspring1 (33): 00000000000000000010 | 0001

Offspring2 (19): 00000000000000000001 | 0011

Figure 2-6 Demonstration of adaptive crossover

Befeore mutation (35): 00000000000000000100[0]11

mutation bit ↑

After mutation (39): 00000000000000000100[1]11

Figure 2-7 Demonstration of adaptive mutation

The proposed method was applied to a gear train design problem as formulated below:

$$\text{Minimize: } f(t_1,\ t_2,\ t_3,\ t_4) = \left( \frac{1}{6.931} - \frac{t_1 * t_2}{t_3 * t_4} \right)^2$$

$$\text{Subject to: } 40 \le t_i \le 60,\ i = 1,...4$$

The results were shown in Table 2-1 and were compared with the one where adaptive crossover and mutation were not applied. They were reported out of ten independent runs. Both of them run for 1000 generations with 100 population size. As can be seen that the algorithm with adaptive crossover and mutation achieves smaller objective value than the one without adaptive crossover and mutation. There are other two advantages of the proposed scheme. First, the different encoding and decoding schemes for the different problems are no longer needed; hence application to different problems is much easier. Secondly, all integer/discrete variables need not to encode to a long binary string for genetic operations and then decode back to individual

integer/discrete variables for function evaluation in each generation; thus efficiency and effectiveness are increased.

There are still $(2^m - n)$ excessive binary strings when $2^m \neq n+1$. This excessive mapping is dealt with by an "Even-Excessive-Distribution" method which will be discussed later.

Table 2-1 Optimal solution of the gear train design

| Items | Optimal solution | | Type of Variable |
|---|---|---|---|
| | W Adaptive | W/O Adaptive | |
| $t_1$ | 19 | 13 | Integer |
| $t_2$ | 16 | 30 | Integer |
| $t_3$ | 43 | 53 | Integer |
| $t_4$ | 49 | 51 | Integer |
| $f(T)$ | $2.7\times10^{-12}$ | $23.08\times10^{-12}$ | |

Continuous design variables

Non-uniform mutation and uniform crossover have been combined as the genetic operator for the continuous variables.

*Non-uniform Mutation*

A special dynamic bounded mutation with local fine tuning capability named non-uniform mutation has been adopted (Michalewicz 1996). The following is suggested:

$$x_i' = \begin{cases} x_i + \Delta(t, U_i - x_i) & \text{if } r[0,1] \leq 0.5 \\ x_i - \Delta(t, x_i - L_i) & \text{if } r[0,1] > 0.5 \end{cases} \tag{2-2}$$

$$\Delta(t,y) = y * \left( 1 - r[0,1]^{\left(1-\frac{t}{T}\right)^{b}} \right) \tag{2-3}$$

$\Delta(t,y)$ returns a value in the range of $[0,y]$ such that the value of $\Delta(t,y)$ becomes smaller with increasing generation. This operator searches globally at the early stage and locally at the later stage. $t$ is the current generation number, $T$ is the generation size, $b$ is a system parameter ($b$ =5 is recommended by Michalewicz 1996). Mutation will operate for each design variable if a random number $r[0,1]$ is smaller than the mutation rate.

*Uniform Crossover*

Uniform crossover is set as the default crossover operator for continuous design variables in this work. A float variable is a 32-bit value and a double is a 64-bit value according to IEEE standard. A one point crossover will operate for each variable/gene if a random number $r[0,1]$ is smaller than the crossover rate. The crossover point is selected by: $\text{int}\left(r[0,1]*m\right)$, $m = 32$ for float type and $m = 64$ for double type as shown in Figure 2-8.

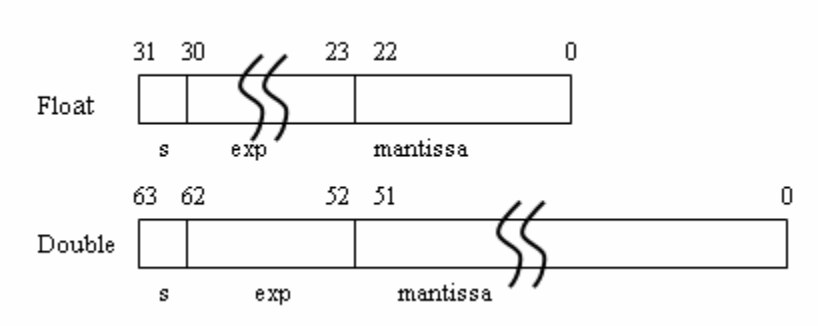


Figure 2-8 Crossover point for the continuous variable

Real-valued crossovers, such as arithmetical crossover, flat crossover, and heuristic crossover are extensively used for numerical optimization. They uniformly pick a value that lies between two points (A & B) which contain the two parents ( $x_1$ & $x_2$ ) as shown in Figure 2-9 for 1-D problem. The real-valued crossovers are also implemented in MIEA and compared with the uniform crossover. They are "assumed" to be more powerful as the crossover operator than the uniform crossover (Schwefel 1981, Wright 1991, Davis 1991). However, as shown in Table 2-2 by five test cases, the real-valued crossover has a much lower performance than that of the uniform crossover when combined with non-uniform mutation. Those five test cases are detailed in Appendix A.1. Radcliffe's (1991) flat crossover was chosen as the real-valued crossover in this comparison. The results were reported out of ten independent runs. G1, G2, G5 and G10 run for 2000 generations with 175 population size and G6-2 run for 10,000 generations with 175 population size. G6-2's global maximum is unknown; 0.833194 is the best result ever reported from the literature.

Table 2-2 Results summery on five test cases

| TC | | Exact opt. | Crossover | Best | Average | Worst |
|---|---|---|---|---|---|---|
| G1 | Minimize | -15.0000 | Uniform | -15.0000 | -15.0000 | -15.0000 |
| | | | Real | -12.8799 | -12.7207 | -12.5623 |
| G2 | Minimize | 7049.33 | Uniform | 7057.38 | 7250.67 | 7560.88 |
| | | | Real | 8619.49 | 19445.14 | 26111.17 |
| G5 | Minimize | 24.036 | Uniform | 24.606 | 24.723 | 24.889 |
| | | | Real | 25.554 | 25.932 | 26.237 |
| G6-2* | Maximize | 0.833194 | Uniform | 0.835202 | 0.826909 | 0.795825 |
| | | | Real | 0.443750 | 0.441113 | 0.439214 |
| G10 | Minimize | -6961.814 | Uniform | -6961.807 | -6960.801 | -6954.905 |
| | | | Real | -6879.350 | -6812.379 | -6706.242 |

Hence, non-uniform mutation with uniform crossover forms a very powerful genetic operator for continuous design variables. There are two main reasons why uniform crossover outperforms real-valued crossover when combined with non-uniform mutation.

First, real-valued crossovers are mostly proposed and tested for the problem with boundary constraints only. They are much less effective when applied to the problem with inequality "$g$ type" and equality "$h$ type" constraints due to their convex combination characteristic. In highly constrained optimization problems, the feasible space is usually small and sparse in the whole search space. A randomly generated initial population is mostly located in infeasible space. This convex combination crossover has lower ability to generate feasible solutions from infeasible solutions; hence it cannot drive the search towards feasible direction.

Secondly, non-uniform mutation is achieving the same power of the real-valued crossover for increasingly focusing search. The only differences between non-uniform

mutation and real-valued crossover are (1) “Step size”: it is self adapted by extent of convergence for real-valued crossover and by the generation for non-uniform mutation. (2) “Perturbation size”: $x_1$ will be perturbed by a region of $[-r_1 I,\ (r_2+1)I]$ for real-valued crossover and a region of $[-r_1 I_1,\ r_2 I_2]$ for non-uniform mutation to generate an offspring as shown in Figures 2-9 and 2-10, where $I = |x_2 - x_1|$, $I_1 = \Delta(g, x_1 - LB)$, $I_2 = \Delta(g, UB - x_1)$. Hence, real-valued crossover is one kind of special mutation operator and its power as crossover operator is very weak.

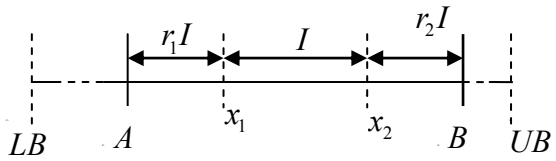


Figure 2-9 Real-valued crossover in a one-dimensional problem

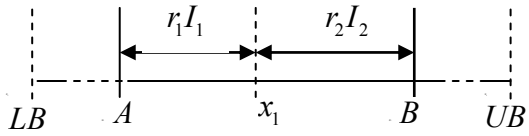


Figure 2-10 Non-uniform mutation in a one-dimensional problem

### 2.3.3 Integrated Constraint Handling

Boundary constraints

An "Even-Excessive-Distribution" method is proposed for boundary constraints. Due to the nature of the GA, the initial population was randomly generated in a given interval $< L_i, U_i >$. Hence, the initial population will be located in legal/search space. If any variable generated by the genetic operators is out of the boundary, which is defined as an illegal solution/offspring, a random value within the boundary will be reassigned to that variable. By this random reassigning scheme, the total effect will even out the distribution of out-of-boundary values back to legal/search space. All the boundary constraints are naturally satisfied and the search is implemented in legal space/search space.

Equality and inequality constraints

The inequality "$g$ type" and equality "$h$ type" constraints make the feasible space different from the search space and determine the ratio $\rho$ between the feasible space and the search space where $\rho = |\mathcal{F}| / |\mathcal{S}|$. A feasible superior, problem independent penalty scheme is proposed as below:

$$fitness(X) = \begin{cases} fitness_f(X) = \dfrac{f(X)}{F(X,t)}, & \text{if } X \in \mathcal{F} \\ fitness_u(X) = \dfrac{f(X)}{F(X,t)} + \dfrac{\sum_{j=1}^{m} p_j(X)}{P(X,t)} + \dfrac{\sum_{j=1}^{m} \varphi_j(X)}{\psi(X,t)} + 2, & \text{if } X \in \mathcal{F}^c \end{cases} \tag{2-4}$$

$$F(X,t) = \max\left\{\max_{X\in\mathcal{S}}\{f(X)\},0\right\} - \min\left\{\min_{X\in\mathcal{S}}\{f(X)\},0\right\} \tag{2-5}$$

$$P(X,t) = \max_{X\in\mathcal{F}^c}\left\{\sum_{j=1}^{m} p_j(X)\right\}, \quad \psi(X,t) = \max_{X\in\mathcal{F}^c}\left\{\sum_{j=1}^{m} \varphi_j(X)\right\} \tag{2-6}$$

$$p_j(X) = \begin{cases} \left(g_j(X) \ge 0\right)?0:g_j(X), & \text{if } 1 \le j \le k \\ \left(\left|h_j(X)\right| \le \varepsilon\right)?0:\left|h_j(X)\right|, & \text{if } k+1 \le j \le m \end{cases} \tag{2-7}$$

$$\varphi_j(X) = \begin{cases} \left(g_j(X) \ge 0\right)?0:1, & \text{if } 1 \le j \le k \\ \left(\left|h_j(X)\right| \le \varepsilon\right)?0:1, & \text{if } k+1 \le j \le m \end{cases} \tag{2-8}$$

All objective values are scaled to [-1, 1] by dividing the range of the objective values in that generation: $F(X,t)$. $\sum_{j=1}^{m} p_j(X)$ is the 'amount' of infeasibility of an infeasible solution and is normalized by the maximum 'amount' of infeasibility among all the solutions in that generation: $P(X,t)$. $\sum_{j=1}^{m} \varphi_j(X)$ is the number of constraints violated by an infeasible solution and is normalized by the maximum number of constraints violated among all the solutions in that generation: $\psi(X,t)$. $p_j(X)$ and $\varphi_j(X)$ are computed by a conditional operator: $d = c\,?\,a:b$. The meaning of this operator is: if $c$ is true; then $d = a$; otherwise $d = b$.

Hence, feasible solutions are evaluated by their objective values only and infeasible solutions are evaluated by their objective values and 'fit' extent. The lower the number of constraints violated, the "fitter" they are; the smaller 'amount' of infeasibility in terms of the degree of constraint violated, the "fitter" they are. The 'fit' extent can be equally evaluated by the number of constraints violated and the amount of infeasibility for infeasible solutions through normalization.

The equality constraints $h_j(X) = 0$ will be replaced by the inequality constraints of $\left|h_j(X)\right| \le \varepsilon$. The variable $\varepsilon$ is an infinitesimal number, which can be given explicitly or be determined from the precision requirement in each problem. For example in precision grinding of Hydraulic Lash Adjuster Body (HLA), the desired bore diameter is 9.2484mm with the dimensional tolerance of $\pm 0.0025mm$. This requirement can be transformed to an equality constraint as in Equation (2-9):

$$D - 9.2485 = 0 \tag{2-9}$$

With the given tolerance, this equality constraints can be relaxed to an inequality constraint as in Equation (2-10) with $\varepsilon$ value equals 0.0025.

$$\left|D - 9.2485\right| \le 0.0025 \tag{2-10}$$

The significant digit requirement will be determined and will be used for all the continuous design variables. $\varepsilon$ can also be estimated from this significant digit requirement. For example, if the significant digit requirement is 6, then $\varepsilon = 10e-6$.

By the aid of normalization, all feasible solutions distribute in [-1, 1]. A value of 2 is "purposely" added to all infeasible solutions to distribute infeasible solutions to (1, 5] as shown in Figure 2-11. Hence all the feasible solutions are better than any infeasible solutions, that is, a feasible superior condition is ensured.

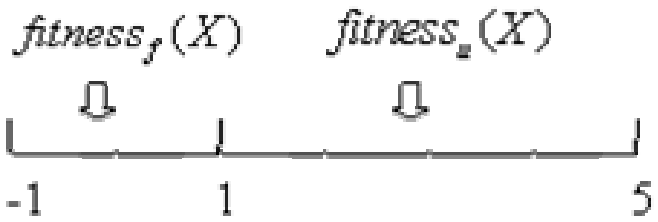


Figure 2-11 Fitness distribution of a population

A feasible superior scheme is preferred for machining process optimization for two reasons. First, a feasible "optimal" solution is a basic requirement for manufacturing processes. Penalty too "heavy" will no longer be equivalent to rejecting methods when "ranking or tournament selection" is used because selection is based on its "rank" instead of its evaluation value. Secondly, the randomly generated initial population is mostly located in the infeasible space due to the small and sparse feasible space in constrained manufacturing problems. "Feasible superior" methods will drive the genetic search

toward the feasible direction because a feasible solution has superior probability to survive.

It is very possible for infeasible solutions to provide better information than some feasible ones about the "feasible global optimal" solution. But a penalty function based on how much information a solution contains about the "unknown feasible global optimal" solution will be too difficult to formulate. So the penalty strategy in this work is not based on how much information a solution contains about the "feasible global optimal" solution, but on how well it can help genetic search to move toward the feasible direction.

Feasible superior method is also implemented in Powell & Skolnick's (1993) method. A different strategy is used to evaluate two infeasible solutions from this study. As the most penalty methods, the Powell & Skolnick method evaluates two infeasible solutions based only on the amount of infeasibility. The number of violations should be equally considered as one of the important indexes to evaluate infeasible solutions. The reason is that not all the design variables are involved in every constraint, when fewer constraints are violated; fewer variables need to be repaired for this infeasible solution to be feasible. They have better chance to generate feasible solutions in the next generation, so as to help the genetic search toward feasible direction.

### 2.3.4 Population Initialization

As are most of the "feasible superior" penalty methods, the proposed penalty method is very sensitive to the pressure of a single feasible solution in the initial

population. However, it is very possible that there is no single feasible solution in a randomly generated initial population for highly constrained manufacturing problems. It is found from this work's numerical tests that when no single solution is feasible in the initial population, genetic operators have difficulty in generating any feasible solution automatically, and the program will end with a premature infeasible solution. It is "reasonable" because GA has no knowledge of feasible solutions when no feasible solution exists in the initial population. The initial population should be uniformly distributed in the whole search space in order to provide enough problem knowledge to the GA. Hence, it is necessary to enforce at least one solution to be feasible in the initial population.

An $(\alpha, \mu)-$population initialization scheme is proposed, where $\mu$ is the population size and $\alpha$ is the number of solutions forced to be feasible in the initial population. Population initialization should not take too much time. The size of $\alpha$ has to be chosen by trading off between efficiency and effectiveness. Initialization time will increase and sometimes important information in the infeasible space may be lost when too many solutions are forced to be feasible in the initial population while $\alpha = 1$ is necessary. In this work $\alpha = 1$ has been used. The initialization scheme is shown in Figure 2-12.

i=1 to $\alpha$
**do** {initialize $X_i := (x_{i1}, x_{i2}...x_{in})$;}
**while** ( $X_i \notin \mathcal{F}$ );
for i= $\alpha + 1$ to $\mu$
{initialize $X_i := (x_{i1}, x_{i2}...x_{in})$;}

Figure 2-12 Initialization scheme

### 2.3.5 Other Components

*Random Numbers*

Genetic Algorithm relies on vast quantities of random values where thousands and thousands of random values need to be generated. A pseudo-random number generator with very unpredictable and large repetition cycle will greatly help the genetic algorithm's performance. One of the pseudo-random number generators, a uniform deviate generator from Ladd (1995), has been adopted in this work.

*Significant Digits*

It is common in engineering that a value is only accurate to a certain number of significant digits. In order to prevent the error from accumulating, all variables are set to a specific number of significant digits. The number of significant digits can be determined online for different precision requirements of each problem in MIEA.

### 2.3.6 Algorithm

The flowchart of MIEA is shown in Figure 2-13. At generation $t = 0$, the initial population is randomly generated while forcing $\alpha$ individuals to be feasible. The fitness values of the initial population are evaluated and sorted. A probability is assigned to each individual based on tournament selection. At each generation t, the best solution from the previous generation is copied to the current generation first. And then genetic operators are applied respectively for integer/discrete and continuous design variables to obtain an offspring population. For each interger/discrete design variable, adaptive crossover and mutation are performed, then the boundary constraint is checked, if the boundary constraint is violated, a random value within the boundary will be reassigned to that variable. For each continuous design variable, uniform crossover is performed and the boundary constraint is checked, then the non-uniform mutation is performed. The offspring populations' fitness values are again evaluated and sorted. A probability value will be reassigned to each individual in the offspring based on the tournament selection. The process will continue until the stopping criterion is met, which is given by the predefined maximum number of generations.

t:=0;
***Initialize*** *the initial population*
i=1 to $\alpha$
*do* {initialize $X_i := (x_{i1}, x_{i2} \ldots x_{in})$;}
*while* ( $X_i \notin \mathcal{F}$ );
*for* $i = \alpha + 1$ *to* $\mu$
{initialize $X_i := (x_{i1}, x_{i2} \ldots x_{in})$;}
***Evaluate & sort*** the fitness of the initial population
***Assign*** $p_i$ based on tournament selection to the initial population
While stopping condition is not met, do
Copy ***elitist*** solution
Do until $\mu$ offspring are obtained:
for each integer/discrete design variable
***Adaptive Crossover***
***Adaptive Mutation***
***Check for boundary constraint***
end
for each continuous design variable
***Uniform Crossover***
***Check for boundary constraint***
***Non-uniform Mutation***
end
end
***Evaluate & sort*** the fitness of the offspring
***Assign*** $p_i$ based on tournament selection to the offspring
t: =t + 1;
end

Figure 2-13 Mixed Integer Evolutionary Algorithm (MIEA)

## 2.4 Application of MIEA to Numerical Cases

The performance of the developed MIEA algorithm has been measured by twelve numerical test cases from (Michalewicz 1996, Michalewicz and Schoenauer 1996) which are listed in Appendix A.1. As reported from Michalewicz and Schoenauer (1996) and shown in Table 2-3, twelve test cases are chosen due to: 1. the type of the objective functions $f$ ; 2. the number $n$ of variables; 3. the number and type of constraints of each category (linear inequalities $LI$ , nonlinear equalities $NE$ and nonlinear inequalities $NI$ ); 4. the number of active constraints $a$ at the optimum; and 5. the ratio $\rho$ between the sizes of the feasible space and the whole search space: $|\mathcal{F}|/|\mathcal{S}|$. $\rho$ was determined numerically by generating 1,000,000 random points from search space $\mathcal{S}$ and checking whether or not they belong to feasible space $\mathcal{F}$. They offer a handy collection for preliminary tests of optimization algorithms, especially for its constraint handling capabilities.

In this work, the population size was chosen to be 175 and all the test cases were run for 2000 generations (except for G6, G7) in order to achieve the same function evaluation trials as those of Michalewicz's (1996) for comparison. G6-1 (20 variables) and G6-2 (50 variables) were run with 175 population size for 10,000 generations and G7 was run with 10 population size for 30,000 generations. The results are shown in Table 2-4, which reports the best, the average, and the worst results; standard deviation; and average execution time in seconds out of 10 independent runs. Feasibility is guaranteed for all the results because the feasible superior scheme is applied in the algorithm.

Table 2-3 Summary of twelve test cases

| TC | $n$ | Type of $f$ | $\rho$ | $LI$ | $NE$ | $NI$ | $a$ |
|---|---|---|---|---|---|---|---|
| G1 | 13 | quadratic | 0.0111% | 9 | 0 | 0 | 6 |
| G2 | 8 | linear | 0.0010% | 3 | 0 | 3 | 6 |
| G3 | 7 | polynomial | 0.5121% | 0 | 0 | 4 | 2 |
| G4 | 5 | nonlinear | 0.0000% | 0 | 3 | 0 | 3 |
| G5 | 10 | quadratic | 0.0003% | 3 | 0 | 5 | 6 |
| G6-1 | 20 | nonlinear | 99.8474% | 0 | 0 | 2 | 1 |
| G6-2 | 50 | nonlinear | 99.8474% | 0 | 0 | 2 | 1 |
| G7 | 20 | polynomial | 0.0000% | 0 | 1 | 0 | 1 |
| G8 | 5 | quadratic | 52.1230% | 0 | 0 | 6 | 2 |
| G9 | 4 | cubic | 0.0000% | 2 | 3 | 0 | 3 |
| G10 | 2 | cubic | 0.0066% | 0 | 0 | 2 | 2 |
| G11 | 2 | nonlinear | 0.8560% | 0 | 0 | 2 | 0 |
| G12 | 2 | quadratic | 0.0000% | 0 | 1 | 0 | 1 |

Table 2-4 Summery of results on twelve test cases

| TC | | Exact opt. | Best | Average | Worst | Standard Deviation | Execution Time (s) |
|---|---|---|---|---|---|---|---|
| G1 | Minimize | -15.000 | -15.000 | -15.000 | -15.000 | 0.0 | 10.433 |
| G2 | Minimize | 7049.331 | 7057.38 | 7250.669 | 7560.88 | 160.348 | 8.613 |
| G3 | Minimize | 680.630 | 680.640 | 680.6549 | 680.696 | 0.0172 | 9.467 |
| G4 | Minimize | 0.054 | 0.0540 | 0.0648 | 0.0982 | 0.0165 | 8.790 |
| G5 | Minimize | 24.036 | 24.606 | 24.723 | 24.889 | 0.0989 | 13.342 |
| G6-1* | Maximize | 0.803553 | 0.803617 | 0.798108 | 0.792601 | 0.0058 | 32.374 |
| G6-2* | Maximize | 0.833194 | 0.835202 | 0.826909 | 0.795825 | 0.0117 | 386.248 |
| G7* | Maximize | 1.0 | 1.00048685 | 1.0003522 | 1.0000958 | 0.000125 | 8.732 |
| G8 | Minimize | -30665.5 | -30665.53 | -30665.51 | -30665.48 | 0.0271 | 6.810 |
| G9 | Minimize | 5126.4981 | - | - | - | - | - |
| G10 | Minimize | -6961.814 | -6961.807 | -6960.801 | -6954.905 | 2.2752 | 3.3326 |
| G11 | Maximize | 0.095825 | 0.095825 | 0.095825 | 0.095825 | 0.0 | 3.410 |
| G12* | Minimize | 0.7500045 | 0.7490002 | 0.7591698 | 0.8005944 | 0.01658 | 3.285 |

As can be seen from Table 2-4, the proposed scheme is able to find the best solutions very close to the known global optimal solution for all the test cases (except the

test case G9) with small standard deviation and within a very short computational time. The proposed constraint handling scheme outperforms all the other six methods listed in Michalewicz's book (1996) for test case G1 – G5; it also works better than those found in the literature (Hadj-Alouane and Bean 1992, Myung 1995, Koziel and Michalewicz 1999) for most test cases.

The proposed method has difficulty for the test case G9 as well as the other methods (Koziel and Michalewicz 1999). Joines and Houck (1994) gave a value of 5126.6653 of the objective function. But no solution was fully feasible due to the three equality constraints in the test case G9. The feasible space of G9 is extremely small. There is not a solution feasible within 1,000,000,000 randomly generated points even though three equality constraints have been relaxed to be $\left|h_j(X)\right| \le 0.0001$ . Therefore it has difficulty in finding a feasible solution in population initialization; however without a feasible solution in the initial population, the problem ends with a premature infeasible solution.

The best solutions for test cases G7 and G12 are better than the known global optimum. The reason is the relaxation of the equality constraints to the inequality constraints. As detailed above, the equality constraints $h_j(X) = 0$ will be replaced by the inequality constraints of $\left|h_j(X)\right| \le \varepsilon$ . The value of $\varepsilon$ determines the relaxation extent of the equality constraints and also affects the final optimal solutions. $\varepsilon = 0.0001$ has been used for the equality constraints in test case G7 and G12.

Worthy of mention is the test case G6. G6 is to maximize a function as shown in Equation (2-11):

$$G6(X) = \left| \frac{\sum_{i=1}^{n} \cos^4(x_i) - 2\prod_{i=1}^{n} \cos^2(x_i)}{\sqrt{\sum_{i=1}^{n} i x_i^2}} \right| \tag{2-11}$$

with the constraints of:

$$0 < x_i < 10,\ i = 1,...n$$

$$\prod_{i=1}^{n} x_i > 0.75$$

$$\sum_{i=1}^{n} x_i < 7.5n$$

G6's global maximum is unknown. As shown in Figure 2-14 for n=2 case where infeasible solutions were assigned value zero, it is a difficult problem on which no known methods gave satisfactory results (Michalewicz and Schoenauer 1996).

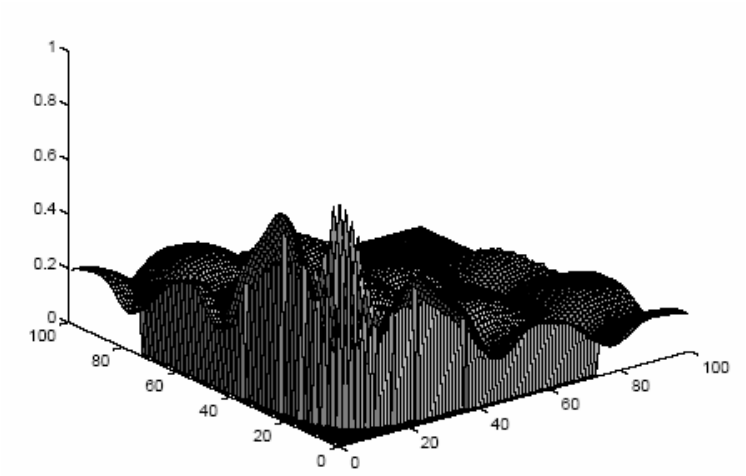


Figure 2-14 The graph of G6 for n=2 (Michalewicz and Schoenauer 1996)

The MIEA gave outstanding results. For the case n=20 (G6-1), it reached the value of 0.803617, which is better than the best value ever found (Keane (1994) gave a best value of 0.76 and Michalewicz (1996) gave a best value of 0.803553) with the optimal solution of:

$X^* = \{3.16043258, 3.12754512, 3.09359360, 3.06049466, 3.02768564, 2.99235296,$
$2.95944715, 2.92219949, 0.49483365, 0.48731905, 0.48034167, 0.47483969,$
$0.47307324, 0.46573946, 0.46269602, 0.45579949, 0.45373166, 0.44978923,$
$0.44504631, 0.44064420\}$

Similarly, for n=50 (G6-2), it reached the value of 0.8352, which is also better than the best value ever reported (best values of 0.8332 and 0.8348 have been reported respectively (Michalewicz 1996)) with the optimal solution of:

$X^* = \{6.28234386, 3.16757345, 3.15456867, 3.14324331, 3.12941480, 3.11366415,$
$3.10167003, 3.08602786, 3.07424927, 3.06255317, 3.04743624, 3.03712273,$
$3.02034664, 3.00651383, 3.00001884, 2.97560692, 2.96612120, 2.95461059,$
$2.93431211, 2.92233706, 0.49643144, 0.48006836, 0.49415991, 0.46941942,$
$0.47801661, 0.47702739, 0.47604510, 0.47386724, 0.47658002, 0.46413743,$
$0.47684807, 0.46653312, 0.47030780, 0.45434538, 0.45569429, 0.45161772,$
$0.45535612, 0.44744486, 0.45442498, 0.44980237, 0.44996986, 0.45574158,$
$0.44432029, 0.44588098, 0.43479106, 0.44538400, 0.45508292, 0.44191003,$
$0.44009739, 0.43020955\}$

The ratio of the feasible solution size to the population size and the best function value changing with the generations for test cases G2 and G5 are shown in Figure 2-14 and Figure 2-15 and for test cases G6 and G7 are shown in Figure 2-16. It can be clearly seen that the penalty scheme used in this study ensures searching toward not only a feasible direction but also an optimal direction, which is the most promising direction desired.

As shown in Table 2-2, for test cases G2, G4, G5, G7, and G12, the ratio $\rho$ between the sizes of the feasible space and the whole search space are very small. It is not surprising to find that no single solution is feasible in the randomly generated initial population. Further feasible solutions are very difficult to generate by genetic operator when no single solution is feasible. When one solution is forced to be feasible in the initial population, more and more feasible solutions will be generated due to the applied penalty method and tournament selection, as shown in Figures 2-15, 2-16 and 2-17. It does not help to force more solutions to be feasible in the initial population; it merely takes more initialization time, because at the second generation the population came back

to only one feasible solution (one solution can be kept feasible at the second generation due to the elitism selection) and the same search procedure happened with $\alpha$ =1.

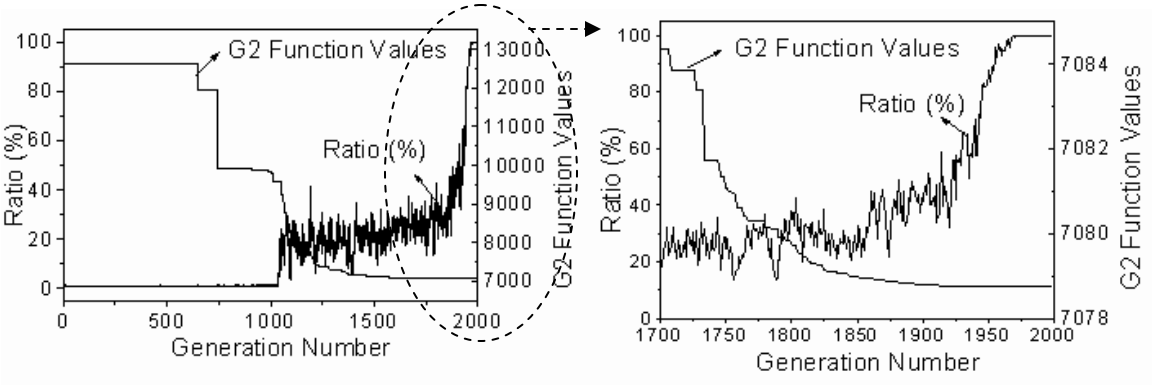


Figure 2-15 The ratio (%) of the feasible solution size to the population size (175) and the best objective function value with the generation for test cases G2

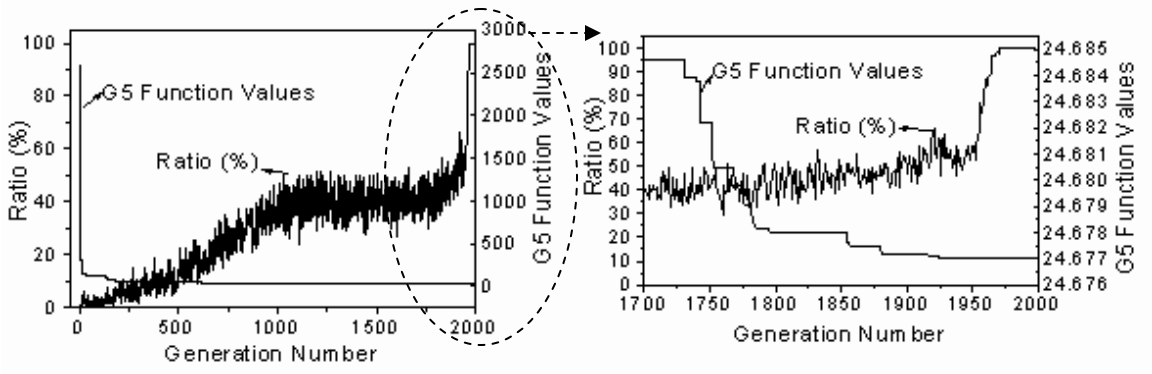


Figure 2-16 The ratio (%) of the feasible solution size to the population size (175) and the best objective function value with the generation for test cases G5

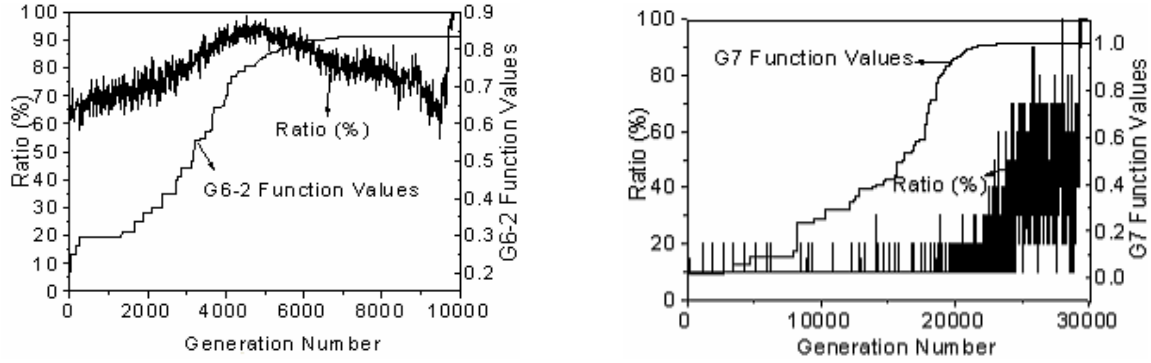


Figure 2-17 The ratio (%) of the feasible solution size to the population size (175) and the best objective function value with the generation for test cases G6-2 and G7

## 2.5 Application of MIEA to General Machining Processes

### 2.5.1 Application to a Unified Metal Cutting Problem

Jang D. Y. (1992) developed a unified optimization approach for selecting the machining parameters that provide the maximum material removal rate. The optimization problem was constrained by surface integrity, the surface residual stress distribution, condition for continuous chip formation, tool failure constraints, including tool fracture, tool plastic deformation, tool flank wear, and tool crater wear constraints. They can be formulated as follows: (Refer to Appendix A.2 and Jang 1992 for detailed models used in this example.)

Maximize:

$$F(V,d,f,R) = V * d * f$$

Subject to:

Speed (continuous): $0 \le V \le 300$ (m/min)

Depth of Cut (continuous): $0 \le d \le 3$ (mm)

Feed (continuous): $0 \le f \le 0.7$ (mm/rev)

Tool edge radius (discrete): $0.1 \le R \le 0.3$ (mm)

Surface Roughness: $h_{\max} \le h_{\text{given}}$

Dimensional Accuracy: $\delta \le \delta_{\text{given}}$

Surface compressive stress: $|\sigma_c| \ge |\sigma_{\text{given}}|$

Depth of the pre-compressed layer: $d_c \ge d_{\text{given}}$

Continuous chips without a built-up edge: $fV^n \ge C_3$

Tool flank wear constraints: $L_2 \le L_1$

Tool-chip interface temperature: $T_C \le T_{\text{softening}}$

Tool fracture constraints: $\sigma_1 \le \sigma_{\max}$

Tool plastic deformation constraints: $T_{\text{pz}} \le T_{\max}$

The design variables are the cutting speed $V$ (m/min), depth of cut d (mm), feed rate $f$ (mm), and tool edge radius R (mm). In this work, tool edge radius is treated as a discrete design variable, which can be selected from 11 discrete values, {0.1, 0.12, 0.14, 0.16, 0.18, 0.2, 0.22, 0.24, 0.26, 0.28, 0.3}, instead of a fixed value in Jang's work.

Jang applied Powell's unconstrained method with the exterior penalty function to solve this problem. The optimal result from Jang is verified to be an infeasible result,

where surface roughness and surface compressive stress constraints are violated. In this work, those two constraints are relaxed to be the same as the work of Jang's and the optimization results are compared in Table 2-5. The MIEA method achieves better results than those of Jang.

Table 2-5 Comparison between the optimum solution for fine cutting

| | **Constraints** | **Jang (1992)** | **MIEA** | **Type of Variable** |
|---|---|---|---|---|
| Feed rate (mm/rev) | $0 \le f \le 0.7$ | 0.12 | 0.12 | continuous |
| Cutting Speed (m/min) | $0 \le V \le 300$ | 217 | 210.307 | continuous |
| Depth of cut (mm) | $0 \le d \le 3$ | 2.8 | 3.0 | continuous |
| Tool edge radius (mm) | $0.1 \le R \le 0.3$ | 0.3 (fixed) | 0.3 (optimal) | discrete |
| $T_{pz}(°C)$ | $T_{pz} \le 830°C$ | 405.7 | 406.2555 | |
| $T_c(°C)$ | $T_C \le 1100°C$ | 1074.2 | 1063.3462 | |
| $L_1$ | $L_2 \le L_1$ | 2.28e-005 | 2.21e-005 | |
| $L_2$ | | 6.51e-014 | 5.10e-014 | |
| $\sigma_1(MPa)$ | $\sigma_1 \le 550$ | 33.7457 | 32.3362 | |
| $d_c$ | $d_c \ge 0.04$ | 0.044 | 0.0436 | |
| $\sigma_c(MPa)$ | $\lvert\sigma_c\rvert \ge \lvert-72.43\rvert$ | -72.43 | -72.43 | |
| $h_{max}(\mu m)$ | $h_{max} \le 5.89$ | 5.89 | 5.89 | |
| $\delta(\mu m)$ | $\delta \le 5$ | 4.5998 | 4.8007 | |
| $MRR$ ($mm^3$/min) | | **72912** | **75709** | |

The advantage of the proposed scheme can be further found in the other two aspects: First, the traditional non-linear optimization methods, such as the Powell method, require a good initial point; otherwise the algorithm is very likely trapped in a

local optimal solution. The MIEA is a population-based algorithm; a judicious choice of an initial point is not required. Secondly, the exterior penalty function used in Jang's method needs lots of penalty parameters and careful tuning of those parameters is necessary; otherwise this method can easily come up with an infeasible solution or can terminate prematurely. Additionally, it will suffer when the "reward" of an infeasible solution higher than its "penalty" and the program will always end with an infeasible solution. The proposed MIEA, on the other hand, uses a problem independent, feasible superior penalty scheme; no additional penalty parameters are required and a feasible optimum is guaranteed.

### 2.5.2 Application to a Generalized Surface Grinding Problem

Vishnupad and Shin (1998) have developed a set of generalized models of the grinding process including maximum chip thickness, tangential force, grinding power, surface roughness, grinding ratio (G-ratio), effective dullness and grinding temperature for Generalized Intelligent Advisory System (GIGAS). Lee (2000) optimized surface grinding processes based on those generalized models. One of the applications is to minimize the total grinding cost using rough grinding and finish grinding. The problem was constrained by the available power and G ratio in rough grinding and G ratio, maximum residual stress and surface finish in finish grinding. It can be formulated as follows:

Minimize Grinding Cost:

$$C_t = C_r(v_w, s_t, a_d, n_r, N_d) + C_f(v_w, s_t, a_d, a_f, N_d)$$

$$C = \frac{M}{3600}\left[\left(\frac{L_w + L_e}{1000 v_w}\right)\times\left(\frac{b_w + b_e}{s_t}\right)\times\frac{T}{a}\right] + \left[\frac{M}{60}\times\frac{t_d}{N_d} + C_s\times\frac{\pi\left(a_d + a_t\right)b_s d_s}{1000 N_d} + \frac{C_d}{N_d N_{td}}\right] + C_s\times\frac{T b_w L_w}{G}$$

$C$ is the grinding cost correspondence to $C_r$ for roughing cost and $C_f$ for finishing cost. Similarly, $T$ and $a$ are the total thickness to remove and the depth of cut correspondence to $T_r$ and $a_r$ for roughing and $T_f$ and $a_f$ for finishing.

Subject to:

$$0.10 \le v_w \le 0.30$$

$$0.5 \le s_t \le 2.3$$

$$12.7 \le a_d \le 50.8$$

$$0.01 \le a_r \le 0.046$$

$$0.01 \le a_f \le 0.046$$

*Rough Grinding:*

Power: $P(k) \le P^*, \quad k = 1, 2, ...N_d$

G ratio: $G \ge G^*$

*Finish Grinding:*

Surface Roughness: $R_a(k) \le R_a^*$

Residual Stress: $\sigma_r(k) \le \sigma_r^* \quad k = 1, 2, ...N_d$

G ratio: $G \ge G^*$

The detail models for surface roughness, grinding force and power, residual stress, and G ratio are listed in appendix A.3 or refer to (Lee 2000) for further details. The design variables in rough grinding include workpiece speed $v_w$ (m/s), crossfeed $s_t$ (mm), dressing depth $a_d$ (um), the number of grinding passes $n_r$, the number of workpieces between dressing $N_d$ and the design variables in finish grinding include workpiece speed $v_w$ (m/s), crossfeed $s_t$ (mm), dressing depth $a_d$ (um), depth of cut $a_f$ (mm) and the number of workpieces between dressing $N_d$.

The population size was set to be 200 and the model was run for 1000 generations. It took around 7 seconds when run on the Pentium 4 personal computer. The optimization results are listed in Tables 2-6 and 2-7.

Evolutionary Strategy (ES) was used by Lee (2000) for this problem and achieved different optimal results. The results are not comparable to this work due to the different models for the accumulated sliding length (A-15, A-16) used. Those two models are not presented in (Lee 2000) and were cited from (Malkin 1976) in this study. The same

Table 2-6 Optimal variables for minimization of grinding cost

| Operation | Design Variable | Value | Type of Variable |
|---|---|---|---|
| Roughing | $v_w$ (m/s) | 0.1935 | continuous |
| | $s_t$ (mm) | 2.3 | continuous |
| | $a_d$ (um) | 50.8 | continuous |
| | $a_r$ (mm) | 0.0333 | continuous |
| | $n_r$ | 3 | Integer |
| | $N_d$ | 36 | Integer |
| Finishing | $v_w$ (m/s) | 0.30 | continuous |
| | $s_t$ (mm) | 2.2675 | continuous |
| | $a_d$ (um) | 15.7423 | continuous |
| | $N_d$ | 37 | Integer |

Table 2-7 Optimization results for minimization of grinding cost

| Operation | Process Output | Constrain Value | Grinding Cost ($/pc) | Total Cost ($/pc) |
|---|---|---|---|---|
| Roughing | $P(1)$ (W) | 343 | 0.6807 | 1.3168 |
| | $P(N_d)$ (W) | 400 | | |
| | G ratio | 61.388 | | |
| Finishing | $R_a(1)$ | 0.60 | 0.6361 | |
| | $\sigma_r(1)$ | 390.2 | | |
| | $\sigma_r(N_d)$ | 400 | | |
| | G ratio | 122.2846 | | |

constraints were active in both results. The computational efficiency of Lee's method was expected to be compromised by the time consuming rejection scheme used to handle the constraints. Michalewicz (1996) reported that the rejecting method needed more computational time, and it had effectiveness and stability issues. The rejecting method

will meet difficulty in highly constrained machining problems whose feasible space is small and sparse while randomly generated initial populations are mostly located in infeasible space and a normal genetic operator often yields infeasible offspring.

## 2.6 Conclusion and Discussion

A novel and systematic optimization scheme based on GA for hard turning process planning and optimization has been proposed. The strengths of this Mixed Integer Evolutionary Algorithm (MIEA) are:

The design variables are represented by the natural data types to implement a one-gene-one-variable scheme; excessivly long binary strings are no longer needed in representing the design variables. This natural representation moves GA closer to the problem space in line with the principle of (ES) and (EP). Consequently, different encoding and decoding schemes for different machining problems are no longer needed; efficiency and effectiveness are increased and application to different machining problems becomes easy.

Binary implementation is combined with the floating point implementation to deal with integer (discrete) and continuous design variables respectively and to take advantage of both bit representation of GA and real-valued representation of ES. Adaptive mutation and crossover is designed for integer variables, while non-uniform mutation with uniform crossover is adopted for continuous variables. The number of crossover points automatically increases with the problems' dimension. Tournament selection with elitism

is used as the selection scheme to strive a balance between population diversity and selective pressure.

A new integrated constraint handling method powered by $(\alpha, \mu)-$population initialization is developed. The boundary constraints are handled by an "Even-Excessive-Distribution" Method. The equality and inequality constraints are handled by a new feasible superior, problem independent penalty technique. At least one solution is forced to be feasible in the initial population in order to uniformly distribute the initial population to the whole search space for highly constrained machining problems.

Twelve numerical cases show that the proposed procedure outperforms the other constraint handling methods. The comparison is not really fair due to the different population initialization, the different selection scheme, and the different genetic operator used, but on the other hand the proposed approach in this work as a systematic scheme has shown its great performance. It searches toward not only the feasible direction but also the optimal direction, which is the most promising direction desired. The proposed scheme has also successfully applied to a unified metal cutting problem and a generalized grinding problem. It has shown higher performance and higher computational efficiency than the other methods, such as Powell's unconstrained method with the exterior penalty function and evolutionary strategy (ES).

# CHAPTER III

# HARD TURNING PROCESS MODELS

## 3.1 Introduction

Good process models in hard turning are desired in model-based process planning and optimization. In this chapter, hard turning process models including cutting temperature, 3-D oblique cutting force, tool wear rate and surface integrity (white layer thickness, residual stress profiles and surface roughness) are presented and some associated coefficients are systematically calibrated by experiments.

Average temperatures along rake face and flank face are calculated from three major heat sources: primary heat source from the shear zone, secondly heat source from the friction zone along chip-tool interface, and third heat source from the rubbing zone along workpiece-tool interface.

Total 3-D oblique cutting forces are obtained as the sum of forces due to chip formation and forces due to tool wear. 3-D oblique cutting geometry will be transformed to equivalent 2-D cutting geometry first. Then based on the equivalent 2-D cutting geometry, forces due to chip formation are predicted from the modified Oxley's orthogonal machining theory and forces due to flank wear are computed from the Waldorf's 2-D worn tool force model. Finally 3D oblique cutting force components decompose from total 2-D force components based on the tool geometry and coordinate

transformation. A Johnson-Cook equation is used as workpiece material constitutive equation and its constants are determined from the machining tests.

Tool flank wear is estimated based on the Huang and Liang's (2004a) unified flank wear rate model. The wear volume loss of the tool insert due to three main wear mechanisms in the hard turning: abrasion, adhesion and diffusion are considered and the flank wear rate is modeled according to the relationship between the wear volume loss and the cutting geometry in the 3-D oblique hard turning.

Surface roughness is simply approximated by the Armarego and Brown (1967) model. However white layer formation and residual stress distribution are the products of complex mechanical, thermal and metallurgical processes, and it is non-trivial to develop the comprehensive physical/analytical models for them while modeling with experimentally gained knowledge can be more effective. Due to the complex nature of the inputs (type of coolant, insert grade, insert nose, clearance angle, rake angle, edge preparation, speed, feed, depth of cut, tool flank wear etc.) and outputs (white layer thickness, residual stress distribution), traditional regression curve fitting methods or pure empirical methods are not able to build up the desired relationships between process input and output variables. Artificial neural networks (ANNs) based on non-linear connectivity have emerged as promising technologies to provide an alternative way of modeling complex systems and processes using the experimental or practical knowledge, whose prediction capability could be higher than the traditional regression methods or pure empirical methods. Among many ANNs, back propagation neural network (BPNN) has been selected to model the white layer formation and residual stress distribution due

to its simplicity and its ability to approximate arbitrary nonlinear functions. The models developed based on ANNs are named as the intelligent models in this study in order to distinguish them from the analytical models.

Tool flank wear is one of the most important inputs in predicting the surface integrity information and is a process output itself. Hence a model with hierarchical structure which consists analytical models and BPNN models is required in predicting white layer thickness and residual stress profiles.

Hard turning of hardened AISI 52100 bearing steels has been extensively studied by numerous researchers. Hardened AISI 1053 is also one of the widely used hardened steels; unfortunately little effort has been devoted to study its machinability. Dry turning of hardened AISI 1053 was performed in this study and its associated material properties were identified.

## 3.2 Thermal Models

Cutting temperatures have a controlling influence on the tool wear rate and a significant effect on the machined part's performance. Hence understanding the temperature behavior in machining is important. There are three major heat sources responsible for the conversion of energy into heat in metal cutting as shown in Figure 3-1: the primary heat source (heat source from the shear zone), the secondary heat source (heat source from the friction zone) along the chip-tool interface (tool rake face), and the third rubbing heat source along the workpiece-tool interface (tool flank face).

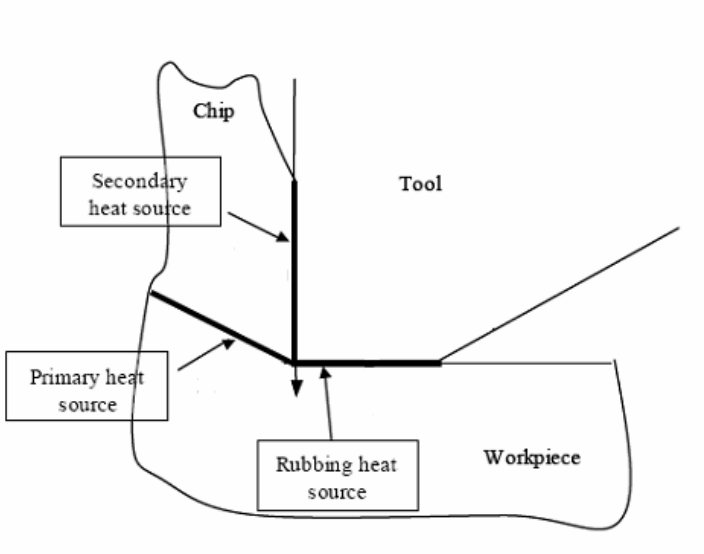


Figure 3-1 Three heat sources in metal cutting (after Huang 2002)

Average temperature along rake face $\bar{T}_{ra}$ can be calculated from those three major heat sources based on the proposed methods from Boothroyd and Oxley (Boothroyd 1963, Boothroyd, *et al.* 1967, Oxley 1989):

$$\bar{T}_{ra} = T_0 + \Delta T_{sz} + \psi \Delta T_M + \Delta T_{VB} \tag{3-1}$$

where $\Delta T_{SZ}$ is the temperature rise due to the primary heat source:

$$\Delta T_{sz} = \frac{(1-\beta)F_s V_s}{\rho C V_c a^* t^*} \tag{3-2}$$

$\Delta T_M$ is the maximum temperature rise in the chip due to the secondary heat source, it can be estimated from the average temperature rise in the chip due to the secondary heat source $\Delta T_c$:

$$\ln\left(\frac{\Delta T_M}{\Delta T_C}\right) = 0.06 - 0.195\delta\left(\frac{R_T t_2}{h}\right)^{1/2} + 0.5\ln\left(\frac{R_T t_2}{h}\right) \tag{3-3}$$

$$\Delta T_c = \frac{F V_{chip}}{\rho C V_c a^* t^*} \tag{3-4}$$

$\Delta T_{VB}$ is the temperature rise due to the third rubbing heat source:

$$\Delta T_{VB} = \frac{\Gamma F_{CW} V_c}{\rho C V_c a^* t^*} \tag{3-5}$$

$F_{CW}$ is the rubbing force along the workpiece-tool interface. $\Gamma$ $(0 < \Gamma \leq 1)$ is the proportion of heat from the third rubbing zone transported by the chip. A value of 0.4 has been used in this study based on the result obtained by Boothroyd (1963).

Average temperature along flank face $\bar{T}_f$ is calculated as a ratio of the average temperature along rake face:

$$\bar{T}_f = \Upsilon \bar{T}_{ra} \tag{3-6}$$

Boothroyd (1963) and Boothroyd *et al.* (1967) showed a ratio of 0.82 to 0.95 (in Kelvin) from experimental measurements in orthogonal cutting of a tubular workpiece. Huang (2002) reported a value of 0.75 to 0.82 (in Kelvin) for various turning cases. A value of 0.80 (in Kelvin) is used in this study.

Figure 3-2 and Figure 3-3 shows the temperature prediction for the typical hard turning process. Hardened AISI 52100 of hardness 60 – 64 HRC and low CBN tools are used in those predictions with the tool geometry: the effective rake angle -25$^o$, the clearance angle 5$^o$ and the nose radius 0.8mm. Figure 3-2 is the predicted average temperatures along the rake face with various cutting speeds for three different depths of cut with fresh tool, where feed rate is fixed at 0.127 mm/rev. Figure 3-3 is the predicted average temperatures along the flank face with various tool flank wear lengths for three different depths of cut, where cutting speed is fixed at 2.287 m/s and feed rate is fixed at 0.1016 mm.

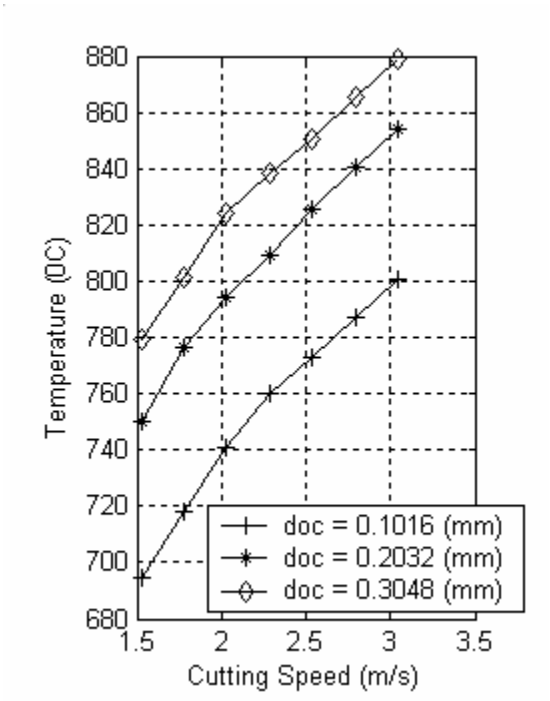


Figure 3-2 Average temperatures along the rake face

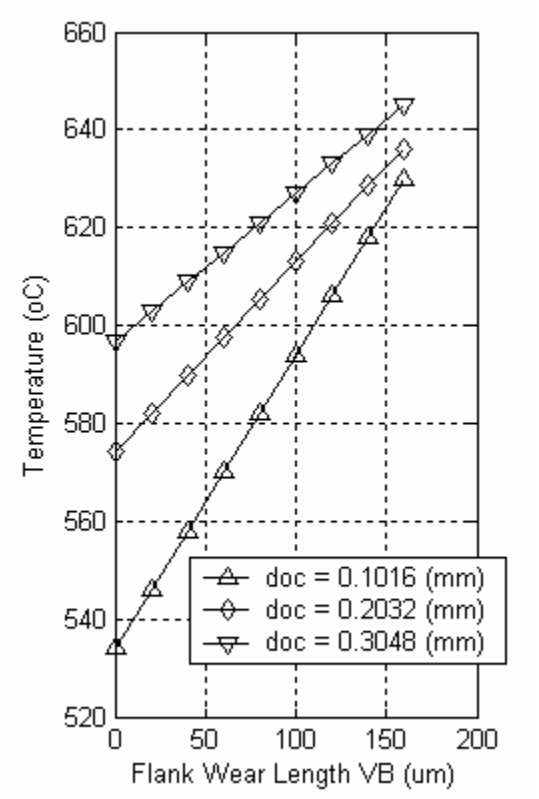


Figure 3-3 Average temperatures along the flank face with the progress of flank wear

## 3.3 Force Models

Force modeling under hard turning conditions is important for thermal modeling, wear rate modeling, chatter prediction, and tool condition monitoring. The hard turning process is normally 3-D oblique cutting with large negative rake angle and large nose radius. The total cutting force generally consists of three components: force due to chip formation, force due to ploughing and force due to sliding (which is the force due to tool wear). Total 3-D oblique cutting forces are estimated as the sum of forces due to chip formation and forces due to tool wear in this study. The magnitude of the plowing

component is usually negligible in comparison with the chip-formation component in turning process.

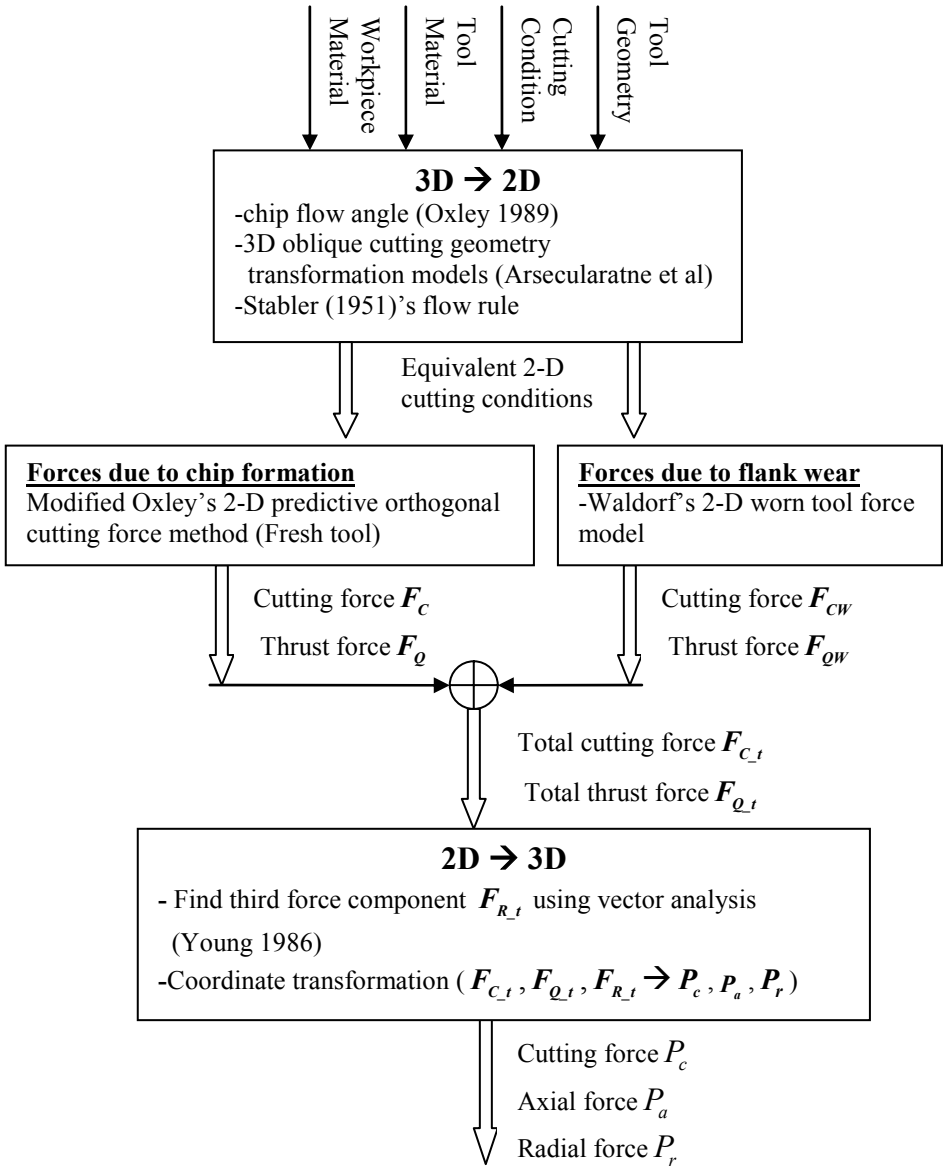


Figure 3-4 The flow chart for 3-D oblique cutting force simulation under hard turning

Figure 3-4 shows the computational procedure for the total 3-D oblique cutting forces under the hard turning condition. Given 3-D tool geometry and cutting conditions together with the known workpiece and tool material properties, 3-D oblique cutting geometry and cutting conditions will be transformed to the equivalent 2-D cutting geometry and cutting conditions, and then forces due to the chip formation and forces due to flank wear will be computed respectively and will be superimposed together to get the total tangential cutting force and thrust cutting force. Finally the total forces in 2-D equivalent cutting geometry will be decomposed to the 3-D cutting forces based on the tool geometry and coordinate transformation. The computation procedures will be detailed as follows.

### 3.3.1 Equivalent 2-D Oblique Cutting Geometry and Condition for 3-D Oblique Cutting

The equivalent 2-D cutting geometry, including the equivalent cutting edge normal rake angle $\alpha_{\mathrm{n}}^{*}$, the equivalent inclination angle $i^{*}$, and the equivalent side cutting edge angle $C_{\mathrm{s}}^{*}$ can be calculated from 3-D oblique cutting geometry transformation models as documented in (Oxley 1989, Arsecularatne *et al.* 1995, Arsecularatne *et al.* 2000):

$$i^{*} = \sin^{-1}(\cos\eta_{0}^{'}\sin i - \sin\eta_{0}^{'}\sin\alpha_{n}\cos i) \tag{3-7}$$

$$\alpha_{n}^{*} = \sin^{-1}\left(\frac{\sec\eta_{0}^{'}\sin i - \sin i^{*}}{\tan\eta_{0}^{'}\cos i^{*}}\right) \tag{3-8}$$

$$C_s^* = C_s + \eta_0 \tag{3-9}$$

The equivalent chip flow angle is estimated based on Stabler's flow rule (Stabler 1951) as in Equation (3-10):

$$\eta_c^* = i^* \tag{3-10}$$

Then the equivalent undeformed chip thickness $t^*$ and width of cut $w^*$ can be calculated by:

$$t^* = f \cos C_s^*, \quad w^* = d / \cos C_s^* \tag{3-11}$$

### 3.3.2 Forces due to Chip Formation

Based on the equivalent 2-D cutting geometry ($\alpha_n^*$, $i^*$ and $C_s^*$) and cutting conditions ($t^*$ and $w^*$), Oxley's predictive 2-D orthogonal cutting force method is modified to predict the tangential cutting force $F_C$ and the thrust cutting force $F_Q$ due to chip formation as documented in APPENDIX B in detail.

Hence the 3-D oblique cutting forces acting in the cutting ($P_c$), axial ($P_a$) and radial ($P_r$) directions for the fresh tool can be calculated respectively from the 2-D orthogonal force components as follows:

$$P_c = F_C, \quad P_a = F_Q \cos C_s^* + F_r \sin C_s^*, \quad P_r = F_Q \sin C_s^* - F_r \cos C_s^* \tag{3-12}$$

where:

$$F_r = \frac{F_C(\sin i^* - \cos i^* \sin \alpha_n^* \tan \eta_c^*) - F_Q \cos \alpha_n^* \tan \eta_c^*}{\sin i^* \sin \alpha_n^* \tan \eta_c^* + \cos i^*} \tag{3-13}$$

### 3.3.3 Forces due to Flank Wear

The force components due to flank wear, that is, the forces due to sliding, are modeled based on the equivalent 2-D cutting geometry as well:

$$F_{CW} = l_c \int_0^{VB} \tau_w(x) dx, \; F_{QW} = l_c \int_0^{VB} \sigma_w(x) dx \tag{3-14}$$

in which $\tau_w(x)$, $\sigma_w(x)$ are computed based on Waldorf's worn tool force model (Waldorf 1996, Waldorf *et al.* 1998) and are detailed in APPENDIX C. $l_c$ is the cutting edge contact length "EFG" as shown in Figure 3-5, which can be calculated as (Huang and Liang 2005):

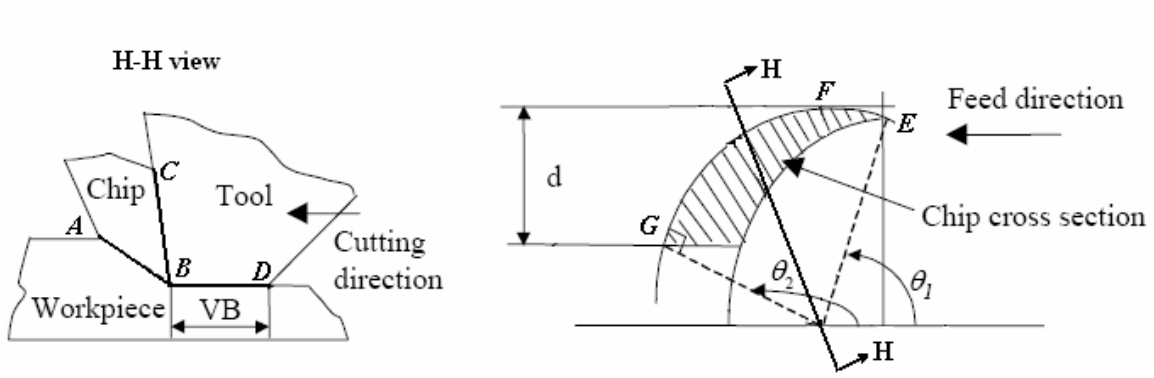


Figure 3-5 Cutting geometry under typical hard turning condition (after Huang 2002)

$$\theta_1 = \cos^{-1}(f/(2R)),\ \ \theta_2 = \pi - \sin^{-1}((R - doc)/R),\ \ l_c = R(\theta_2 - \theta_1) \qquad (3\text{-}15)$$

### 3.3.4 Total 3-D Oblique Forces

The total 2-D orthogonal force components are the summation of the forces due to chip formation when the tool is fresh and the forces due to flank wear, that is:

$$F_{C\_t} = F_C + F_{CW},\ F_{Q\_t} = F_Q + F_{QW} \qquad (3\text{-}16)$$

Thereafter, the total cutting forces acting in the cutting ($P_{c\_t}$), axial ($P_{a\_t}$) and radial ($P_{r\_t}$) directions can be decomposed from the total 2-D orthogonal force components as follows:

$$P_{c\_t} = F_{C\_t},\quad P_{a\_t} = F_{Q\_t}\cos C_s^* + F_{r\_t}\sin C_s^*,\quad P_{r\_t} = F_{Q\_t}\sin C_s^* - F_{r\_t}\cos C_s^* \quad (3\text{-}17)$$

where:

$$F_{r\_t} = \frac{F_{C\_t}(\sin i^* - \cos i^* \sin \alpha_n^* \tan \eta_c^*) - F_{Q\_t} \cos \alpha_n^* \tan \eta_c^*}{\sin i^* \sin \alpha_n^* \tan \eta_c^* + \cos i^*} \tag{3-18}$$

The shear angle and the shear flow stress will be determined from the established force model as well. The other process information, such as heat intensity of the rubbing heat source ( $q_r$ ), and the average stress ( $\bar{\sigma}$ ) along the worn tool face could be computed as in Equation (3-19) and (3-20):

$$q_r = \frac{F_{CW} V_c}{VBl_c} \tag{3-19}$$

$$\bar{\sigma} = \frac{F_{CW}}{VBl_c} \tag{3-20}$$

Based on the estimated cutting forces, the cutting power can be simply obtained as in Equation (3-21):

$$P = P_{c\_t} * V_c \tag{3-21}$$

### 3.3.5 Constitutive Equation of Workpiece Material

The constitutive equation of hardened steels is represented by the Johnson-Cook equation (Johnson and Cook 1983) as in equation (3-22):

$$\sigma = \left(A + B\varepsilon^{n}\right)\left(1 + C\ln\frac{\dot{\varepsilon}}{\dot{\varepsilon}_{o}}\right)\left(1 - \left(\frac{T - T_{r}}{T_{m} - T_{r}}\right)^{m}\right) \tag{3-22}$$

This constitutive model could capture the strain hardening behavior, strain rate effect and softening at high temperature of the hardened steels under the high strain, high strain rate and high temperature machining conditions.

Its constants ( $A$, $B$, $C$, $m$, $n$ ) are determined based on the machining tests by minimizing the least square errors between the predicted and experimental force components for the forces due to chip formation only.

### 3.3.6 Experimental Results

A series of experiments was performed to determine the unknown Johnson-Cook parameters of AISI 1053 with hardness of 58 - 60 HRC and to verify the proposed force models in finish hard turning process.

Dry turning of hardened 1053 was performed on a horizontal lathe (Hardinge T-42) with Kennametal low CBN tool inserts (KB5625). The tool holder was a Kennametal DCLNR – 164C which provides a 5 $^{o}$ side cutting-edge angle, a 5 $^{o}$ end cutting-edge

angle, a negative 5 $^{o}$ back rake angle, and a negative 5 $^{o}$ side rake angle. A kistler 9257B dynamometer was mounted on the tool post to measure the 3-D oblique cutting forces.

Determination of the workpiece material properties

KB5625 (Kennametal CNGA432S0420) has a nose radius of 0.8mm, a chamfer length of 0.1mm, and a negative chamfer angle of 20$^{o}$. Hence the effective rake angle is -25 $^{o}$, and inclination angle is -5 $^{o}$.

Test matrix as shown in Table 3-1 is used to calibrate the unknown constants of the Johnson-Cook Equation ($A$, $B$, $C$, $m$, $n$) for hardened AISI 1053. They are determined by minimizing the least square errors between the measured 3-D cutting forces and predicted 3-D cutting forces for the fresh tool as shown in Equation (3-23):

$$\min\left\{\sqrt{\sum\left[\left(P_{c,m}-P_{c,p}\right)^2+\left(P_{a,m}-P_{a,p}\right)^2+\left(P_{r,m}-P_{r,p}\right)^2\right]}\right\} \tag{3-23}$$

Table 3-1 Calibration test matrix

| | **Speed** (m/s) | **Feed** (mm/rev) | **DOC** (mm) |
|---|---|---|---|
| T1 | 2.033 | 0.076 | 0.127 |
| T2 | 2.033 | 0.127 | 0.127 |
| T3 | 2.541 | 0.076 | 0.127 |
| T4 | 2.541 | 0.127 | 0.127 |

The established force model requires several other physical constants for workpiece and cutting tool material. These are given in Table 3-2.

Table 3-2 Physical properties of workpiece and cutting tool

| | Low PCBN tool (Shatla 2001) | AISI 1053 (HRC 58 - 60) |
|---|---|---|
| Density $(Kg/m^3)$ | 4370.1 | 7870 |
| Thermal conductivity $(W/m \cdot k)$ | 44 | $51.9 - 0.0298T$ |
| Specific heat capacity $(J/Kg \cdot k)$ | 750 | $486 + 0.504T$ |
| $T_m$ $(k)$ | | 1760 |

The resulting Johnson-Cook constants for hardened AISI 1053 are given in Table 3-3.

Table 3-3 Resulting Johnson-Cook constants for hardened AISI 1053

A = 447.6 (MPa)
B = 69.1 (MPa)
n = 0.453
C = 0.030
m = 2.978

Further experiments as shown in Table 3-4 have been conducted to verify the established force model with fresh tool inserts based on the determined Johnson-Cook constants for hardened AISI 1053. The comparisons are shown in Figure 3-6, 3-7 and 3-8.

Table 3-4 Verification test matrix

| | **Speed** (m/s) | **Feed** (mm/rev) | **DOC** (mm) |
|---|---|---|---|
| V1 | 1.524 | 0.102 | 0.102 |
| V2 | 1.524 | 0.152 | 0.152 |
| V3 | 2.287 | 0.051 | 0.102 |
| V4 | 2.287 | 0.102 | 0.152 |
| V5 | 3.049 | 0.051 | 0.152 |
| V6 | 3.049 | 0.152 | 0.102 |

As listed in Table 3-5, the average error for cutting force prediction is 8.2%; that for radial force prediction is 22.7% and that for axial force prediction is 15.4%. Maximum prediction errors up to 21.2%, 44.0% and 32.1% for cutting, radial and axial force respectively occur for test case V3 where feed rate and depth of cut is very small, which are 0.051mm/rev (0.002ipr) and 0.102mm (0.004inch) respectively. Relatively large prediction errors up to 13.2%, 33.1% and 18.1% happen for test case V5, where feed rate is very small, which is 0.051mm/rev (0.002ipr). When the tool with large nose radius and large negative rake angle is used with very small values of feed rate and depth of cut as in test cases V3 and V5, the ploughing effect is rather pronounced and contributes a large portion of the total cutting forces. Unfortunately the force components due to the ploughing effect are not addressed in the established force model.

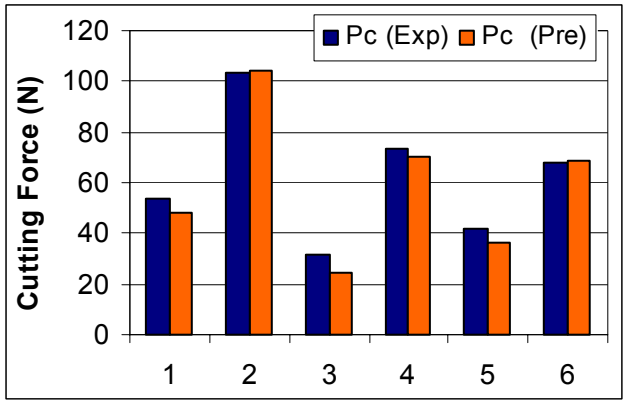


Figure 3-6 Cutting force comparison when turning hardened 1053 steel

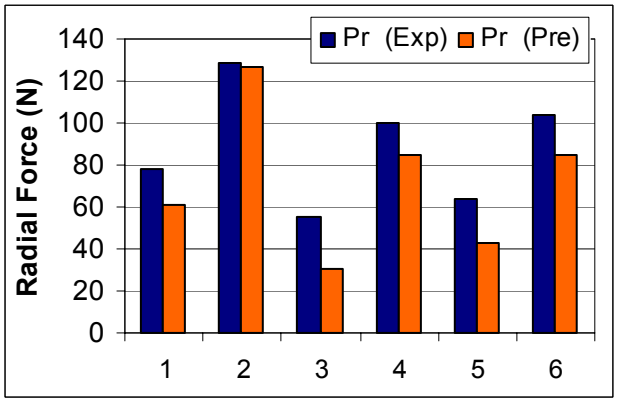


Figure 3-7 Radial force comparison when turning hardened 1053 steel

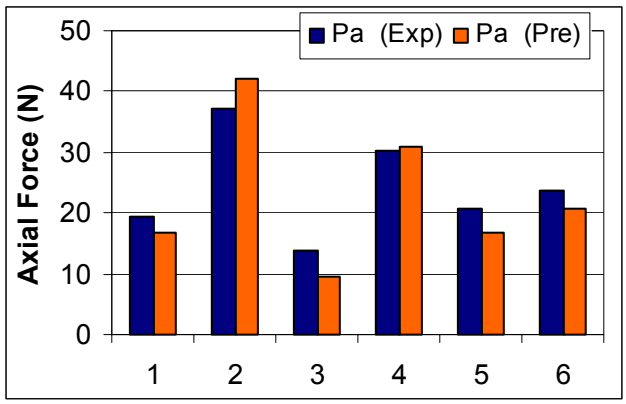


Figure 3-8 Axial force comparison when turning hardened 1053 steel

Table 3-5 Prediction errors for the verification tests

| | **Pc** | **Pr** | **Pa** |
|---|---|---|---|
| | **Error (%)** | **Error (%)** | **Error (%)** |
| V1 | 9.4 | 22.4 | 14.1 |
| V2 | 0.2 | 1.5 | 13.8 |
| V3 | 21.3 | 44.9 | 32.1 |
| V4 | 4.3 | 15.9 | 2.5 |
| V5 | 13.2 | 33.2 | 18.2 |
| V6 | 1.2 | 18.7 | 11.9 |
| Average | 8.3 | 22.7 | 15.4 |

Validation for the total cutting forces

Total cutting forces with the progress of flank wear were measured for cutting conditions of: cutting velocity = 2.287 m/s, feed rate = 0.051 mm/rev, and depth of cut = 0.1016 mm. KB5625 (Kennametal CNGA434S0420) is used which has nose radius of 1.6 mm, chamfer length of 0.1mm, and negative chamfer angle of $20^{o}$. Tool wear is

measured by a Zygo NewView 200 microscope. The total cutting forces including forces due to the chip formation and forces due to the flank wear. The estimated cutting, radial and axial forces are 25.4N, 32.4N, 6.8N respectively with the fresh tool. And the measured and predicted total cutting forces with the progress of flank wear are shown in Figure 3-9, 3-10 and 3-11 where experimental data are given by circles and model predictions by lines.

Another case is shown in Figure 3-12 with the same tool geometry and cutting conditions of: cutting velocity = 1.601 m/s, feed rate = 0.127 mm/rev, and depth of cut = 0.1016 mm. The estimated cutting, radial and axial forces are 63N, 82N, 15N respectively with the fresh tool.

Overall, the developed model gives reasonably good results. However the forces at larger flank wear are all underestimated. One of the error sources could be accumulated from the tool wear measurements.

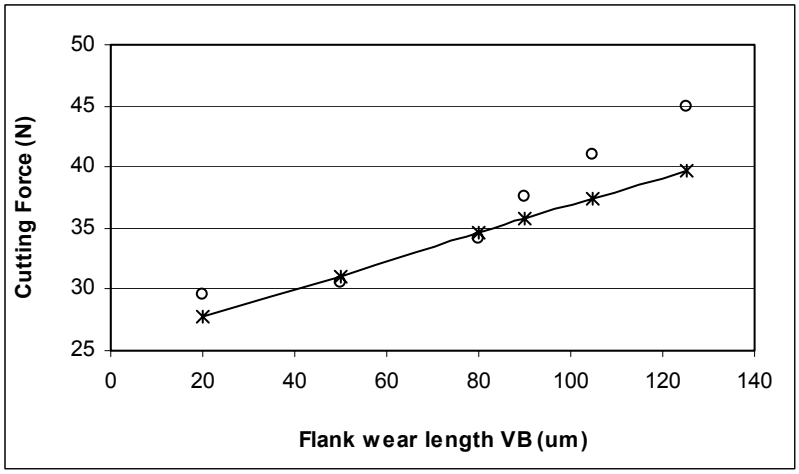


Figure 3-9 Total tangential cutting forces with the progress of flank wear (cutting velocity = 2.287 m/s, feed rate = 0.051 mm/rev, and depth of cut = 0.1016 mm)

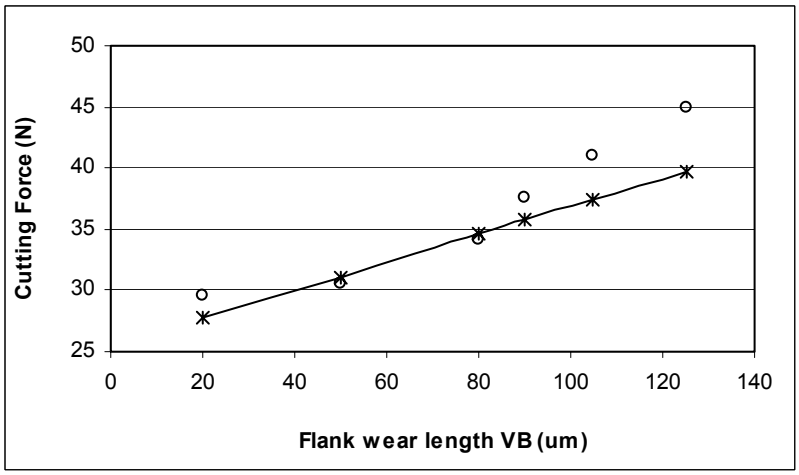


Figure 3-10 Total radial forces with the progress of flank wear (cutting velocity = 2.287 m/s, feed rate = 0.051 mm/rev, and depth of cut = 0.1016 mm)

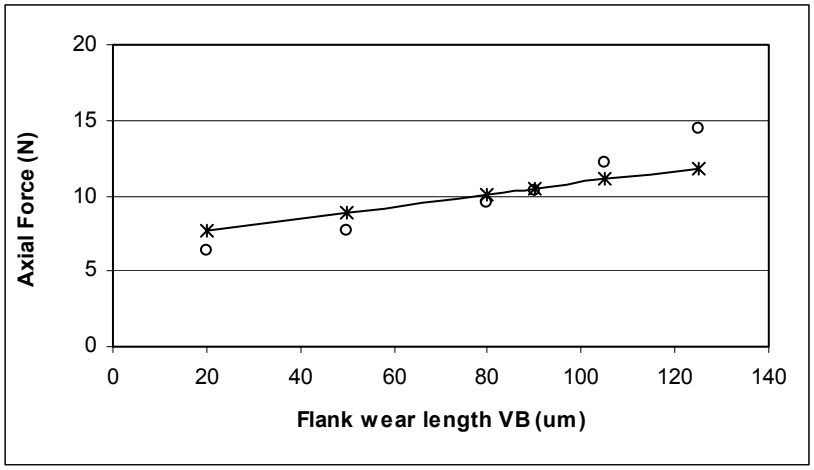


Figure 3-11 Total axial forces with the progress of flank wear (cutting velocity = 2.287 m/s, feed rate = 0.051 mm/rev, and depth of cut = 0.1016 mm)

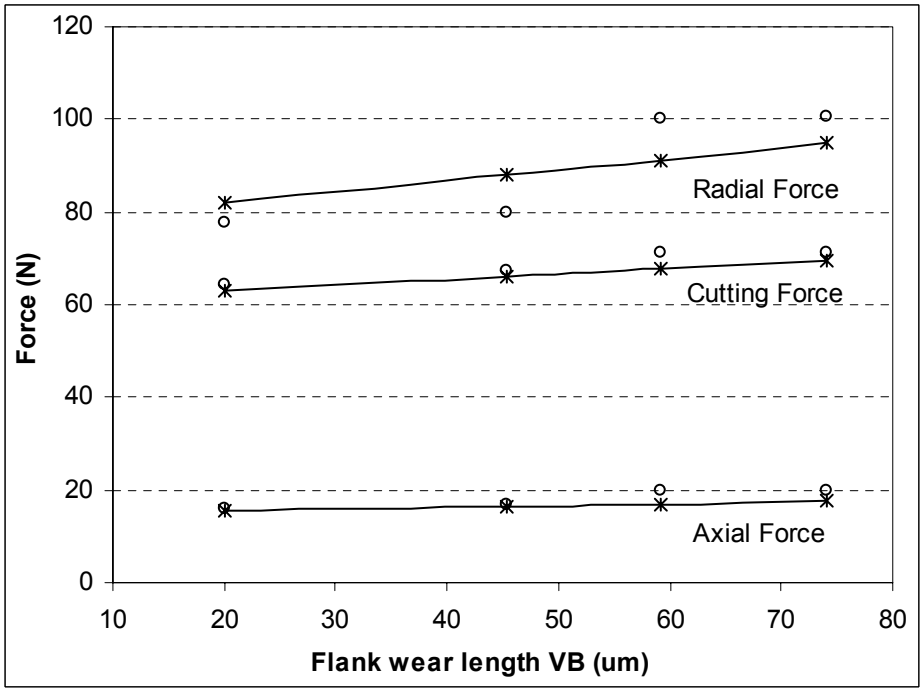


Figure 3-12 Total cutting forces with the progress of flank wear (cutting velocity = 1.601 m/s, feed rate = 0.127 mm/rev, and depth of cut = 0.1016 mm)

## 3.4 Tool Wear Models

### 3.4.1 Computational Procedure

With the process information predicted by the thermal model and overall cutting force model, the tool flank wear rate can be estimated for every specific tool flank wear length as Equation (3-24) from Huang and Liang (2004a). The wear volume loss of the tool insert due to three main wear mechanisms in the hard turning: abrasion, adhesion and diffusion are considered and the flank wear rate is modeled according to the PCBN tool geometry.

$$\frac{dVB}{dt} = \frac{(\cot\gamma + \tan\alpha)R}{VB(R - \tan\gamma)} \left\{ K_{abrasion} K \left( \frac{H_a^{\,n-1}}{H_t^{\,n}} \right) V_c VB\bar{\sigma} + K_{adhesion} e^{a\bar{T}_f} V_c \bar{\sigma} + K_{diff} \sqrt{V_c VB}\, e^{-\frac{K_Q}{\bar{T}_f + 273}} \right\} \tag{3-24}$$

Based on the flank wear rate model, flank wear length can be predicted as the initial value problem as in Equation (3-25). Initial flank wear length after the break-in period is assumed to be 10 $\mu m$.

$$VB_{n+1} = VB_n + \frac{dVB}{dt}\left( VB_n, \bar{T}_n, \bar{\sigma}_n, \text{cutting condition, tool geometry} \right)\Delta t \tag{3-25}$$

Figure 3-13 shows a unified approach for flank wear prediction. Knowing the tool and workpiece material properties (including Johnson-Cook constants and the calibrated wear coefficients), cutting condition, and tool geometry; process information (including shear angle, the shear flow stress, the normal stress, the rubbing heat source, average cutting temperature along flank face, etc) can be predicted from the established thermal and force models. With all this information, flank wear rate can be estimated based on the wear rate model as Equation (3-24) and new flank wear length can be predicted after a time interval as Equation (3-25). Non-uniform time steps should be applied to compensate non-uniform wear rate during the whole tool life. Inasmuch as the new flank wear length will be fed back to the thermal and force models to update the process information due to the progression of the tool wear, a new wear rate can be estimated based on the updated process information and new flank wear length. The iteration goes on until the end of the cutting to get a final flank wear length.

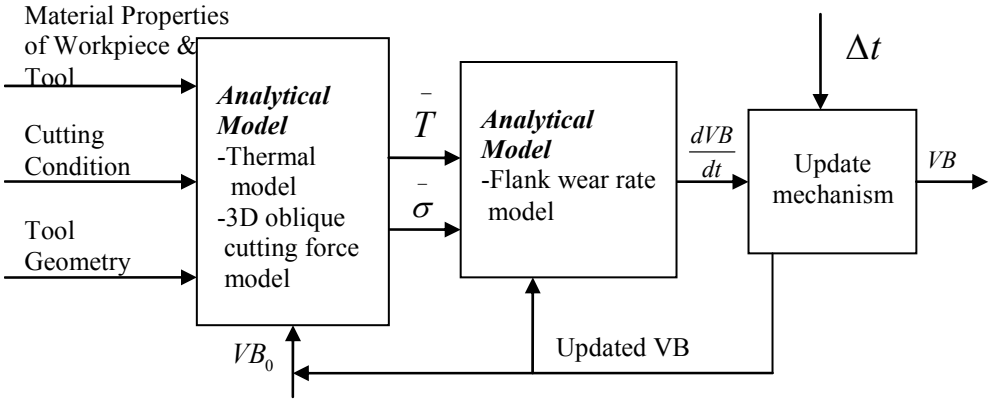


Figure 3-13 The unified approach for the flank wear prediction

### 3.4.2 Calibration for Wear Coefficients

The coefficients of the wear rate model ($K_{abrasion}$, $K_{adhesion}$, $K_{diff}$, $a$, $K_Q$) are not general and should be determined for any workpiece and tool insert combination. They can be calibrated from the experiment by minimizing the least square errors between the predicted and measured tool wear data.

Three cutting tests as shown in Table 3-6 are performed to calibrate the unknown wear coefficients for hardened AISI 1053 with hardness 58 – 60 HRC and Kennametal low CBN tool insert KB5625. KB5625 tool inserts with geometry specified as CNGA432S0420, CNGA433S0420 and CNGA434S0420 were used for test case 1, 2 and 3 respectively. All three inserts have -20$^o$ and 0.1mm wide edge chamfer with different tool nose radius of 0.8mm, 1.2mm and 1.6mm. The tool holder was a Kennametal DCLNR – 164C. Turning without cutting fluid was performed on a horizontal lathe (Hardinge T-42). The flank wear progressions are measured at each test case with a Zygo NewView 200 optical microscope.

Table 3-6 Calibration cutting tests for wear coefficient calibration

| | Tool Geometry | | Cutting Condition | | |
|---|---|---|---|---|---|
| | Chamfer angle | Insert nose (mm) | Cutting speed (m/s) | Feed rate (mm/rev) | Depth of cut (mm) |
| 1 | 20 | 0.8 | 3.05 | 0.102 | 0.152 |
| 2 | 20 | 1.2 | 1.52 | 0.152 | 0.203 |
| 3 | 20 | 1.6 | 2.29 | 0.051 | 0.102 |

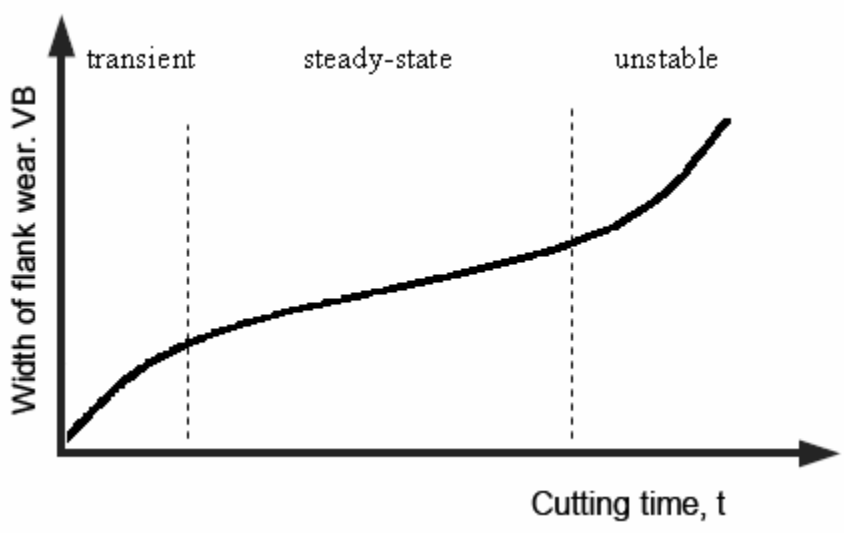


Figure 3-14 A typical curve of flank wear progression with the cutting time

The unknown coefficients of the flank wear rate model are determined by minimizing the least square errors between the measured wear rates and predicted wear rates at the different flank wear lengths as in Equation (3-26). Figure 3-14 shows a typical curve of flank wear progression with cutting time. There are three stages of the tool wear behavior: transient, steady state and unstable. In the transient stage, wear rate is relatively high. In the steady state, wear rate becomes approximately constant. And in the unstable stage, wear rate rises abruptly where temperature at the trailing end of the wear land reaches the thermal softening point of the workpiece material (Shaw 2002). In finish hard turning, the tool usually fails before the unstable stage due to the chipping or broken conditions. The wear data collected in the transient period could vary quite a lot and those in the steady state are more repeatable. Hence only the wear rate data in the steady state are used to calibrate the wear coefficients in this study.

$$\min\left\{\sqrt{\sum\left[\left(\frac{dVB}{dt}\right)_{VB,m}-\left(\frac{dVB}{dt}\right)_{VB,p}\right]^2}\right\} \tag{3-26}$$

The calibrated wear coefficients for hardened AISI 1053 with KB5625 tool are listed in Table 3-7.

Table 3-7 Calibrated wear coefficients

| | |
|---|---|
| $K_{abrasion}$ | 2.2638e-8 |
| $K_{adhesion}$ | 8.3046e-15 |
| $K_{diff}$ | 1.9580e+7 |
| $a$ | 2.5385e-3 |
| $K_Q$ | 20304 |

The predicted flank wear progressions and wear rates (only wear rate values on steady state are listed) are compared with the measured ones based on the calibrated wear coefficients for test case 1, 2, and 3 in Figure 3-15, where triangular markers represent the measurements and solid lines represent the predictions.

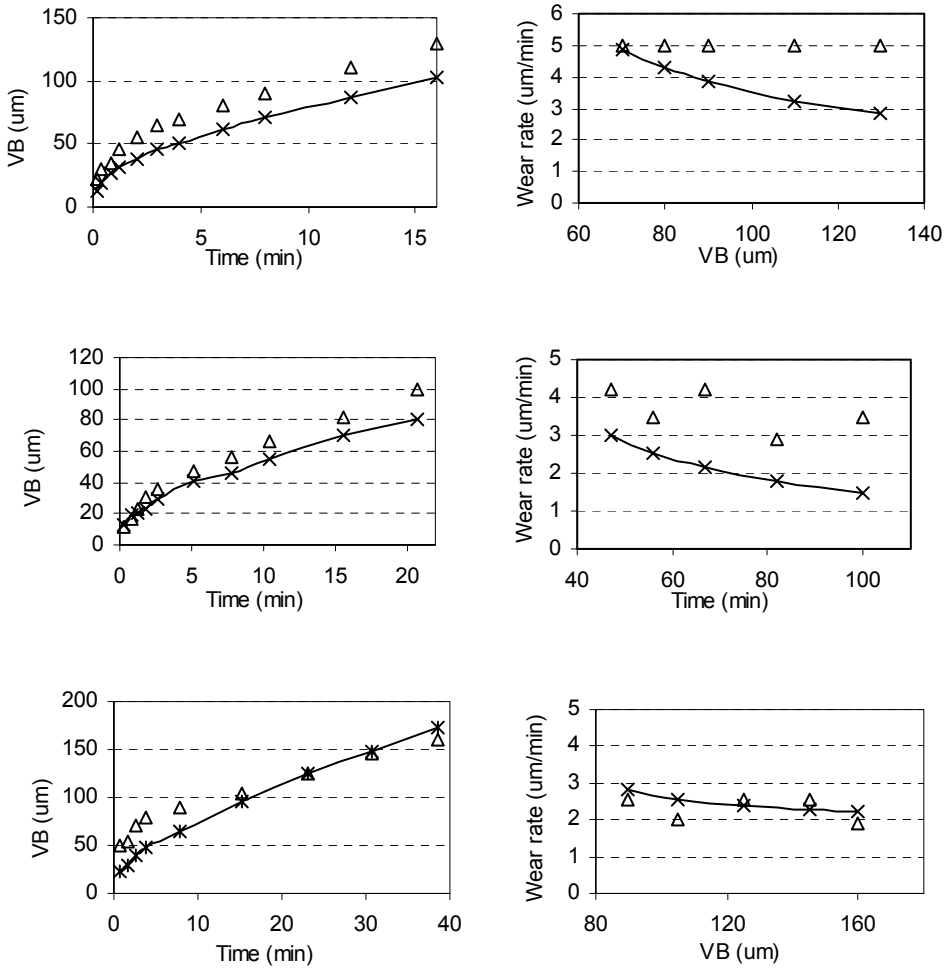


Figure 3-15 The comparison of measured and predicted flank wear and wear rate for test case 1, 2, and 3 (from top to bottom) based on the calibrated wear coefficients

## 3.5 Surface Integrity Models

### 3.5.1 Surface Roughness

In most hard turning applications, cutting takes place only along the tool nose radius, hence the surface roughness ( $Ra$ ) equation from (Armarego and Brown 1967) is adopted:

$$Ra \approx \frac{f^2}{32R} \tag{3-27}$$

Dawson (2002) proved its validity in predicting surface roughness during hard turning of AISI 52100 in his experimental work. Additionally, it is assumed that the surface roughness will not deteriorate with the progress of the tool wear.

### 3.5.2 White Layer Formation and Residual Stress Distribution

Experimental data for white layer formation and residual stress distribution from the industrial site (Delphi Corporation) were used in this work to establish the BPNN models. In this section, back propagation neural network will be introduced first, and then the details of the experimental procedures in the industrial site and modeling schemes for both white layer thickness and residual stress profile prediction are presented. Prediction results are discussed and compared with the experimental results. Finally, a hierarchical modeling scheme needed in predicting surface integrity information is illustrated.

Back propagation neural network (BPNN)

The back propagation algorithm as a learning procedure executes the model training equations based on iterative processes, and thus can be easily implemented on a computer (Kartalopoulos 1996).

BPNN with biases, an input layer, a sigmoid hidden layer, and a linear output layer are capable of approximating any function with a finite number of discontinuities (Mathworks, 2002). Hence a general topology of the network including an input layer (the inputs to the network), a hidden layer with sigmoid transfer function and an output layer (the outputs from the network) with linear transfer function as shown in Figure 3-16 is selected in this study. $f1$ represents a sigmoid transfer function and $f2$ represents a linear transfer function. This general topology has $R$ inputs (input neurons), $S^1$ neurons in the hidden layer and $S^2$ output (output neurons). $w^1_{i,j}$ are the connection weights between input layer and hidden layer and $w^2_{i,j}$ are the connection weights between hidden layer and output layer. $b^1_j$ and $b^2_j$ are the bias for the first and second layers, which are set as zero in this study. $p_{1,}\ p_2 ... p_R$ are the $R$ inputs. Here the superscript represents the layer number and the subscript represents the neuron number.

The output from the neuron $j$ in the hidden layer is:

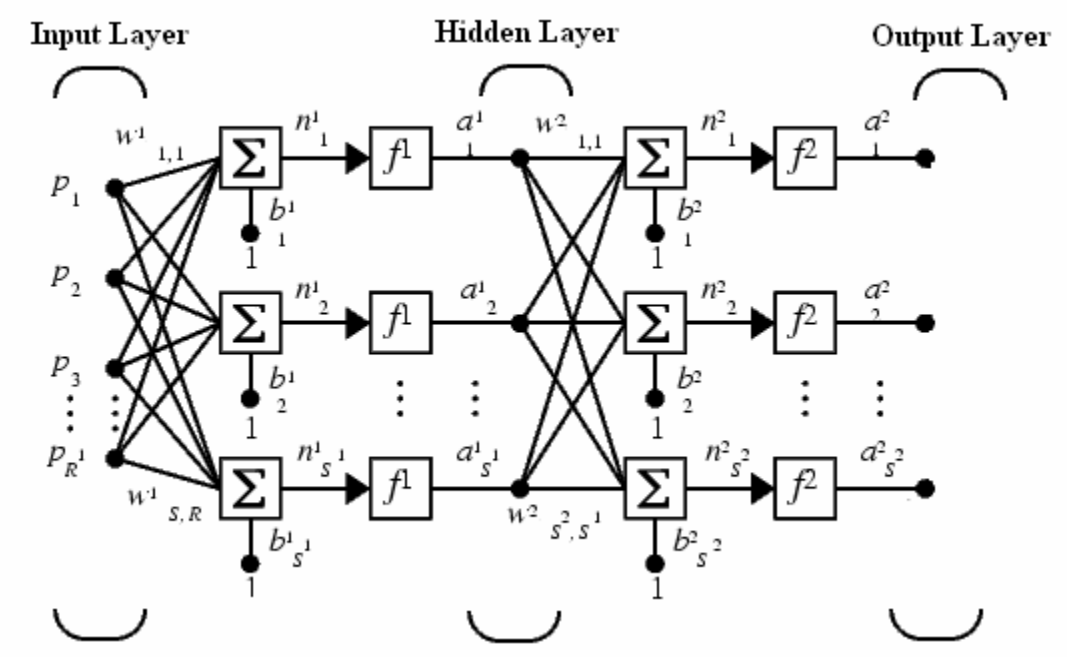


Figure 3-16 A general topology of BPNN with input layer, one hidden layer and output layer (after Mathworks 2002)

$$a_j^1 = f_1\left(n_j^1\right), \quad j = 1, 2...S^1 \tag{3-28}$$

where $$n_j^1 = \sum_{i=1}^{R} w_{i,j}^1 p_i + b_j^1, \quad j = 1, 2...S^1$$

And output j from the output layer is:

$$a_j^2 = f_2\left(n_j^2\right), \quad j = 1, 2...S^2 \tag{3-29}$$

$$\text{where} \quad n_j^2 = \sum_{i=1}^{S^1} w_{i,j}^2 a_i^1 + b_j^2, \quad j = 1, 2 \ldots S^2$$

$a_j^2$ are the actual outputs from the BPNN. $n_j^1$ and $n_j^2$ are defined as the potentials of neuron j at the first and second layer respectively.

The connection weights: $w_{i,j}^1$ and $w_{i,j}^2$ and the biases $b_j^1$ and $b_j^2$ (if applied) are randomly generated initially, hence the actual output from BPNN will be very far from the desired output. Those connection weights and biases will be updated during the BNPP training session in order to achieve the most desirable output from the network, which is also referred to the learning process (biases are set as zero in this study).

During the model training session, a pair of sample patterns is applied: $\left(X_k, T_k\right)$, where $X_k$ is the input pattern and $T_k$ the target/desired output pattern. They can be represented as:

$$X_k = \begin{bmatrix} p_1(k) \\ . \\ . \\ . \\ p_R(k) \end{bmatrix}, \quad T_k = \begin{bmatrix} t_1(k) \\ . \\ . \\ . \\ t_{S^2}(k) \end{bmatrix}$$

The input pattern is presented to the first layer (input layer) and is processed to the hidden layer by a linear combination followed with a sigmoid transfer function to produce an output which in turn becomes an input to the neurons of output layer to obtain

the actual output. The difference between the actual output and the desired output yields an error signal. This error signal depends on the connection weights and biases used in the network layers. The main purpose of the learning process is to minimize this error by updating the values of those weights. The algorithm recalculates the weights at the last layer and continues computing the error and updating weights moving backward, toward the input layer, until the input layer is reached (Back-Propagation Learning). The training for all input-output patterns will be repeated until the error between the actual output from the neural network and the desired output diminishes to a specified bound or other stopping criteria are met.

The weights of BPNN are updated based on a gradient descent algorithm, as in Equation (3-27). The other standard optimization techniques have been used in BPNN as well, such as conjugate gradient and Newton methods.

$$\Delta w_{ij}^{q} = -\lambda \frac{\partial E}{\partial w_{ij}^{q}} \tag{3-30}$$

Where $q = 1, 2$ for the topology used in this study. $\lambda$ is the learning rate with value $0 < \lambda < 1$. $E$ is the error function, which is defined as in Equation (3-31) for a pattern $(X_k, T_k)$:

$$E(k) = \frac{1}{2} \sum_{r=1}^{S^2} (a_r^2 - t_r(k))^2 \tag{3-31}$$

Hence the weights could be updated based on the partial derivative of the error function, which can be analytically obtained by the generalized chain rule as detailed below:

$$\frac{\partial E}{\partial w_{ij}^q} = \frac{\partial E}{\partial n_j^q} \frac{\partial n_j^q}{\partial w_{ij}^q} \tag{3-32}$$

Substitute Equation (3-32) back to the Equation (3-30):

$$\Delta w_{ij}^q = -\lambda \frac{\partial E}{\partial n_j^q} \frac{\partial n_j^q}{\partial w_{ij}^q} \tag{3-33}$$

Where the first part as in Equation (3-34) is defined as the error signal:

$$\psi_j^q = -\frac{\partial E}{\partial n_j^q} \tag{3-34}$$

The second part gives:

$$\frac{\partial n_j^q}{\partial w_{ij}^q} = \frac{\partial}{\partial w_{ij}^q} \left( \sum_{r=1}^{k^{(q-1)}} w_{rj}^q a_r^{(q-1)} \right) = a_i^{(q-1)} \tag{3-35}$$

The error term can be computed using the chain rule:

$$\psi_j^q = -\frac{\partial E}{\partial a_j^q}\frac{\partial a_j^q}{\partial n_j^q} \tag{3-36}$$

As $a_j^q = f_q(n_j^q)$, the second term of $\psi_j^{(q)}$ gives:

$$\frac{\partial a_j^q}{\partial n_j^q} = f_q\,'(n_j^q) \tag{3-37}$$

The first term $\frac{\partial E}{\partial a_j^q}$ has two possible computations based on the given topology in this study:

$\underline{q = 2}$

$$\frac{\partial E}{\partial a_j^2} = \frac{\partial}{\partial a_j^2}\left(\frac{1}{2}\sum_{r=1}^{S^2}(a_r^2 - t_r(k))^2\right) = a_j^2 - t_j(k) \tag{3-38}$$

Then:

$$\psi_j^2 = (t_j(k) - a_j^2) f_2\,'(n_j^2) \tag{3-39}$$

Hence:

$$\Delta w_{ij}^2 = \lambda(t_j(k) - a_j^2) f_2\,'(n_j^2) a_i^1 \tag{3-40}$$

$q = 1$

In order to use the error terms of layer $q = 2$, we can write:

$$\begin{aligned}\frac{\partial E}{\partial a_j^1} &= \sum_{r=1}^{S^2} \frac{\partial E}{\partial n_r^2} \frac{\partial n_r^2}{\partial a_j^1} \\ &= \sum_{r=1}^{S^2} \frac{\partial E}{\partial n_r^2} \frac{\partial}{\partial a_j^1} \left(\sum_{l=1}^{S^1} w_{lr}^2 a_l^{(1)}\right) \\ &= -\sum_{r=1}^{S^2} \psi_r^2 w_{jr}^2\end{aligned} \tag{3-41}$$

Then,

$$\psi_j^1 = \left(\sum_{r=1}^{S^2} \psi_r^2 W_{jr}^2\right) f_1'(a_j^1) \tag{3-42}$$

And,

$$\Delta w_{ij}^{(1)} = \lambda \left(\sum_{r=1}^{S^2} \psi_r^{(2)} w_{jr}^{(2)}\right) f_1'(n_j^{(1)}) p_i(k) \tag{3-43}$$

Hence, the connection weights will be updated based on Equation (3-40) and (3-43). The number of neurons in the hidden layer and the value of the learning rate are selected in order to minimize the model's training and verification error as in equation (3-44):

$$E(k)=\frac{1}{2}\left( w_1\sum_{r=1}^{N_v}(X_r(v)-T_r(v))^2+w_2\sum_{r=1}^{N_t}(X_r(t)-T_r(t))^2 \right) \quad (3\text{-}44)$$

White layer formation

*Experimental Procedure*

Inner Diameter (ID) bore finish turning of inner rings was carried out in a vertical turning center on hardened AISI 52100 bearing steel with hardness of HRC 60 to 62. The bore diameter was 41 mm and length was 15 mm. The depth of cut was fixed to be 0.25 mm. There are five main factors that could drastically affect the white layer formation in finish hard turning: 1 Insert grade 2 tool geometry, including rake angle, clearance angle, nose radius and edge preparation (chamfer length and angle for chamfered tool and hone radius for honed tool); 3 cutting conditions, including cutting speed, feed rate and depth of cut; 4 tool wear progression; 5 type of cooling method. Consequently, eight factors including type of cooling method (two levels, represented as A1 and A2), insert grade (three levels, represented as B1, B2 and B3), insert nose (three levels, represented as C1, C2 and C3), clearance angle (three levels, represented as D1, D2 and D3), rake angle (two levels, represented as E1 and E2), edge preparation (three levels, represented as F1, F2 and F3), cutting speed (three levels, represented as G1, G2 and G3, where G1<G2<G3), and feed rate (three levels, represented as H1, H2 and H3, where H1<H2<H3), are selected as control factors and tool wear is considered as a noise factor at two levels (fresh and worn). L18 ($2^1 3^7$) orthogonal matrix is used as experimental

Table 3-8 Experimental design matrix (L18)

| L18 | | Type of coolant | Insert grade | Insert nose | Clearance angle | Back rake angle | Chamfer angle | Speed (SFM) | Feed (in/rev) | Tool Flank wear (um) |
|---|---|---|---|---|---|---|---|---|---|---|
| Factors | | 1 | 2 | 3 | 4 | 5 | 6 | 7 | 8 | 9 |
| 1 | F | A1 | B1 | C1 | D1 | E1 | F1 | G1 | H1 | 10 |
| 2 | W | A1 | B1 | C1 | D1 | E1 | F1 | G1 | H1 | 261.9 |
| 3 | F | A1 | B1 | C2 | D2 | E2 | F2 | G2 | H2 | 10 |
| 4 | W | A1 | B1 | C2 | D2 | E2 | F2 | G2 | H2 | 445.4 |
| 5 | F | A1 | B1 | C3 | D3 | E1 | F3 | G3 | H3 | 10 |
| 6 | W | A1 | B1 | C3 | D3 | E1 | F3 | G3 | H3 | 339.4 |
| 7 | F | A1 | B2 | C1 | D1 | E2 | F2 | G3 | H3 | 10 |
| 8 | W | A1 | B2 | C1 | D1 | E2 | F2 | G3 | H3 | 480.8 |
| 9 | F | A1 | B2 | C2 | D2 | E1 | F3 | G1 | H1 | 10 |
| 10 | W | A1 | B2 | C2 | D2 | E1 | F3 | G1 | H1 | 397.8 |
| 11 | F | A1 | B2 | C3 | D3 | E1 | F1 | G2 | H2 | 10 |
| 12 | W | A1 | B2 | C3 | D3 | E1 | F1 | G2 | H2 | 397.2 |
| 13 | F | A1 | B3 | C1 | D2 | E1 | F3 | G2 | H3 | 10 |
| 14 | W | A1 | B3 | C1 | D2 | E1 | F3 | G2 | H3 | 386.9 |
| 15 | F | A1 | B3 | C2 | D3 | E2 | F1 | G3 | H1 | 10 |
| 16 | W | A1 | B3 | C2 | D3 | E2 | F1 | G3 | H1 | 558 |
| 17 | F | A1 | B3 | C3 | D1 | E1 | F2 | G1 | H2 | 10 |
| 18 | W | A1 | B3 | C3 | D1 | E1 | F2 | G1 | H2 | 308.7 |
| 19 | F | A2 | B1 | C1 | D3 | E1 | F2 | G2 | H1 | 10 |
| 20 | W | A2 | B1 | C1 | D3 | E1 | F2 | G2 | H1 | 486.8 |
| 21 | F | A2 | B1 | C2 | D1 | E1 | F3 | G3 | H2 | 10 |
| 22 | W | A2 | B1 | C2 | D1 | E1 | F3 | G3 | H2 | 455.6 |
| 23 | F | A2 | B1 | C3 | D2 | E2 | F1 | G1 | H3 | 10 |
| 24 | W | A2 | B1 | C3 | D2 | E2 | F1 | G1 | H3 | 340.7 |
| 25 | F | A2 | B2 | C1 | D2 | E1 | F1 | G3 | H2 | 10 |
| 26 | W | A2 | B2 | C1 | D2 | E1 | F1 | G3 | H2 | 570.2 |
| 27 | F | A2 | B2 | C2 | D3 | E1 | F2 | G1 | H3 | 10 |
| 28 | W | A2 | B2 | C2 | D3 | E1 | F2 | G1 | H3 | 287.9 |
| 29 | F | A2 | B2 | C3 | D1 | E2 | F3 | G2 | H1 | 10 |
| 30 | W | A2 | B2 | C3 | D1 | E2 | F3 | G2 | H1 | 527.8 |
| 31 | F | A2 | B3 | C1 | D3 | E2 | F3 | G1 | H2 | 10 |
| 32 | W | A2 | B3 | C1 | D3 | E2 | F3 | G1 | H2 | 447.6 |
| 33 | F | A2 | B3 | C2 | D1 | E1 | F1 | G2 | H3 | 10 |
| 34 | W | A2 | B3 | C2 | D1 | E1 | F1 | G2 | H3 | 491.9 |
| 35 | F | A2 | B3 | C3 | D2 | E1 | F2 | G3 | H1 | 10 |
| 36 | W | A2 | B3 | C3 | D2 | E1 | F2 | G3 | H1 | 1113.8 |

Table 3-9 Confirmation run

| Confirmation Run | | Type of coolant | Insert grade | Insert nose | Clearance angle | Back rake angle | Chamfer angle | Speed (SFM) | Feed (in/rev) | Tool Flank wear (um) |
|---|---|---|---|---|---|---|---|---|---|---|
| Factors | | 1 | 2 | 3 | 4 | 5 | 6 | 7 | 8 | 9 |
| 1 | F | A1 | B1 | C3 | D1 | E1 | F1 | G1 | H3 | 10 |
| 2 | W | A1 | B1 | C3 | D1 | E1 | F1 | G1 | H3 | 228.7 |
| 3 | F | A1 | B3 | C3 | D1 | E1 | F2 | G1 | H3 | 10 |
| 4 | W | A1 | B3 | C3 | D1 | E1 | F2 | G1 | H3 | 206.1 |

Where: "F" means fresh tool and "W" means Worn tool

layout based on Taguchi Method as shown in Table 3-8. Additional two tests were carried out as confirmation runs/validation cases as in Table 3-9.

There are a total of 20 runs. In each run, 100 pieces were cut with 5 paths. White layer thickness was measured after 1st and 500th cuts using optical microscope and tool wear was measured after 500th cut using a SmartScope Flash video gage. Tool flank wear VB = 10 μm was assumed after the 1st cut. The machined surface in each test is sectioned, mounded, polished and etched in order to reveal the microstructure for white layer measurement. The thickness of the white layer is not uniform and its depth was measured at several points along the machined surface to get an average value.

*Modeling Scheme*

A general topology structure with input layer, one hidden layer, and the output layer as stated in previous section is used in this model. There are nine inputs $X = \{x_1, x_2, x_3, x_4, x_5, x_6, x_7, x_8, x_9\}$ to represent cooling method, insert grade, insert

nose radius, clearance angle, rake angle, edge preparation, cutting speed, feed rate and tool flank wear and one outputs $O = \{o_1\}$ to represent white layer thickness (WL). All inputs and outputs need to be normalized within (-1, +1) to facilitate the convergence. There are 36 training sample patterns and 4 verification sample patterns.

First, the initial connection weights will be generated randomly, and then BPNN will be trained with 36 experimental data (input-output pattern) to update the connection weights to achieve the desired output. After the system has been successfully trained, the final weights will be established and stored. Then, the established model will be verified by the remaining 4 verification data to check its generalization capability.

*Results and Analysis*

The actual output from the established BPNN model for the training samples (Experiment 1 to 18) and the verification samples (Experiment 19 – 20) of worn tools are shown in Figure 3-17, where the results from linear regression are included as well for comparison. The overall prediction including training data sets and verification data sets have 12.4% error for intelligent model and 24.5% error for linear regression model. Hence the intelligent model based on BPNN achieves higher performance than the traditional linear regression method.

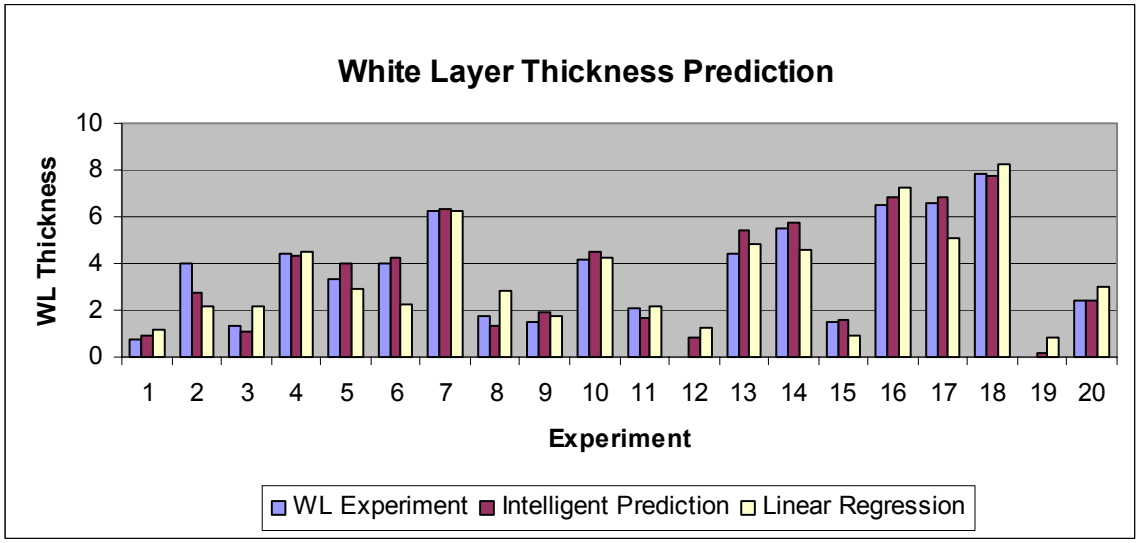


Figure 3-17 Comparison between the experimental and prediction results

*White Layer Thickness Prediction Toolbox*

Based on the established intelligent model, a white layer thickness prediction toolbox has been built for future predictions. Its interface is shown in Figure 3-18. Both "Linear regression" and "Intelligent prediction" methods have been integrated in this toolbox. Any combination of "Type of Coolant", "Insert Grade", "Nose Radius", "Clearance Angle", "Rake Angle", "Tool Strength", "Speed" "Feed" and "Flank wear length" can be selected to predict the possible white layer thickness. When linked to the database where new experimental or practical data are stored, the BPNN model can be retrained based on the new available data to improve its prediction fidelity.

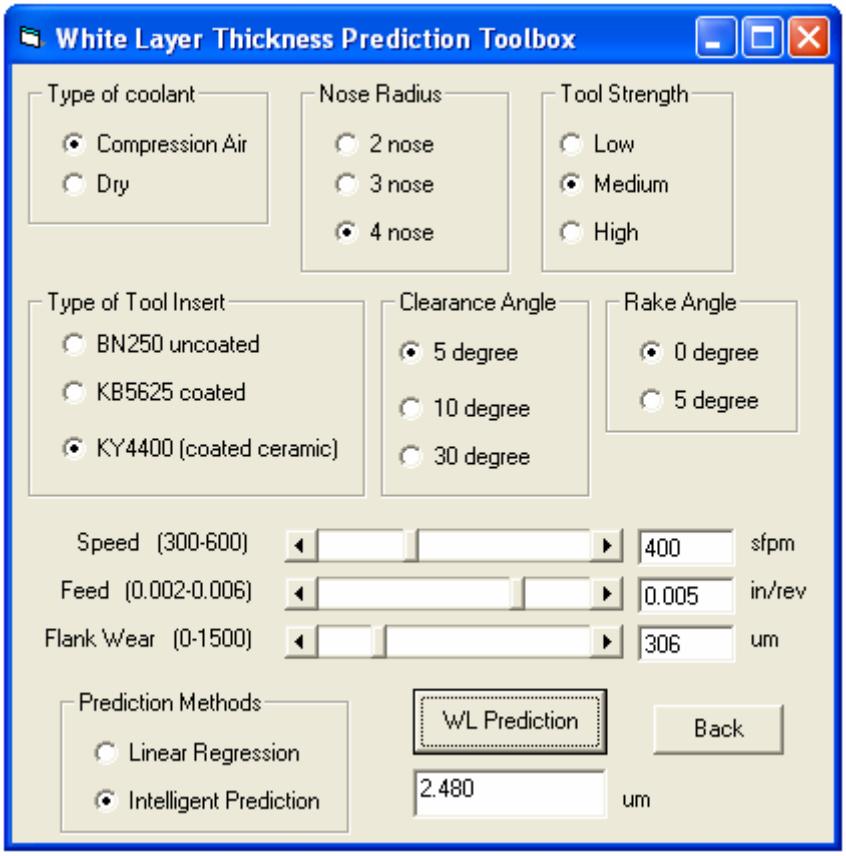


Figure 3-18 White layer thickness prediction toolbox

Residual stress distribution

*Experimental Procedure*

Outer Diameter cuttings were performed in a vertical turning center. AISI 1053 and AISI 1070 bearing steels were used as machining specimens. Both AISI 1053 and AISI 1070 were induction hardened to 58 ~ 62 HRC prior to machining. Two types of low CBN content inserts (CBN KDO50 and CBN KB5625) were used in the experiment. There are nine factors considered in the experiment: cooling methods (three levels, represented as A1, A2, A3), workpiece material (AISI 1053 and AISI 1070), insert grade

(CBN KDO50 and CBN KB5625), nose radius (two levels, represented as B1, B2), edge preparation – chamfer angle (three levels, represented as C1, C2, C3), cutting speed (three levels, represented as D1, D2, D3), feed rate (three levels, represented as E1, E2, E3), depth of cut (three levels, represented as F1, F2, F3) and tool flank wear. It is very important to have an appropriate experimental design in order to minimize the number of runs and meanwhile train the ANN with enough information to explore the permissible ranges for all the inputs. Experimental design using the Taguchi Method has been adopted in this work as shown in Table 3-10.

Circumferential ($\sigma_C$) and longitudinal ($\sigma_L$) residual stresses were measured using X–ray diffraction techniques with a Proto XRD 3000 Residual Stress Analyzer. Stresses were read at five depths (0, 5.08, 12.70, 25.40, 50.80 $\mu m$) along the workpiece. Residual stress profiles were approximated using smooth lines through those five points.

There are a total of 12 runs. For each run, circumferential and longitudinal residual stress profiles were measured at fresh tool (after cutting the first piece, tool flank wear VB = 10 μm was assumed) and worn tool (after cutting 150 pieces, tool flank wear was measured using a SmartScope flash video gage). Thus, there are a total of 23 experimental data points available (one experimental data point was failed due to early tool breakage), where 21 data points (runs 1,2,3,4,5,6,7,8,9,10,11) will be used as the training samples in the BPNN, and 2 data points (run 12 fresh and worn) will be used for model verification.

Table 3-10 Experimental design matrix

| | | Coolant | Workpiece | Tool Insert | Tool Nose Radius | Chamfer Angle | Cutting Speed (SFPM) | Feed Rate (in/rev) | DOC (inch) | Flank Wear (um) |
|---|---|---|---|---|---|---|---|---|---|---|
| Factors | | 1 | 2 | 3 | 4 | 5 | 6 | 7 | 8 | 9 |
| 1 | F | A1 | 1053 | CBN KD050 | B1 | C1 | D1 | E2 | F2 | 10 |
| | W | A1 | 1053 | CBN KD050 | B1 | C1 | D1 | E2 | F2 | 139 |
| 2 | F | A2 | 1070 | CBN KD050 | B1 | C2 | D2 | E1 | F1 | 10 |
| | W | A2 | 1070 | CBN KD050 | B1 | C2 | D2 | E1 | F1 | 205 |
| 3 | F | A3 | 1053 | CBN KD050 | B1 | C3 | D3 | E3 | F3 | 10 |
| | W | A3 | 1053 | CBN KD050 | B1 | C3 | D3 | E3 | F3 | 326 |
| 4 | F | A2 | 1053 | CBN KD050 | B2 | C3 | D1 | E2 | F1 | 10 |
| | W | A2 | 1053 | CBN KD050 | B2 | C3 | D1 | E2 | F1 | 116 |
| 5 | F | A3 | 1053 | CBN KD050 | B2 | C1 | D2 | E1 | F3 | 10 |
| | W | A3 | 1053 | CBN KD050 | B2 | C1 | D2 | E1 | F3 | 386 |
| 6 | F | A1 | 1070 | CBN KD050 | B2 | C2 | D3 | E3 | F2 | 10 |
| | W | A1 | 1070 | CBN KD050 | B2 | C2 | D3 | E3 | F2 | 168 |
| 7 | F | A3 | 1053 | CBN KD5625 | B1 | C2 | D1 | E1 | F2 | 10 |
| | W | A3 | 1053 | CBN KD5625 | B1 | C2 | D1 | E1 | F2 | 485 |
| 8 | F | A1 | 1053 | CBN KD5625 | B1 | C3 | D2 | E3 | F1 | 10 |
| | W | A1 | 1053 | CBN KD5625 | B1 | C3 | D2 | E3 | F1 | 184 |
| 9 | F | A2 | 1070 | CBN KD5625 | B1 | C1 | D3 | E2 | F3 | 10 |
| | W | A2 | 1070 | CBN KD5625 | B1 | C1 | D3 | E2 | F3 | 897 |
| 10 | F | A2 | 1053 | CBN KD5625 | B2 | C2 | D1 | E3 | F3 | 10 |
| | W | A2 | 1053 | CBN KD5625 | B2 | C2 | D1 | E3 | F3 | 322 |
| 11 | F | 3 | 1070 | CBN KD5625 | B2 | C3 | D2 | E2 | F2 | 10 |
| | W | A3 | 1070 | CBN KD5625 | B2 | C3 | D2 | E2 | F2 | failed |
| 12 | F | A1 | 1053 | CBN KD5625 | B2 | C1 | D3 | E1 | F1 | 10 |
| | W | A1 | 1053 | CBN KD5625 | B2 | C1 | D3 | E1 | F1 | 193 |

Where: “F” means fresh tool and “W” means Worn tool

*Modeling Scheme*

The modeling scheme is shown in Figure 3-19. Longitudinal ($\sigma_L$) and circumferential ($\sigma_C$) residual stresses have been measured at five depths in the experiment to approximate the residual stress profiles. The behavior of the residual stress is different at different depths along the workpiece. In order to precisely describe the behavior of the residual stress distribution along the workpiece depth, five sub-BPNNs have been adopted to learn the different behavior at the different depths. Each BPNN predicts one $\sigma_C$ and $\sigma_L$ at one depth, five $\sigma_C$ and $\sigma_L$ are predicted for five different

depths. Longitudinal ($\sigma_L$) and circumferential ($\sigma_C$) residual stress profiles are generated using smooth lines through those five data points.

A general topology structure with input layer, one hidden layer, and the output layer is selected. There are nine inputs $X = \{x_1, x_2, x_3, x_4, x_5, x_6, x_7, x_8, x_9\}$ to represent cooling method, workpiece material, insert grade, tool nose radius, chamfer angle, cutting speed, feed rate, depth of cut and tool flank wear; and two outputs $O = \{o_1, o_2\}$ to represent $\sigma_C$ and $\sigma_L$. All inputs and outputs need to be normalized within (-1, +1) to facilitate the convergence. There are 21 sample patterns to train each sub BPNN. The other 2 sample patterns (run 12) are reserved for model verification.

Each BPNN will be trained using experimental data (input-output pattern), which is referred to the learning process. After the system has been successfully trained, the final weights will be established and stored. Circumferential ($\sigma_C$) and longitudinal ($\sigma_L$) residual stress profiles can be predicted based on the finalized/stored weights.

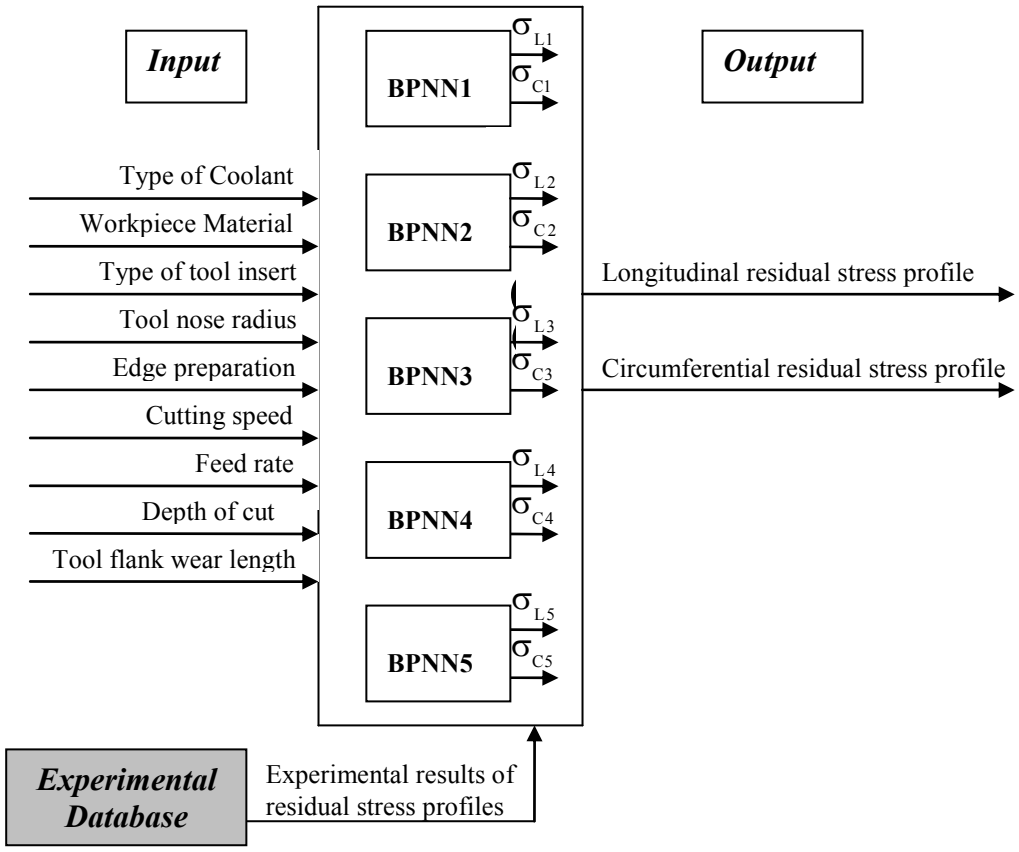


Figure 3-19 Intelligent modeling scheme

*Results and Analysis*

The optimal number of neurons in the hidden layer and the learning rate, the sum of the absolute training errors and percentage errors for each BPNN are shown in Table 3-11. The sum of the absolute errors and percentage errors from linear regression methods are included as well for comparison. BPNN models achieve much smaller errors at all the depths than those of the linear regression methods, especially at the depth 1 and 2 where tensile residual stresses tend to be generated. The proposed BPNN method is

able to identify the tensile residual stresses generated at the workpiece surface while linear regression method has difficulty in predicting the tensile residual stresses.

Table 3-11 Training results for each BPNN

| | Number of neurons | Learning rate | BPNN | | Linear regression | |
|---|---|---|---|---|---|---|
| | | | Sum errors | Percentage errors (%) | Sum errors | Percentage errors (%) |
| Depth 1 | 9 | 0.75 | 110.156 | 9.7 | 438.774 | 38.9 |
| Depth 2 | 12 | 0.35 | 131.556 | 8.0 | 550.715 | 33.3 |
| Depth 3 | 11 | 0.4 | 147.663 | 6.7 | 325.415 | 14.9 |
| Depth 4 | 9 | 0.9 | 138.927 | 5.5 | 172.711 | 6.8 |
| Depth 5 | 16 | 0.65 | 94.286 | 3.2 | 104.602 | 3.6 |

The trained circumferential (CRS) and longitudinal (LRS) residual stress profiles (dotted curve) from the BPNN are compared with the experimental profiles (solid curve) as shown in Figure 3-20 for test cases: run 6 and run 7 and Figure 3-21 for test case: run 9. The results (dashed curve) from linear regression method are also included in the figure for comparison. The trained BPNN system and the established linear regression model are used to predict the residual stress profiles for run 12. The results are compared in Figure 3-22. All the results shown in the figures are normalized to a fixed value.

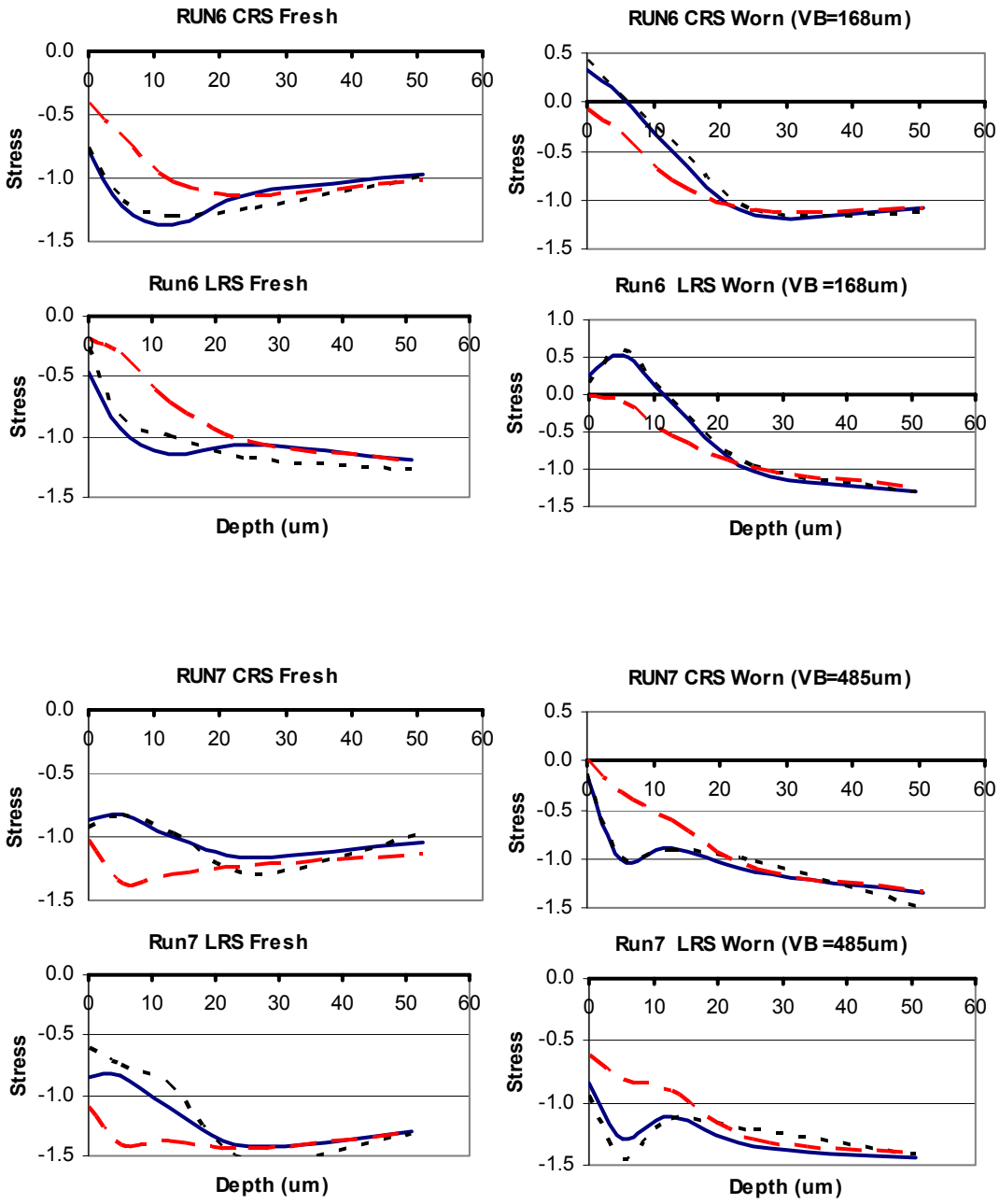


Figure 3-20 Training results for test cases: run 6 and run7: measured residual stress profiles (solid lines), prediction by intelligent model (dotted lines) and prediction by regression model (dashed lines)

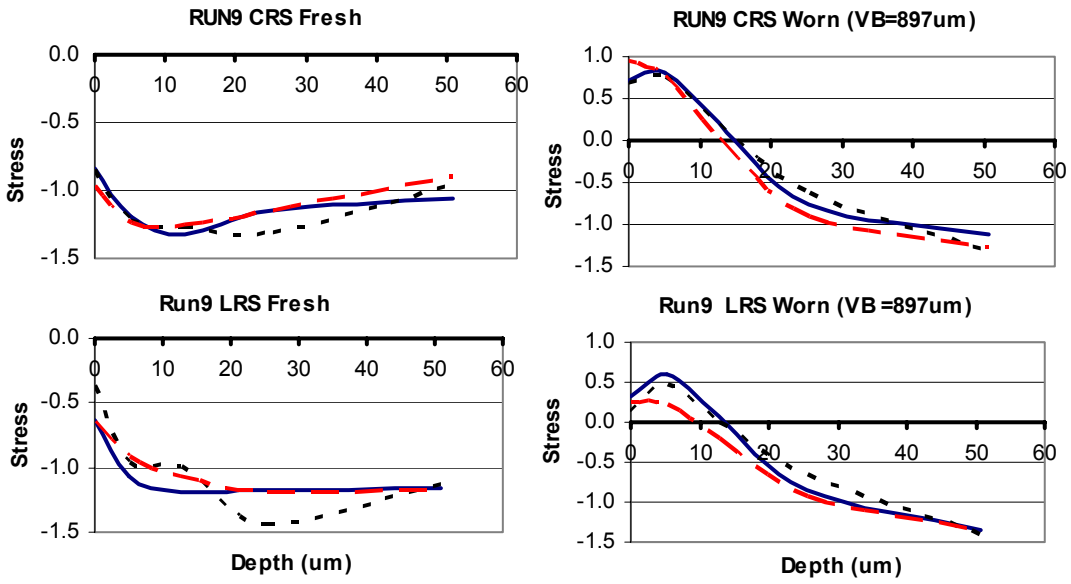


Figure 3-21 Training results for test case: run 9: measured residual stress profiles (solid lines), prediction by intelligent model (dotted lines) and prediction by regression model (dashed lines)

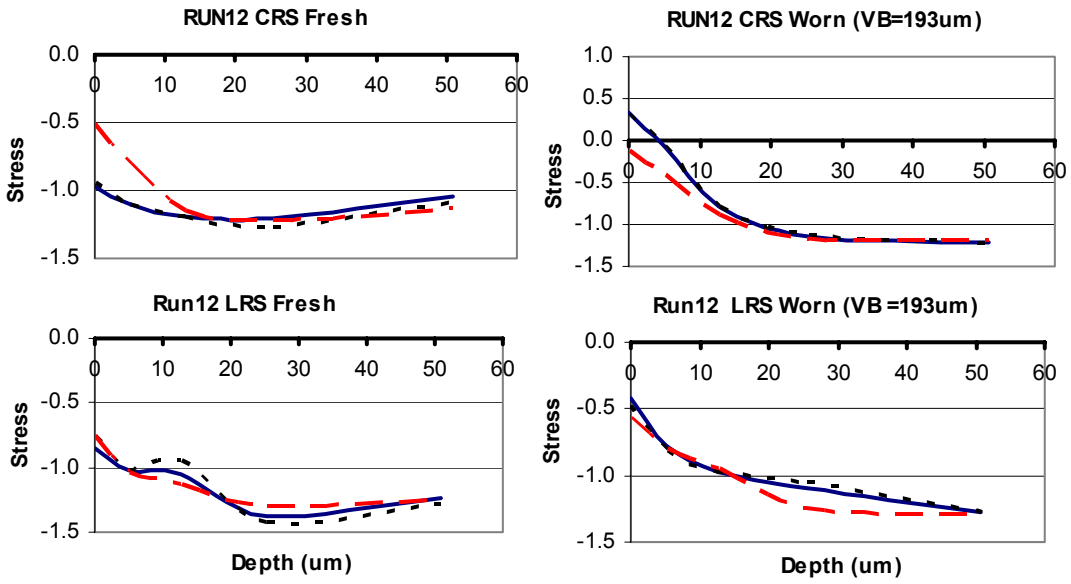


Figure 3-22 Verification results for run 12: measured results (solid lines), prediction by intelligent model (dotted lines) and prediction by regression model (dashed lines)

Residual stress profiles predicted from the intelligent model are sufficiently accurate for all the cases and have much higher performance relative to the linear regression model.

BPNN1 has been used to predict the surface residual stress; its prediction results are tabulated in Table 3-12 for worn tools, including the training cases and the verification cases (run 12, which are bolded in the table). Results from the linear regression are included as well for comparison. As can be seen from the table, the proposed model can precisely predict surface residual stress with 7.8% error in circumferential residual stress and 8.1% error in longitudinal residual stress, while the

linear regression model has 1111.4% error in circumferential residual stress and 20.6% error in longitudinal residual stress.

Table 3-12 Surface residual stress prediction (normalized)

| | Circumferential (worn tool) | | | Longitudinal (worn tool) | | |
|---|---|---|---|---|---|---|
| Run Case | Experiment | Model Prediction | Regression Prediction | Experiment | Model Prediction | Regression Prediction |
| 1 | 0.1167 | 0.1585 | -0.1611 | -0.3537 | -0.2955 | -0.4349 |
| 2 | -0.3357 | -0.2747 | -0.1105 | -0.5940 | -0.5581 | -0.5147 |
| 3 | -0.4260 | -0.2775 | -0.4390 | -0.4097 | -0.3360 | -0.3264 |
| 4 | -0.0180 | 0.0783 | -0.1949 | -0.2935 | -0.2831 | -0.4635 |
| 5 | 0.0915 | 0.1465 | 0.1001 | -0.7105 | -0.8050 | -0.5581 |
| 6 | 0.3313 | 0.4207 | -0.0669 | 0.2562 | 0.1469 | -0.0205 |
| 7 | -0.1483 | -0.1317 | 0.0074 | -0.8356 | -0.9397 | -0.6200 |
| 8 | 0.0469 | 0.0521 | -0.3937 | -0.1470 | -0.2523 | -0.2694 |
| 9 | 0.7072 | 0.6949 | 0.9581 | 0.3236 | 0.1352 | 0.2583 |
| 10 | 0.0600 | 0.0486 | -0.1491 | -0.1767 | -0.2496 | -0.2445 |
| **12** | **0.3231** | **0.3134** | **-0.1147** | **-0.4156** | **-0.4811** | **-0.5729** |
| **Error (%)** | | **7.8** | **1111.4** | | **8.1** | **20.6** |

Tool flank wear is found to be the most critical factor affecting the residual stresses. Tool insert type and tool geometry are found to be very strong effect factors while workpiece material and cutting condition are found to be weaker effect factors on the residual stress distribution. Residual stresses tend to be tensile with the progression of the tool flank wear. With the proposed intelligent model, the onset of the tensile residual stress for the specific conditions can be predicted. As shown in Figures 3-23 and 3-24, two cases have been studied.

Case study 1 is dry turning of hardened AISI 1053 with KB5625 low CBN tool insert. The tool has nose radius of 0.8 mm, negative chamfer angle of 15°, back rake angle of -5°, and clearance angle of 5°. Cutting Condition is cutting speed 1.524 m/s, feed rate 0.1016 mm/rev and depth of cut 0.1016 mm. Flank wear is 149 μm at the onset of the tensile residual stress. Case study 2 is dry turning of hardened AISI 1070 with Kennametal KD050 low CBN tool insert. The tool has nose radius of 1.6 mm, negative chamfer angle of 20°, back rake angle of -5°, and clearance angle of 5°. Cutting Condition is cutting speed 2.287 m/s, feed rate 0.1524 mm/rev and depth of cut 0.2032 mm. Flank wear is 98 μm at the onset of the tensile residual stress. Therefore with integrated tool flank wear model, it is possible to predict the quantity of the pieces cut before the onset of the tensile residual stress at the workpiece surface.

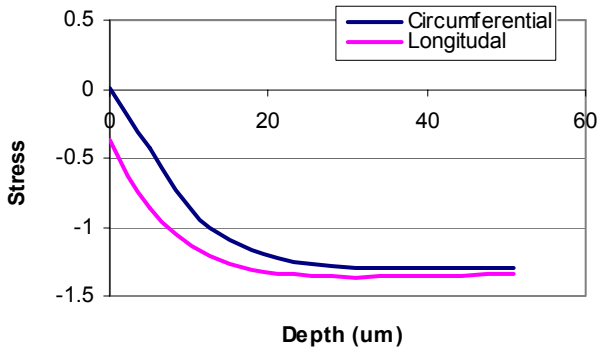


Figure 3-23 Onset of tensile residual stress for case study 1

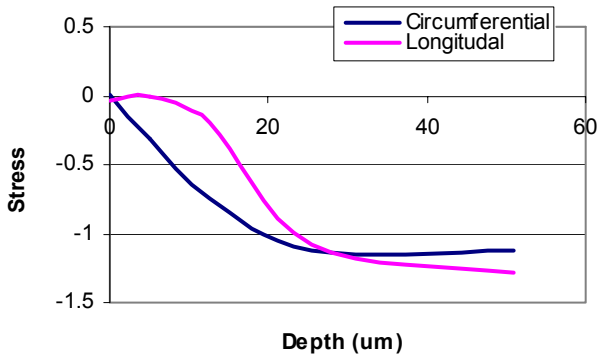


Figure 3-24 Onset of tensile residual stress for case study 2

*Residual Stress Profile Prediction Toolbox*

An easy-to-use prediction toolbox, as illustrated in Figure 3-25, has been designed with the developed intelligent model embedded. When linked to a database, the embedded intelligent model can be automatically retrained with accumulated experimental and practical process data stored in the database to further improve its prediction capability. The developed toolbox can not only be used to study the residual stress distribution for certain process setting, but can also be used for machining quality online control.

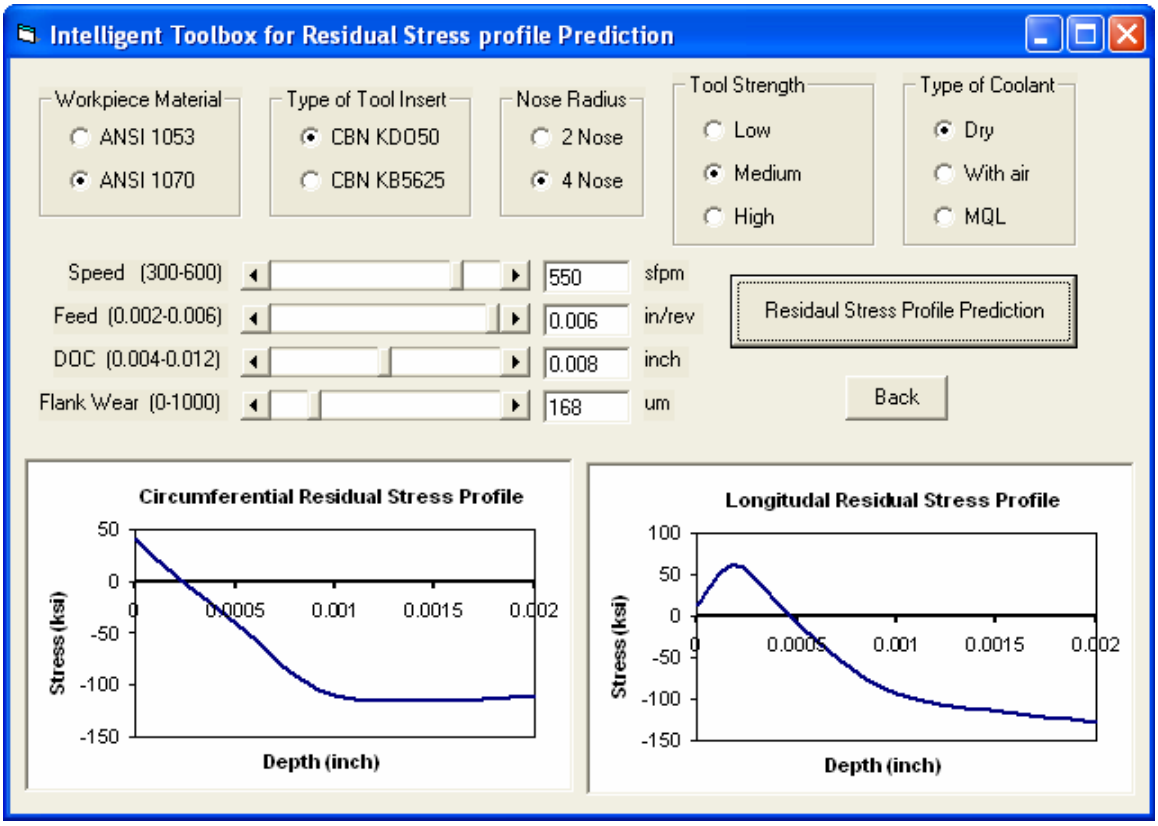


Figure 3-25 The prediction toolbox for residual stress profile

Hierarchical modeling scheme

Tool flank wear is one of the inputs in the established BPNN models to predict the white layer thickness and residual stress profiles, which is also a process output in itself and should be predicted in the simulation. A flank wear prediction model as presented in Section 3.4 should be integrated in predicting white layer thickness and residual stress profiles. Hence a model with hierarchical structure which consists of analytical models and BPNN models as shown in Figure 3-26 is required.

Given workpiece material and tool insert type together with the tool geometry (clearance angle, back rake angle, insert nose radius and edge preparation) and cutting conditions (cutting speed, feed rate and depth of cut), tool flank wear can be estimated based on the unified approach detailed in Section 3.4, and then the predicted flank wear length will be used as one of the inputs to the BPNN models together with the other process inputs (tool geometry and cutting condition) to predict the white layer thickness and residual stress profiles.

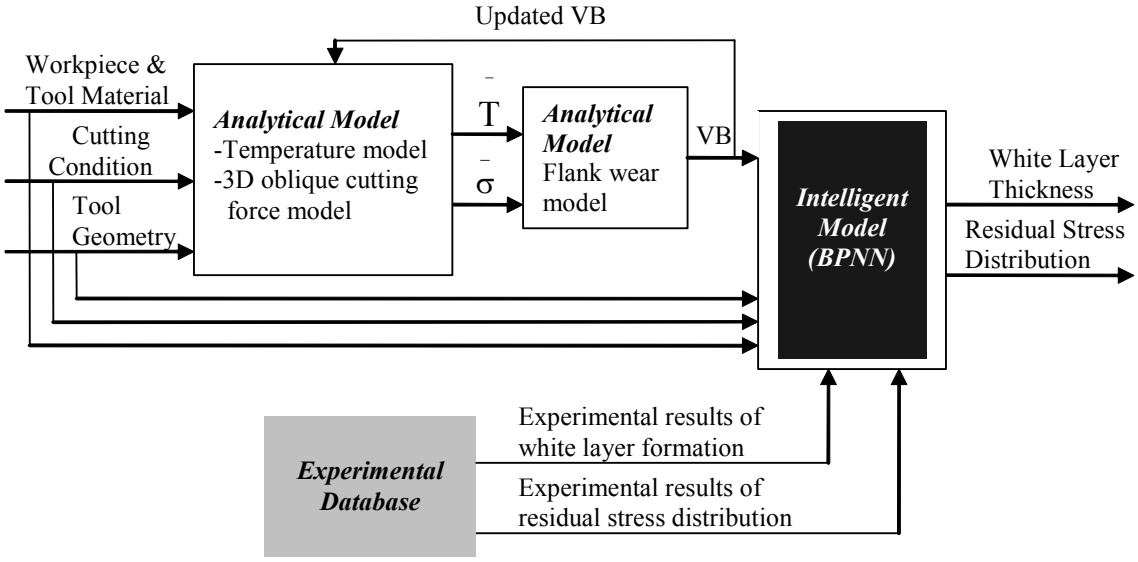


Figure 3-26 A hierarchical modeling structure

## 3.6 Conclusion

Hard turning process models are indispensable in providing the process information in process planning and optimization. In this chapter, hard turning process models, including thermal model, 3-D oblique cutting force model, tool wear rate model and surface integrity models (including surface roughness, white layer thickness, and residual stress profiles) are addressed.

Average temperatures along rake face and flank face are calculated from three major heat sources in metal cutting. 3-D oblique cutting forces are modeled by taking modified Oxley's machining theory and Waldorf's worn tool force model as its kernel. A unified approach in modeling the CBN tool flank wear rate from Huang *et al.* (Huang and Liang 2004a) is used to estimate the tool flank wear progression in hard turning. Surface roughness is determined by feed rate and tool nose radius. BPNN models are constructed based on the experimentally accumulated knowledge in predicting the white layer thickness and residual stress profiles; the prediction results from BPNN models match the experimental results well, and much higher performance relative to the conventional linear regression method has been achieved. A hierarchical structure is needed in prediction white layer thickness and residual stress profiles to integrate the tool wear information. Dry turning of hardened AISI 1053 with KB5625 tool inserts is performed on a horizontal lathe in order to determine its Johnson-Cook parameters and wear coefficients.

# CHAPTER IV

# HARD TURNING PROCESS PLANNING AND OPTIMIZATION

## 4.1 Introduction

The objective of hard turning process optimization is to design optimal tool geometry (edge preparation, rake angle, clearance angle, tool nose radius, etc) and cutting condition (cutting speed, federate, and depth of cut) to achieve specific performance goals (such as minimum cost per part, maximum production rate) with satisfactory surface finish (surface roughness, white layer thickness and residual stress distribution) and any other practical constraints in finish hard turning processes.

Based on the developed optimization algorithm in Chapter 2 and process models in Chapter 3, two case studies have been implemented for finish hard turning process planning and optimization. The first case is to achieve minimum cost per part and maximum production rate simultaneously in outer diameter finish turning of hardened AISI 52100. The second case is to achieve maximum material removal rate, minimum tool wear, and best surface finish simultaneously in finish turning of hardened AISI 1053. The optimal process conditions determined for the second case are verified by experiments in order to demonstrate the capability and feasibility of the developed methodology.

The overall framework of process optimization is shown in Figure 4-1. Given material properties of workpiece and tool together with initial randomly generated cutting conditions and tool geometries, cutting temperatures and 3D oblique cutting forces will be predicted. Tool flank wear length can be calculated based on the process information estimated from the thermal and force models. Experimental knowledge from the experimental database will be used to train the BPNN in order to establish the process models for white layer thickness and residual stress profile prediction. Based on the specified process performance goals, further cutting conditions and tool geometries will be generated from the optimization algorithm to search for the optimal cutting condition and tool geometry until the stopping criteria are met. Finally, optimal cutting condition and tool geometry will be reached and process information such as cost per part, cycle time per part, final tool wear, and surface integrity (surface roughness, white layer thickness, and residual stress profile) will be given.

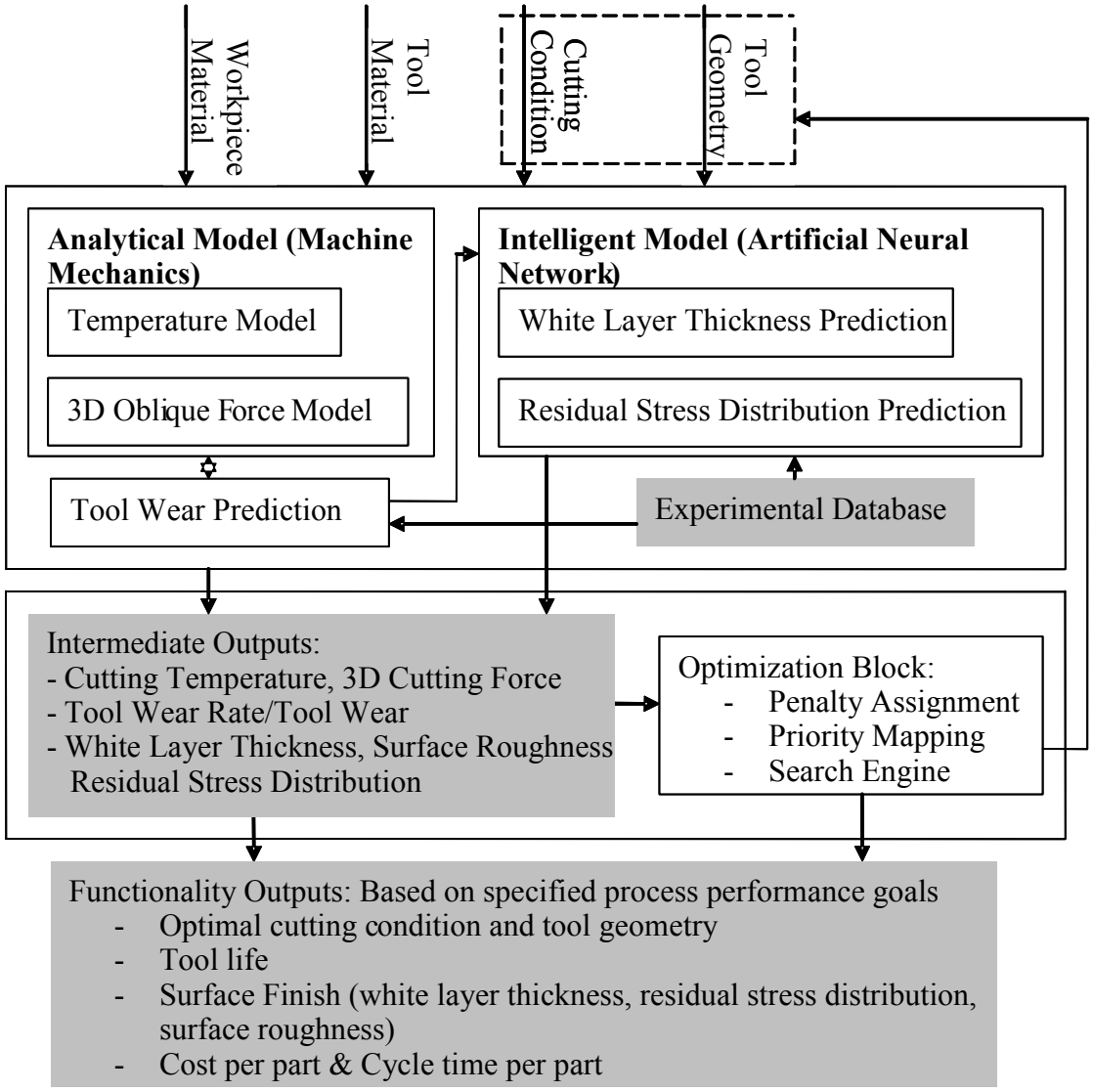


Figure 4-1 Overall process optimization flow chart

## 4.2 Case Study 1

Process optimization of inner ring outer diameter (OD) finish hard turning with low CBN tool insert (Kennametal KB5625) is studied here. The inner ring is made of hardened AISI 52100 steel with hardness 60 – 64 HRC, a diameter of $D$ (mm), and a

length of $L$ (mm). Required stock removal (depth of cut $doc$) is 0.25mm. The objective is to design the optimal cutting condition (cutting speed $V_c$ and federate $f$), tool geometry (back rake angle $\alpha$, chamfer angle $\varphi$, clearance angle $\gamma$ and tool nose radius $R$) and the number of parts cut per insert $N$ to achieve minimum cost per part and maximum production rate.

The material properties for hardened AISI 52100 are listed in Table 4-1. The parameters of Johnson-Cook model for AISI 52100 from Dawson (2002) are used. They were determined by minimizing the least square errors between the measurements in orthogonal machining tests and the predictions from the modified Oxley's 2-D orthogonal model. The wear coefficients for hardened 52100 bearing steel with KB5625 tool insert were recalibrated with the experimental data from Huang (2002) based on the method elaborated in Section 3.2.3, the reference temperature is defined as 300k.

The wear coefficients calibrated by Huang (2004a) for hardened 52100 and KB5625 tool insert are not readily applicable here. The main reason is due to the different thermal and force models applied in Huang's work and in this study. Hence different process information is estimated which are the inputs to the flank wear prediction model. Large prediction errors can be expected when using wear coefficients from Huang (2004a), which were calibrated based on his thermal and force models. Those wear coefficients should be recalibrated based on the thermal and force models used in this study to maintain consistency. A better calibration scheme should be applied to avoid this unsystematic scheme.

Table 4-1 Material properties of AISI 52100

| | | |
|---|---|---|
| Specific heat capacity $(J/Kg\cdot k)$ | | $475+0.504T$ |
| Thermal conductivity $(W/m\cdot k)$ | | $46.6-0.0298T$ |
| Density $(Kg/m^3)$ | | 7827 |
| Melting point $(k)$ | | 1760 |
| Parameters of Johnson-Cook Model (Dawson, 2002) | A $(MPa)$ | 688.2 |
| | B $(MPa)$ | 150.8 |
| | C | 0.043 |
| | m | 2.779 |
| | n | 0.336 |
| Wear Coefficients with Kennametal KB5625 tool insert | $K_{abrasion}$ | 4.4286e-7 |
| | $K_{adhesion}$ | 6.8356e-16 |
| | $K_{diff}$ | 3.7779e+7 |
| | $a$ | 7.0689e-3 |
| | $K_Q$ | 509050 |

The optimization is subject to several constraints. First, tool geometry could be selected only from several discrete values which are listed as the standard design from Kennametal's category. The cutting condition is subjected to the recommended range for practical finish hard turning applications. The process is also constrained by the required surface integrity (surface roughness, white layer thickness, and residual stress), maximum allowable tool flank wear and available horsepower.

Tool life is mainly determined by the tool flank wear criteria (Groover 1975, Huang 2004c) or Taylor's generalized equation (Ermer 1987, Gopalakrishnan 1991, Dawson 2002), and the number of parts cut per insert is computed directly from the tool life. However, several factors may limit the tool life and therefore affect machining cost. In a finishing process, surface integrity (surface roughness, white layer thickness, and

residual stress) is often of great concern because of its impact on product performance. A tool insert should be changed when a chipping or broken condition happens or when it cannot generate desired surface integrity before the tool fails. Hence, the number of parts cut per insert $N$ should be determined by maximum allowable tool flank wear length and required surface integrity.

The optimization problem can be formulated as:

***Minimize:***

$$f(\alpha,\varphi,\gamma,R,V_c,f,N) = 0.5\frac{C_p}{C_p^*} + 0.5\frac{t_t}{t_t^*}$$

$$C_p = (C_m^{'} + C_w^{'})t_t + \frac{C_t}{N} \tag{4-1}$$

$$t_t = t_{load} + \frac{t_{mach}}{f_{mach}} + \frac{t_{ct}}{N} \tag{4-2}$$

$$t_{mach} = \frac{\pi DL}{1000 f V_c} \tag{4-3}$$

***Subject to:***

$$1.5244(\text{m/s})/300(\text{sfpm}) \le V_c \le 3.0488(\text{m/s})/600(\text{sfpm})$$

$$0.0508(\text{mm/rev})/0.002(\text{ipr}) \le f \le 0.1524\ (\text{mm/rev})/0.006(\text{ipr})$$

$$R \in \{0.4\text{mm}, 0.8\text{mm}, 1.2\text{mm}, 1.6\text{mm}\}$$

$$\alpha \in \{0^{\circ}, -5^{\circ}\}$$

$$\varphi \in \{0^{\circ}, -15^{\circ}, -20^{\circ}\}$$

$$\gamma \in \{5^{\circ}, 8^{\circ}, 10^{\circ}, 12^{\circ}, 16^{\circ}, 20^{\circ}, 25^{\circ}, 30^{\circ}\}$$

Flank wear length: $VB \le VB^{*}$

Surface roughness: $R_a \le R_a^{*}$

White layer thickness: $WL(k) \le WL^{*}$

Maximum circumferential residual stress: $\sigma_{C\max}(k) \le \sigma_C^{*}$

Maximum longitudinal residual stress: $\sigma_{L\max}(k) \le \sigma_L^{*}$

Horse Power: $P(k) \le P^{*}$

where $k = 1, 2, ...N$

The parameter values used for this optimization problem are listed in Table 4-2. The population size was chosen to be 100 and run for 1000 generations. The residual stress models were established only for hardened AISI 1053 and AISI 1070, which is used to predict the residual stress profiles for hardened AISI 52100 as well.

The optimal values of the design variables are listed in Table 4-3 and the process outputs of the optimal design are listed in Table 4-4. Predicted circumferential and longitudinal residual stress profiles for the last workpiece ( $N$ ) (before the tool change) are shown in Figure 4-2.

Though the process models are computationally expensive, the proposed Mixed-Integer Evolutionary Algorithm has excellent search capability and computational efficiency. It took around 11.23 minutes when run on a Pentium 4 personal computer. The Evolutionary Strategy with rejecting constraint handling method which has been applied in grinding process optimization by Lee and Shin (2000) will be very ineffective in this problem with computationally expensive process evaluation. Numerous solutions have to be generated and evaluated in order to find one feasible offspring with rejecting constraint handling method for this highly constrained problem.

Table 4-2 Parameters used for this optimization problem

| Symbol | Definition | Value |
|---|---|---|
| $D$ | Diameter of Inner Ring (mm) | 50.518 |
| $L$ | Length of Inner Ring (mm) | 20 |
| $C_p^*$ | Target cost per part ($/pc) | 10 |
| $t_t^*$ | Target cycle time per part (min/pc) | 10 |
| $C_m^{'}$ | Machine related cost ($/min) | 0.3472 |
| $C_w^{'}$ | Labor related cost ($/min) | 0.7 |
| $C_t$ | Cost of a single cutting edge ($/edge) | 23 |
| $t_{load}$ | Loading time (min/part) | 0.75 |
| $f_{mach}$ | Fraction of active machining time once loaded (%) | 75 |
| $t_{ct}$ | Tool change time (min) | 1.5 |
| $VB^*$ | Maximum flank wear length allowed ( $\mu m$ ) | 250 |
| $R_a^*$ | Maximum surface roughness allowed ( $\mu m$ ) | 0.8 |
| $WL^*$ | Maximum white layer thickness allowed ( $\mu m$ ) | 3 |
| $\sigma_C^*$ | Maximum circumferential residual stress allowed (MPa) | 0 |
| $\sigma_L^*$ | Maximum longitudinal residual stress allowed (MPa) | 0 |
| $P^*$ | Maximum horsepower allowed (W) | 1119 |

Table 4-3 Optimal design variable values

| Design Variable | Value | Type of Variable |
|---|---|---|
| Rake angle $\alpha$ | $-5^\circ$ | Discrete |
| Chamfer angle $\varphi$ | $-20^\circ$ | Discrete |
| Clearance angle $\gamma$ | $30^\circ$ | Discrete |
| Nose radius $R$ | 1.2mm | Discrete |
| Cutting speed $v_c$ | 600(sfpm)/3.0488(m/s) | Continuous |
| Federate $f$ | 0.006(ipr)/0.1524(mm/rev) | Continuous |
| $N$ | 560 | Integer |

Table 4-4 Optimization results

| Process Output | Constraint Value | Process Output | Constraint Value |
|---|---|---|---|
| $P(1)$ (W) | 618.15 | $\sigma_{C\max}(N)$ (Mpa) | -0.79 |
| $P(N)$ (W) | 836.72 | $\sigma_{L\max}(1)$ (Mpa) | -38.56 |
| VB ($\mu m$) | 229.82 | $\sigma_{L\max}(N)$ (Mpa) | -20.21 |
| $R_a$ ($\mu m$) | 0.605 | $MRR(mm^3/\min)$ | 6969.5 |
| $WL(1)$ ($\mu m$) | 0 | Objective | 0.094637 |
| $WL(N)$ ($\mu m$) | 1.42 | Cost per part ($/pc) | 0.9883 |
| $\sigma_{C\max}(1)$ (Mpa) | -138.21 | Cycle Time (min/pc) | 0.9045 |

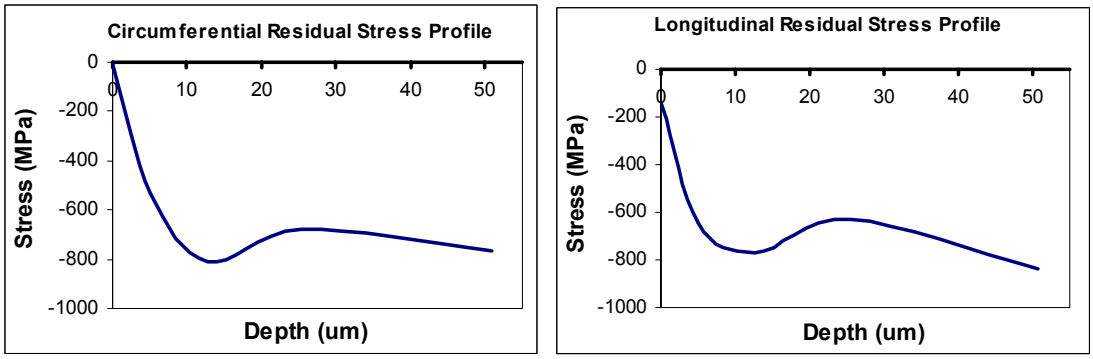


Figure 4-2 Predicted circumferential and longitudinal residual stress profiles for the last workpiece

The optimal chamfer angle and tool nose radius given in this work are comparable with the experimental results from Shintani et al. (1989). Shintani et al. investigated the optimal CBN tool geometry: the angle of negative land (negative chamfer angle), the width of negative land, the nose radius and the honing radius for fine turning of

carburized steel bar on the basis of tool life. Tool flank wear length and surface roughness were used as tool life criteria, respectively. The same constraints have been set for the tool flank wear length and surface roughness in this work. It was found in Shintani *et al.* (1989) that tool life indicated by both tool flank wear and surface roughness first increased as negative chamfer angle was increased until the chamfer angle reached 30-35$^{o}$ and then decreased as negative chamfer angle continued to increase. It is reasonable to find the optimal rake angle as -5$^{o}$ and chamfer angle as -20$^{o}$ in this work. Tool life indicated by tool flank wear increased as nose radius was increased and remained constant for nose radius larger than 0.8mm, while tool life indicated by surface roughness reached a maximum when nose radius was 0.8mm. Optimal nose radius in this work is found to be 1.2mm, because white layer thickness and residual stress distribution of the finished surface are also considered as factors limiting the tool life, including surface roughness. Larger nose radius was found to produce smaller white layer thickness and better residual stress profiles.

Liu and Mittal (1998) optimized the cutting condition (speed, feed, and depth of cut) to achieve the maximum fatigue life and maximum material removal rate for rolling contact under the constraint of surface roughness in superfinish hard turning of through hardened 52100 steel. The optimal cutting speed is mostly 600 – 650 sfpm for different roller bearing applications as selected from 200sfpm to 650sfpm; this is comparable to the optimal speed (600sfpm) in this work. The optimal feed is mostly 0.0005 – 0.001 ipr as selected from 0.0005ipr to 0.005ipr; which deviate from the optimal feed (0.006 ipr) in this work.

## 4.3 Case Study 2 and Experimental Verification

The main purpose of this case study is to check and establish the validity of the developed methodology for hard turning process optimization by experiment. The process used for experimental validation is finish turning of hardened AISI 1053 (58 – 60 HRC) with Kennametal low CBN tool KB5625. The length of cut is 25.4 mm/1 inch and initial bar diameter is 48.00 mm/1.890 inch. The objective is to select the optimal tool geometry (chamfer angle $\varphi$ and tool nose radius $R$) and cutting condition (cutting speed $V_c$ and federate $f$) to achieve maximum material removal rate, minimum tool wear and best surface finish (considering surface roughness only) after turning 100 passes. The back rake angle is -5$^o$, clearance angle is 5$^o$ and depth of cut is 0.1016mm.

The problem can be mathematically formulated as:

***Minimize:***

$$f(\varphi, R, V_c, f) = -w_1 * \frac{MRR}{MRR^t} + w_2 * \frac{VB}{VB^t} + w_3 * \frac{Ra}{Ra^t}$$

***Subject to:***

$$1.5244(\text{m/s})/300(\text{sfpm}) \le V_c \le 3.0488(\text{m/s})/600(\text{sfpm})$$

$$0.0508(\text{mm/rev})/0.002(\text{ipr}) \le f \le 0.1524\ (\text{mm/rev})/0.006(\text{ipr})$$

$$R \in \{0.8\text{mm}, 1.2\text{mm}, 1.6\text{mm}\}$$

$$\varphi \in \{0^{\circ}, -15^{\circ}, -20^{\circ}\}$$

Material Removal Rate: $MRR \geq 20mm^3 / s$

Flank wear length: $VB \leq 250\mu m$

Surface roughness: $R_a \leq 1.2\mu m$

$w_1$, $w_2$ and $w_3$ are the weighting factors, $w_1 = 1.0$, $w_2 = 1.0$, $w_3 = 1.0$ were chosen in this case study. $MRR^t$, $VB^t$ and $Ra^t$ are the target material removal rate, flank wear limitation and surface roughness limitation respectively. They are selected to be:

$$MRR^t = 50mm^3 / s,\ VB^t = 250\mu m,\ Ra^t = 1.5\mu m$$

The overall experimental validation scheme is shown in Figure 4-3. First total of nine cutting tests designed based on Taguchi Method as in Table 4-5 were performed in the experiment. Cutting force, tool wear and surface roughness will be monitored and the measured results will be compared with the prediction results from the prediction models used in the optimization scheme. If the results do not match, prediction models will be recalibrated/recorrected to match the measured results. Thus the evaluation for the

validity of the process planning and optimization methodology affected by process models can be minimized. After that, optimal design will be computed based on the re-corrected prediction models using the developed optimization algorithm. The constraints will be tightened by taking the prediction errors under consideration to ensure the feasibility of the optimal solution. The optimal solution from the simulation will be run experimentally and its experimental results will be compared with the other nine experimental results based on the specified process performance goals used in the optimization scheme to verify its optimality.

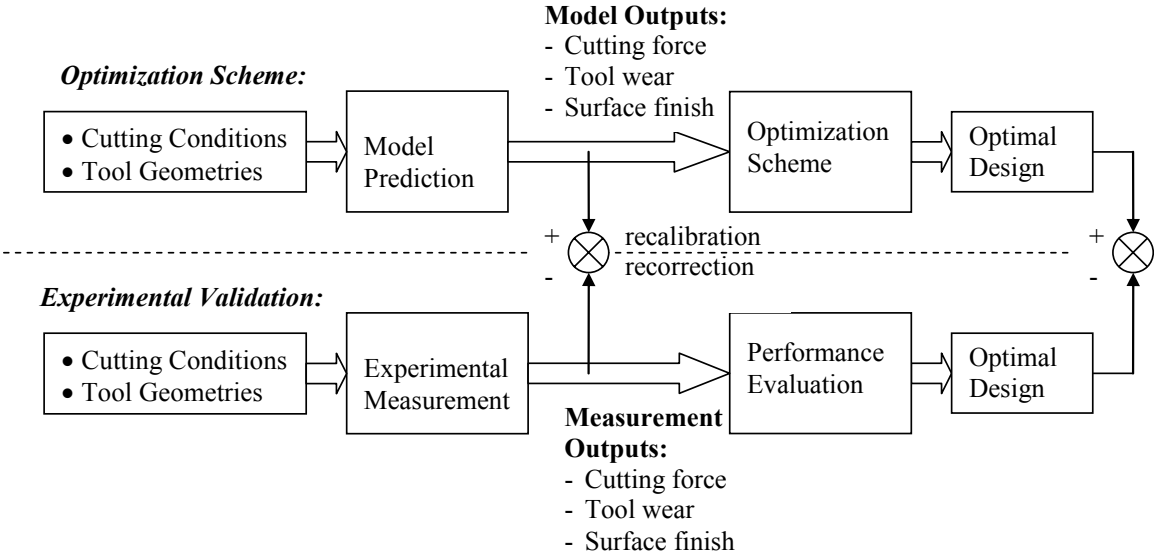


Figure 4-3 The experimental validation scheme for process optimization

Table 4-5 The test matrix for optimization validation

| TC# | Insert Type | Chamfer Angle | Insert Nose (mm) | Cutting Speed (m/s) | Feed Rate (mm/rev) | Depth of Cut (mm) |
|---|---|---|---|---|---|---|
| TC1 | CNGA432S | 0 | 0.8 | 1.524 | 0.0508 | 0.1016 |
| TC2 | CNGA433S | 0 | 1.2 | 2.287 | 0.1016 | 0.1016 |
| TC3 | CNGA434S | 0 | 1.6 | 3.049 | 0.1524 | 0.1016 |
| TC4 | CNGA432S0415 | 15 | 0.8 | 2.287 | 0.1524 | 0.1016 |
| TC5 | CNGA433S0415 | 15 | 1.2 | 3.049 | 0.0508 | 0.1016 |
| TC6 | CNGA434S0415 | 15 | 1.6 | 1.524 | 0.1016 | 0.1016 |
| TC7 | CNGA432S0420 | 20 | 0.8 | 3.049 | 0.1016 | 0.1016 |
| TC8 | CNGA433S0420 | 20 | 1.2 | 1.524 | 0.1524 | 0.1016 |
| TC9 | CNGA434S0420 | 20 | 1.6 | 2.287 | 0.0508 | 0.1016 |

The validation scheme including experimental procedure, prediction verification, model recalibration/recorrection and optimal design validation will be presented as follows.

### 4.3.1 Experimental Procedure

Finish dry turning was performed on a horizontal lathe (Hardinge T-42). Solid bars of AISI 1053 with 152.4 mm/6 inch length and 48.56 mm/1.912 inch diameter were used, which have been through hardened to 60 HRC. All bars were first clean cut to 48.00 mm/1.890 inch to remove the scale from heat treatment and initial out-of-roundness. Then the turning was carried out for 20 passes for every inch length (25.4 mm) at the 0.004inch (0.1016mm) depth of cut up to total five inches. Hence there were a total of 100 passes at 1 inch length of cut. The diameter of the bar was reduced from 1.890 inch/48.00mm to 1.730 inch/43.94mm.

3-D oblique cutting forces were recorded with a kistler 9257B dynamometer. Surface roughness was measured with a contact profilometer and tool flank wear was measured with a surface microscope (Zygo New View 200). They were all monitored after cutting 2, 4, 7, 10, 20, 40, 60, 80 and 100 passes.

*Hardness Testing*

Solid bars of AISI 1053 were through hardened to 60 HRC. Unavoidably, the hardness achieved is uneven from the outer surface toward the middle of the bar. Hardness tests on the material were performed with Micromet 2100 series Microhardness Tester to check the hardness consistency from the outer diameter to the diameter of 41.91mm/1.650 inch.

Microhardness Tester has two operation modes: Vickers (HV) and Knoop (HK) operation. Vickers (HV) operation is selected with applied load of 2000gf. The measured value will be converted to HRC scale and displayed in the screen. Readings were taken at four different diameters for five times and the testing values are shown in Table 4-6.

Table 4-6 Averaged hardness readings of AISI 1053 solid bar

| Diameter (mm/inch) | #1 | #2 | #3 | #4 | #5 | Average (HRC) |
|---|---|---|---|---|---|---|
| 48.13/1.895 | 59.8 | 59.2 | 60.1 | 59.5 | 58.9 | 59.5 |
| 45.34/1.785 | 60.2 | 59.9 | 57.5 | 57.1 | 58.0 | 58.5 |
| 43.94/1.730 | 57.6 | 59.7 | 58.3 | 56.4 | 58.4 | 58.1 |
| 41.96/1.652 | 54.0 | 52.1 | 57.0 | 54.8 | 55.3 | 54.6 |

As can be seen, hardness values are within the target values (58 to 60 HRC) from the outer diameter to the diameter of 43.94 mm/1.730 inch. Hence, the solid bars were turned from diameter 48.00 mm/1.890 inch down to 43.94mm/1.730 inch only in order to keep the hardness within the target values.

### 4.3.2 Model Verification and Recalibration

*Model Verification for Cutting Force*

The measured 3-D cutting forces are compared with the predicted values for those nine test cases at the second pass (flank wear was assumed to be 20 um for all the cases) in Figure 4-4, 4-5 and 4-6.

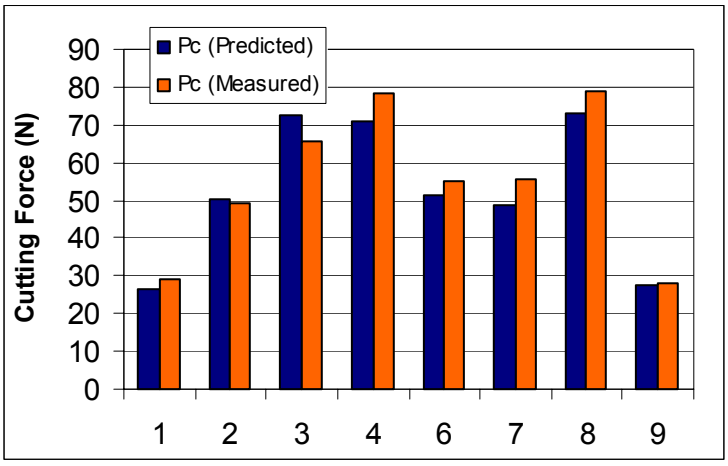


Figure 4-4 Cutting force comparison when turning hardened 1053 steel

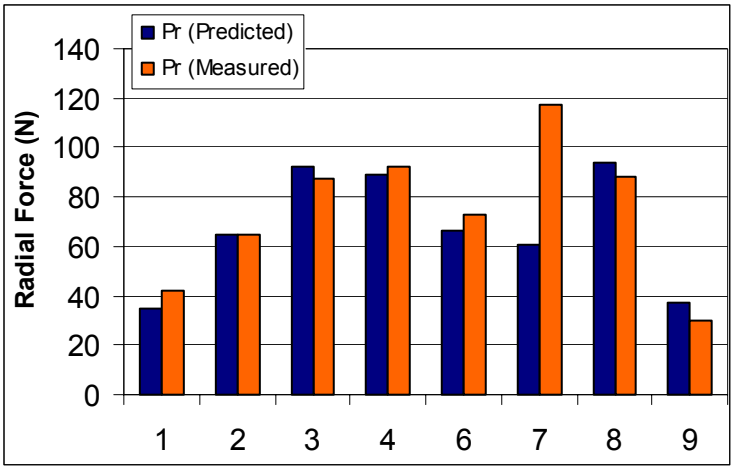


Figure 4-5 Radial force comparison when turning hardened 1053 steel

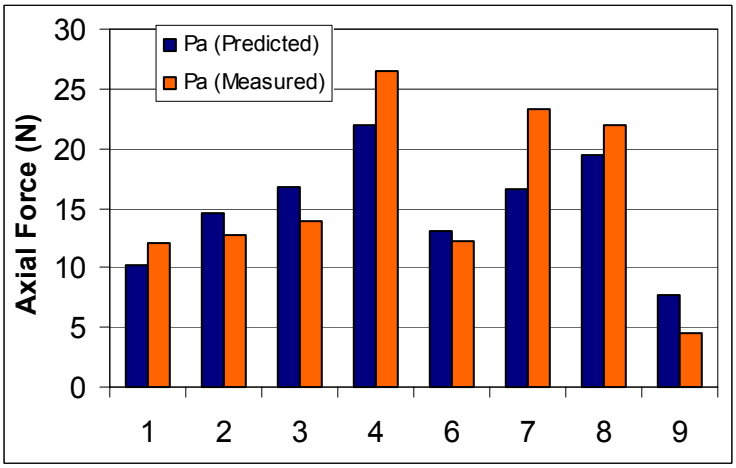


Figure 4-6 Axial force comparison when turning hardened 1053 steel

The prediction values match the measured ones very well (the force data for test case #5 were not measured) with the average error for cutting force prediction 7.7%, radial force prediction 20.2% and axial force prediction 20.9%. Prediction errors increase at the smaller value of feed rate where plouing effect pronounces.

*Model Verification for Tool Wear*

The calibrated wear coefficients for hardened AISI 1053 with KB5625 low CBN insert in Section 3.2 are used to predict the flank wear progression. The predicted results are compared with the measured ones in Figure 4-7, where triangular is the measurements and solid line is the predictions. As suggested from those Figures, the calibrated flank wear model predicts the tool flank wear progression pretty well. The average prediction error of the final flank wear length after cutting 100 passes of all the test cases is 10.3%.

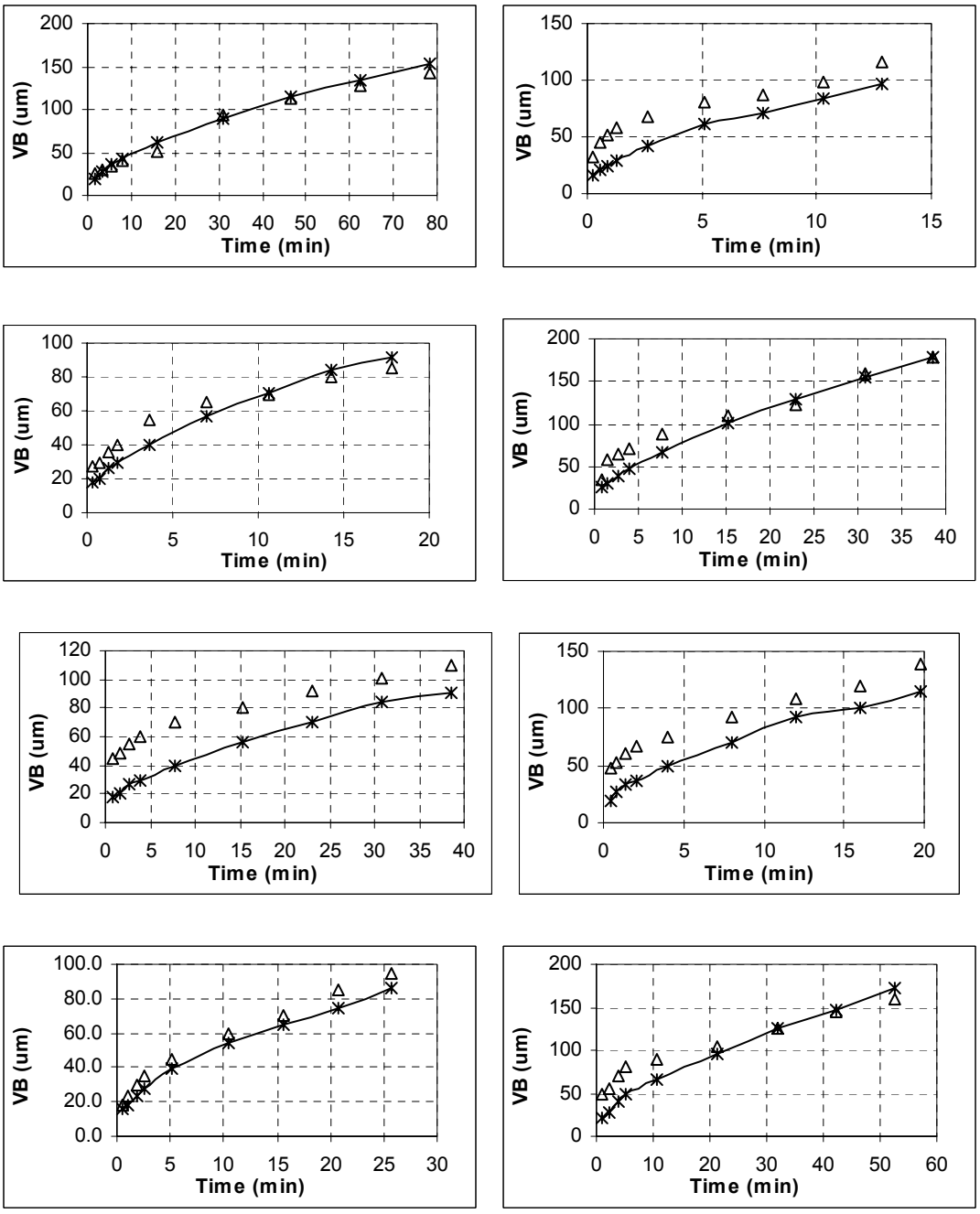


Figure 4-7 The comparison of flank wear progression for test cases 1, 3, 4, 5, 6, 7, 8, 9 (from top to bottom and from left to right)

*Model Verification and Recalibration for Surface Roughness*

Surface roughness was monitored with the progression of the tool wear for each test. The measured results are shown in Figure 4-8. For test case 4, 6, 8, and 9, surface roughness increases with the progression of tool wear at early stage and reaches to a relatively stable value at later stage. For test case 3 and 7, surface roughness remains relatively constant with the progression of tool wear. However for test case 1 and 5, surface roughness first decreases with the progression of tool wear and increases after a certain flank wear value. Hence, the variation of surface roughness with the progression of tool wear varies from the case to case and the assumption where surface roughness will not deteriorate with the progression of tool wear is not valid.

Additionally, as shown in Figure 4-9, the measured surface roughness values greatly deviate from the model prediction from Equation (3-27), where the initial and average surface roughness from the measurement are compared with the prediction results. Consequently, the model for surface roughness needs to be recorrected in order for predicted values to match the measured results better. The major focus herein is to verify the optimization results from the developed methodology instead of building an accurate prediction model. Therefore, an empirical model is simply built based on those eight experimental results as shown in Equation (4-4), where average surface roughness values during the hard turning are used:

$$Ra = R_0 f^x R^y V_c^z \tag{4-4}$$

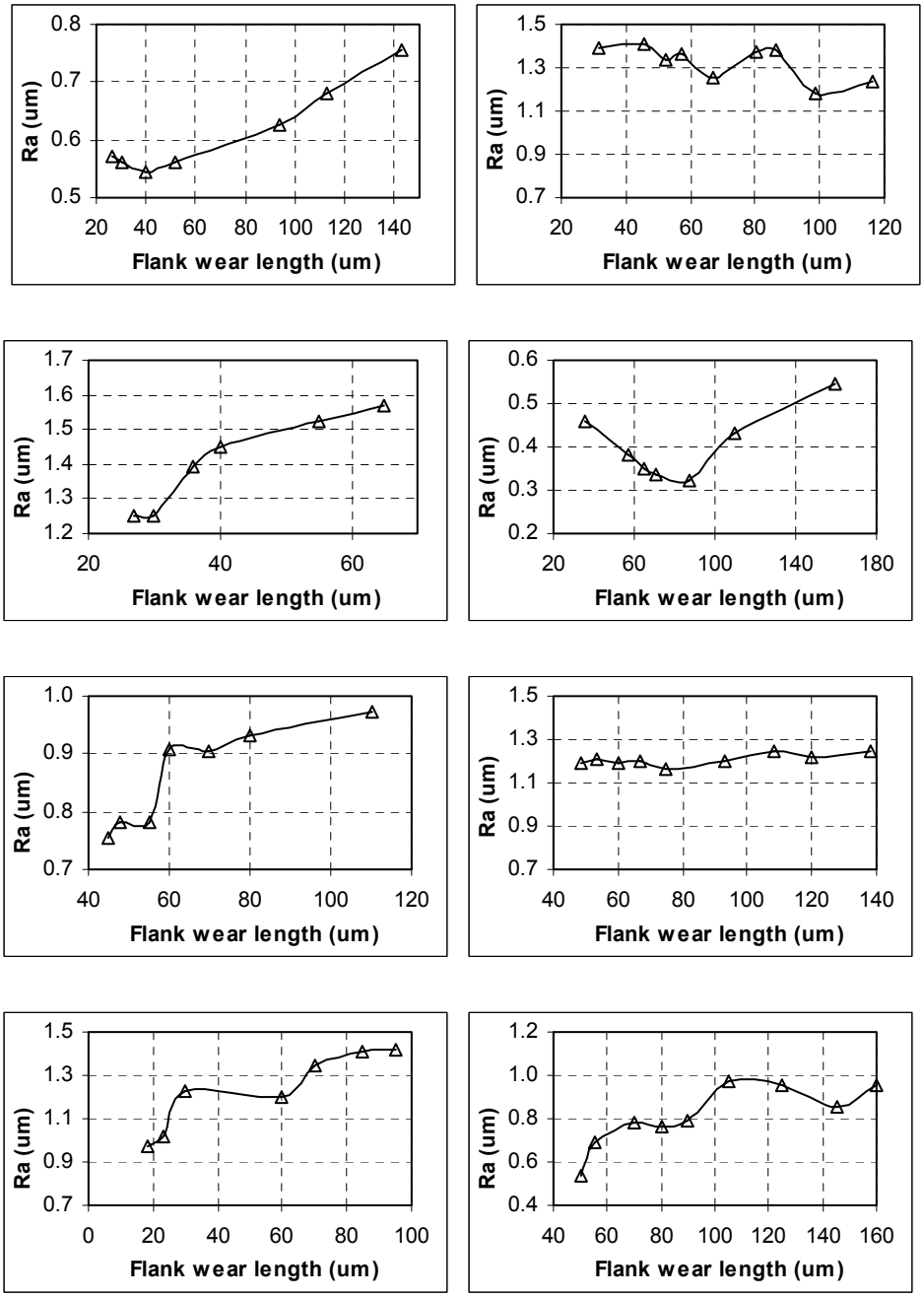


Figure 4-8 Measured surface roughness with flank wear progression for test case 1, 3, 4, 5, 6, 7, 8, 9 (from left to right and from top to bottom)

The values of $R_0$, $x$, $y$, $z$ were determined to be 2.474, 0.503, -0.143, 0.420. The empirical model implicates that not only feed rate and tool nose radius will affect surface roughness but cutting speed also plays a critical role. Prediction results from the recalibrated model are also compared with measured results in Figure 4-9, which match the experimental data much better with average prediction error of 14.1%.

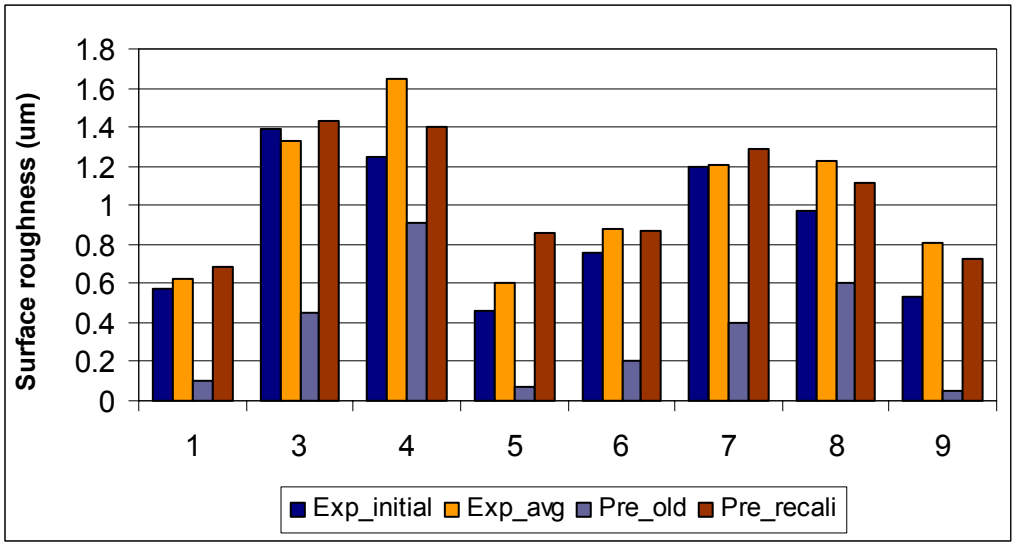


Figure 4-9 The comparison of measured and predicted surface roughness for test case 1, 3, 4, 5, 6, 7, 8, 9

### 4.3.3 Optimal Results and Experimental Validation

The developed mixed integer evolutionary algorithm was applied to solve the optimization problem in this case. The developed and recalibrated process models and the related coefficients in finish turning of hardened AISI 1053 with KB5625 were used. In

order to ensure the feasibility of the optimal results, tool wear and surface roughness constraints are tightened by taking the model prediction error into consideration. For example, the required surface roughness should be smaller than 1.2 $\mu m$, and there is an average 14.1% prediction error from the model used in the optimization scheme. In order to ensure part surface roughness smaller than the required value, the surface roughness constraint is tightened to be: 1.2/(1+0.141) =1.0 $\mu m$. Similarly, tool flank wear constraint is tightened to be 250/(1+0.1) $\approx$ 227 $\mu m$.

The optimal results from the simulation are shown in Table 4-7. The surface roughness constraint is an active constraint which will limit the selection of tool nose radius, cutting speed and federate.

Table 4-7 Optimization results for case study 2

| Design Variable | Optimal Value |
|---|---|
| Nose Radius | Nose 4 (1.6 mm) |
| Chamfer Angle | -20° |
| $V_c$ | 315 (sfpm)/1.6006 (m/s) |
| $f$ | 0.005 (ipr)/0.1270 (mm/rev) |

The simulated optimal results were compared with the other eight non-optimal conditions listed in Table 4-5, the comparison results are shown in Table 4-8 (Chatter happened at test case #2 after cutting several passes, hence comparison for this test case were not included). As can be seen, the predicted process output matches the experimental results fairly well. In the simulation, test cases 3, 4, 6, 7, 8 achieve smaller

objective values; however they are all infeasible solutions. The test cases 3, 4, 7, 8 violate the surface roughness constraints both in simulation and experiment, test case 6 violate the constraint for required material removal rate.

The predicted optimal results had distinguished to be optimal not only in the simulation but also in the experiment. Hence the reliability and validity of the proposed methodology for hard turning process planning and optimization are proved experimentally.

Table 4-8 Results of experimental validation for case study 2

| Condition | Process Output | Predicted | Experiment | Objective | |
|---|---|---|---|---|---|
| | | | | Predicted | Experiment |
| Optimal | $MRR\,(mm^3/s)$ | 20.7 | 20.7 | 0.6180 | 0.7192 |
| | $VB\ (\mu m)$ | 91.4 | 83.4 | | |
| | $Ra\ (\mu m)$ | 0.998 | 1.198 | | |
| TC1 | $MRR\,(mm^3/s)$ | 7.9 | 7.9 | 0.9076 | 0.8332 |
| | $VB\ (\mu m)$ | 152.9 | 142.9 | | |
| | $Ra\ (\mu m)$ | 0.681 | 0.628 | | |
| TC3 | $MRR\,(mm^3/s)$ | 47.2 | 47.2 | 0.3972 | 0.4058 |
| | $VB\ (\mu m)$ | 96.3 | 116.5 | | |
| | $Ra\ (\mu m)$ | 1.434 | 1.326 | | |
| TC4 | $MRR\,(mm^3/s)$ | 35.4 | 35.4 | 0.5921 | 0.7322 |
| | $VB\ (\mu m)$ | 91.2 | 85.0 | | |
| | $Ra\ (\mu m)$ | 1.403 | 1.650 | | |
| TC5 | $MRR\,(mm^3/s)$ | 15.7 | 15.7 | 0.9721 | 0.7986 |
| | $VB\ (\mu m)$ | 178.2 | 177.8 | | |
| | $Ra\ (\mu m)$ | 0.860 | 0.603 | | |
| TC6 | $MRR\,(mm^3/s)$ | 15.7 | 15.7 | 0.6335 | 0.7130 |
| | $VB\ (\mu m)$ | 91.2 | 110.0 | | |
| | $Ra\ (\mu m)$ | 0.874 | 0.882 | | |
| TC7 | $MRR\,(mm^3/s)$ | 31.5 | 31.5 | 0.6899 | 0.7306 |
| | $VB\ (\mu m)$ | 114.8 | 138.3 | | |
| | $Ra\ (\mu m)$ | 1.291 | 1.210 | | |
| TC8 | $MRR\,(mm^3/s)$ | 23.6 | 23.6 | 0.6167 | 0.7273 |
| | $VB\ (\mu m)$ | 86 | 95.0 | | |
| | $Ra\ (\mu m)$ | 1.117 | 1.229 | | |
| TC9 | $MRR\,(mm^3/s)$ | 11.8 | 11.8 | 0.9417 | 0.9398 |
| | $VB\ (\mu m)$ | 172.6 | 160.0 | | |
| | $Ra\ (\mu m)$ | 0.731 | 0.804 | | |

## 4.4 Conclusion

Process planning and optimization is crucial to help establish the economic and quality viability of hard turning process as a potential replacement for grinding. Based on the developed optimization algorithm in Chapter 2 and the process models in Chapter 3, two case studies have been implemented in this Chapter. Kennametal KB5625 low CBN tool insert is used for both case studies.

First case is to design tool geometry and select cutting conditions for inner ring outer diameter (OD) finish hard turning to achieve minimum cost per part and maximum production rate. The inner ring is made of hardened AISI 52100 steel with hardness 60 – 64 HRC. The optimal results for this case study showed its rationality by comparing with the other documented experimental and analytical work.

Second case is to optimize the finish hard turning of hardened AISI 1053 with hardness of 58 – 60 HRC. The main purpose of this case study is to check the validity of the developed methodology by experiment. In the evaluation, both optimal and other nine non-optimal conditions were performed experimentally. Cutting force, tool wear and surface roughness were monitored in the experiments. The prediction results for cutting force components and tool wear progression match the experimental results pretty well; however surface roughness prediction greatly deviates from the measured values. An empirical model was reestablished for surface roughness and the optimal result was obtained based on the reestablished surface roughness model. The predicted optimal results had distinguished to be optimal not only in the simulation but also in the

experiment. Hence the reliability and validity of the proposed methodology for hard turning process planning and optimization are proved experimentally.

It is also demonstrated that the proposed Mixed Integer Evolutionary Algorithm has excellent search capability and computational efficiency for the mixed-integer, highly constrained, highly non-linear, non-explicit, and not analytically differential optimization problems presented in hard turning process planning and optimization.

# CHAPTER V

# INTELLIGENT ADVISORY SYSTEM FOR HARD TURNING PROCESSES

## 5.1 Introduction

An intelligent advisory system, named IAS101, for hard turning process planning and optimization is developed as shown in Figure 5-1. The goal of the developed system is to consolidate all the accumulated knowledge and data (including experimental, numerical and analytical knowledge) gathered from the NIST-ATP Project entitled "Enabling Technologies for Lean Manufacturing of Critical Hardened Steel Applications" into one user-friendly software package with prediction and optimization functions which could be used to predict the hard turning process variables and to help run critical hard turning processes in an optimal manner given specific objectives and practical constraints.

The current Intelligent Advisory System has two modules: a prediction module and an optimization module. A training module and a database module are separated modules and have not been integrated into system yet. Some of the advantages of IAS101 are:

- simplicity and easy to use,

- running in a PC environment,
- a very short calculation time for both process prediction and optimization,
- allowing for the customized tool insert and workpiece material selection,
- allowing for the use of customized tool geometry and cutting conditions,
- predicting the hard turning process variables needed in practice, and
- generating the results in organized format and with graphics in case of predicted residual stresses' profiles (stress vs. depth).

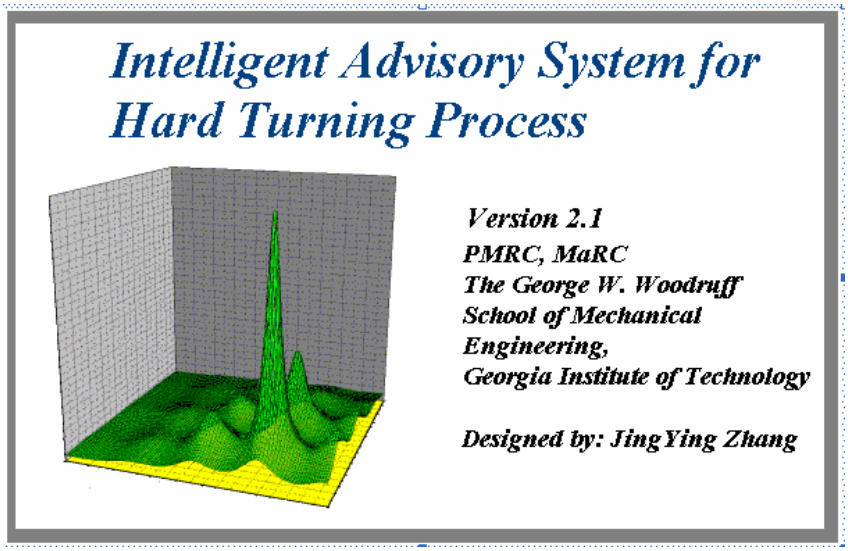


Figure 5-1 Intelligent Advisory System for Hard Turning Process

The functionality of the developed system is limited by the available knowledge and data. The current system could easily be extended to a more comprehensive system once more knowledge and data are accumulated to predict hard turning process

performance. In the mean time, IAS101's major functions have already been implemented for most commonly used workpiece materials and tool inserts.

## 5.2 Intelligent Advisory System

The structure of the IAS101 program is illustrated in Figure 5-2 and Figure 5-3. The program has two major functions: prediction and optimization. Input parameters for the prediction module are: tool insert grade (or user defined tool insert), workpiece material (or user defined workpiece material), wear coefficients for this combination of tool insert and workpiece material, tool geometry (insert nose radius, edge preparation, rake angle, and clearance angle), cutting condition (cutting speed, feed rate and depth of cut), process condition (length of cut, part diameter, number of part to be cut). The outputs from the prediction module are: cutting temperature, 3-D cutting force components, tool flank wear, surface roughness, white layer thickness, circumferential and longitudinal residual stress profiles.

The input parameters required for the optimization module are: tool insert grade (or user defined tool insert), workpiece material (or user defined workpiece material), wear coefficients for this combination of tool insert and workpiece material, process condition (length of cut, part diameter), boundary constraints for cutting condition, available tool geometry (the standard tool geometries from Kennametal tool catalog are listed in current IAS101 system), process requirements and practical constraints (including maximum allowable tool crater wear, tool flank wear, surface roughness, white layer thickness; available horsepower; required residual stress profiles), economic

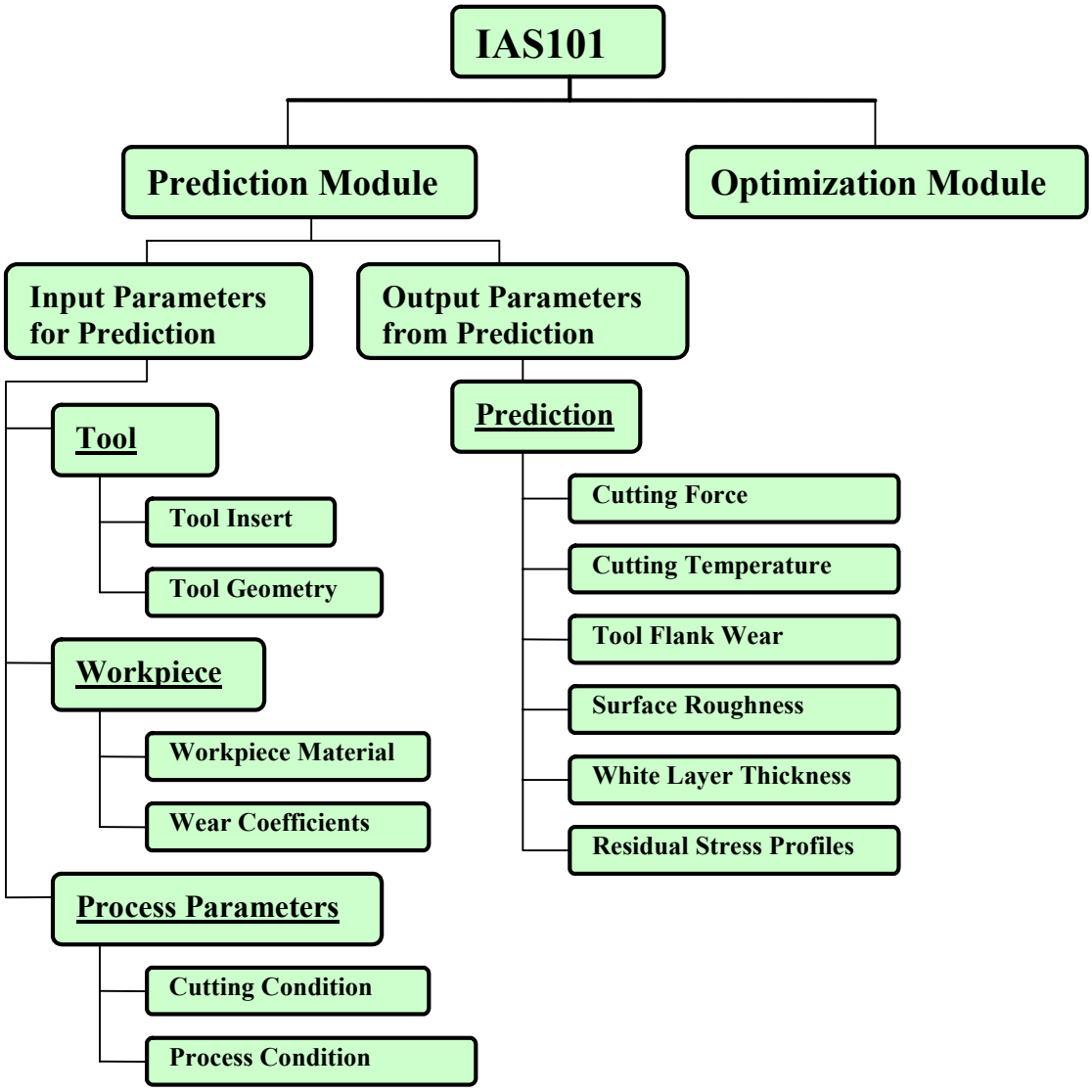


Figure 5-2 Flow chart for Intelligent Advisory System (prediction module)

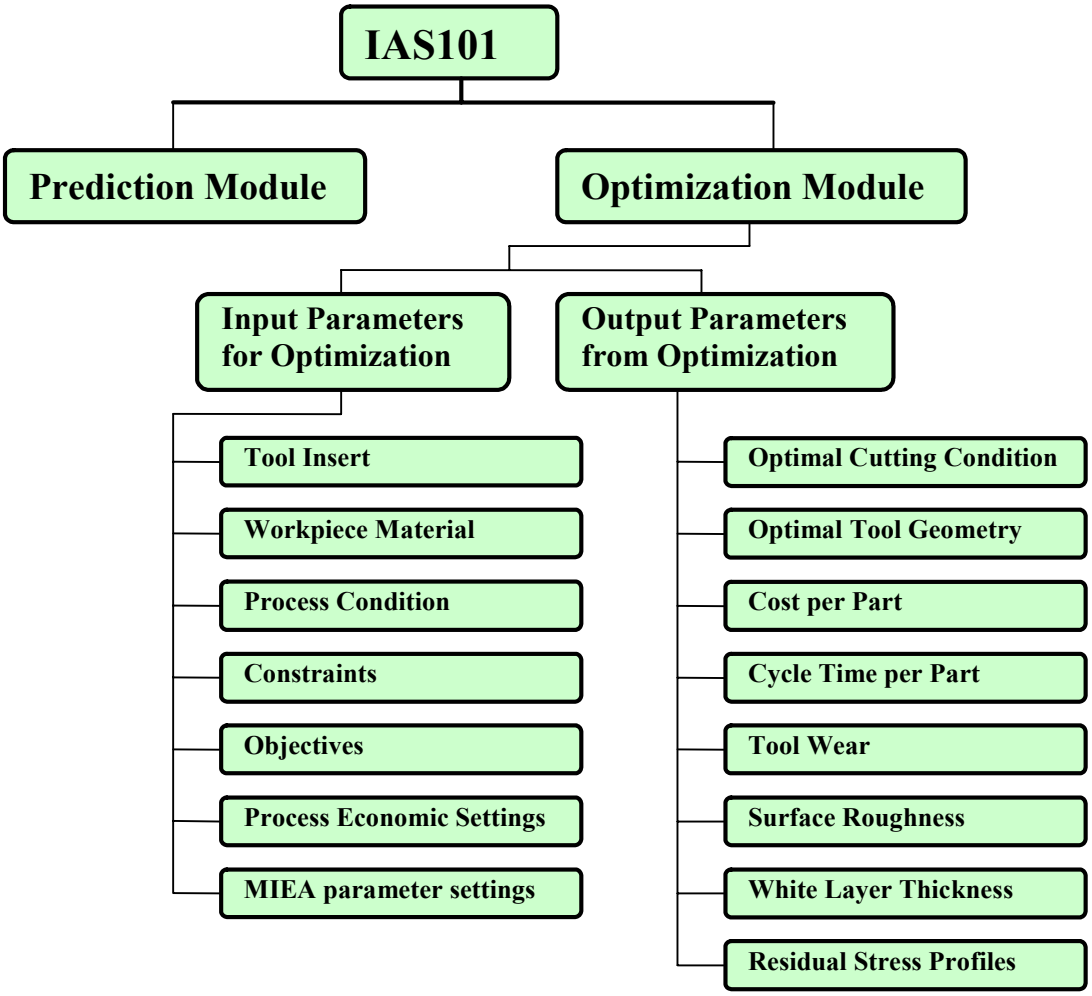


Figure 5-3 Flow chart for Intelligent Advisory System (optimization module)

parameter settings for specific hard turning process, parameter settings for mixed integer evolutionary algorithm.

Prediction module and optimization module in IAS101 will be elaborated in the following sections.

### 5.2.1 Prediction Module

Input parameters for prediction

There are two submenus under the Prediction Menu: Set Prediction Parameters and Predict. When Set Prediction Parameters is selected, a dialog as shown in Figure 5-4 will pop up for users to enter the input parameters for prediction.

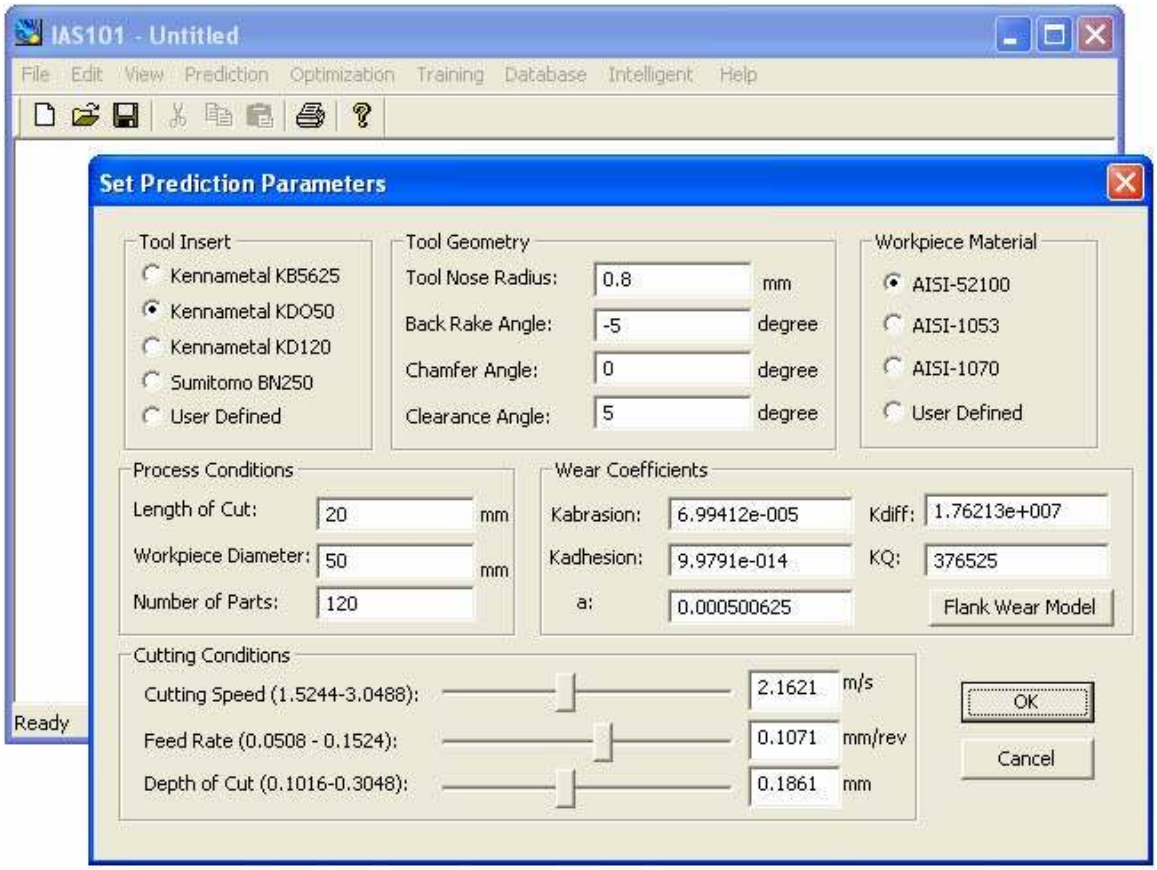


Figure 5-4 Dialog window to set prediction parameters for prediction module

The predefined tool inserts are limited to four:

- Kennametal KB5625 (coated low CBN 65%),
- Kennametal KD050 (low CBN 50%),
- Kennametal KD120 (high CBN 93%),
- Sumitomo BN250 (low CBN 60%) or

For other tool insert grades, "User Defined" tool should be selected from the dialog. After tool insert grade is selected or defined, tool geometry should be specified, including too nose radius, chamfer angle, back rake angle and clearance angle.

The user can choose one of three predefined workpiece materials (AISI-52100, AISI-1053, AISI-1070) available in the program or use a "User Defined" material in which the users are required to identify some material properties (specific heat, thermal conductivity, density, melting point, and Johnson-Cook parameters for Material Constitutive Equation) as shown in Figure 5-5.

Those three predefined workpiece materials are selected due to their widespread use and industrial significance, which are valid only for hardness values ranging from 58 to 62 HRC. Hardness properties and the chemical composition of the workpiece material are not explicitly specified but are reflected in the constitutive equation (the Johnson-cook equation). As a result, the Johnson-Cook parameters are uniquely determined by the specific workpiece material and hardness combination. Consequently, different Johnson-cook parameters might associate with the same workpiece material having a different hardness value.

The user should enter the coefficients ($K_{abrasion}$, $K_{adhesion}$, $K_{diff}$, $a$, $K_Q$) of the wear rate model as in Equation (3-24). They are required to calculate the tool flank wear

and are uniquely determined by the combination of the workpiece material and cutting tool materials. They could be determined from the machining tests.

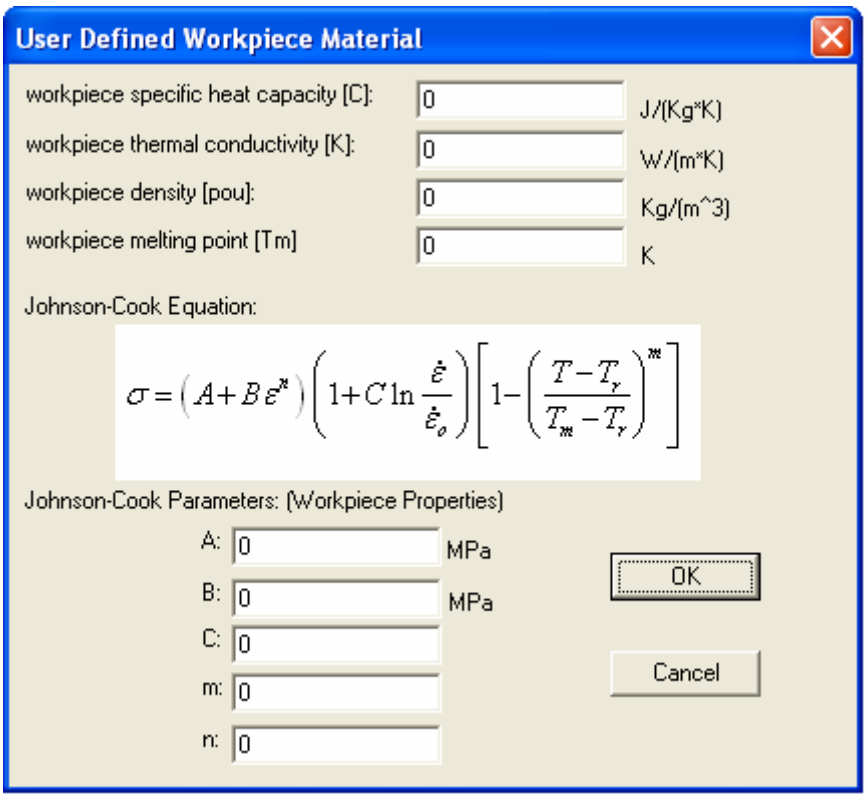


Figure 5-5 User defined workpiece material

In order to build up a comprehensive advisory system, a database could be further embedded into the system to store the calibrated wear coefficients for the specific workpiece and tool combinations. When the user selects a workpiece material and a tool insert, wear coefficients will be automatically extracted from the database.

After entering cutting tool and workpiece information, process parameters should be specified. The parameters include cutting conditions: cutting speed (m/s), feed rate (mm/rev), and depth of cut (mm) and process conditions: length of cut $L$ (mm), workpiece diameter $D$ (mm), and number of parts to be cut ($N$). Figure 5-6 and Figure 5-7 include definition for the cutting conditions and the process conditions.

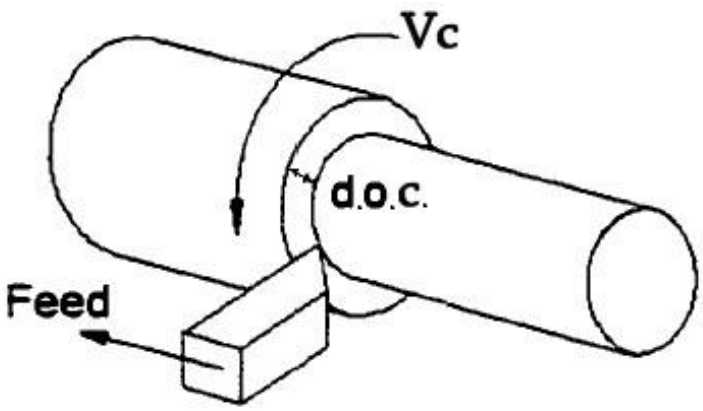


Figure 5-6 Cutting speed (Vc), feed rate (Feed), and depth of cut (doc) (After OSU report 2005)

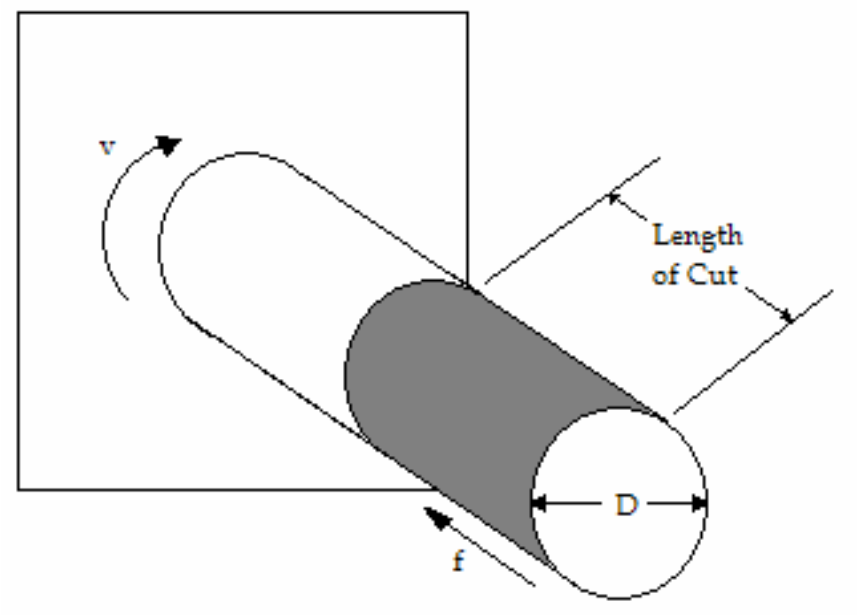


Figure 5-7 Definition of length of cut (L) and workpiece diameter (D) (after OSU internal report 2005)

With the process parameters defined, total cutting time can be computed as in Equation (5-1), which will be used in predicting tool flank wear in the system.

$$t_{m\_t} = \frac{\pi DL}{1000 f V_c} * N \tag{5-1}$$

Output parameters from prediction

After all the input parameters for prediction are defined, the user can select Predict to predict one process variable or all the process variables as listed in Figure 5-8. Cutting temperature, 3D oblique cutting force components, tool flank wear, surface

roughness and white layer thickness will be generated in the output window. An excel window will be automatically activated to display the circumferential and longitudinal residual stress profiles graphically at the end of computation. The outputs from the IAS101 system are shown in Figure 5-9 and 5-10 for all the process variables when input parameters are selected as in Figure 5-4.

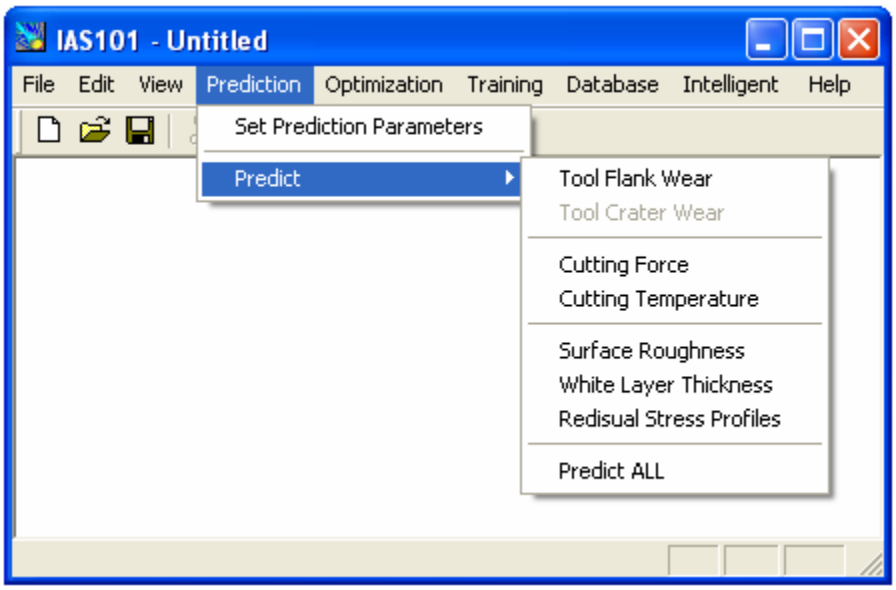


Figure 5-8 Selection menus for process prediction

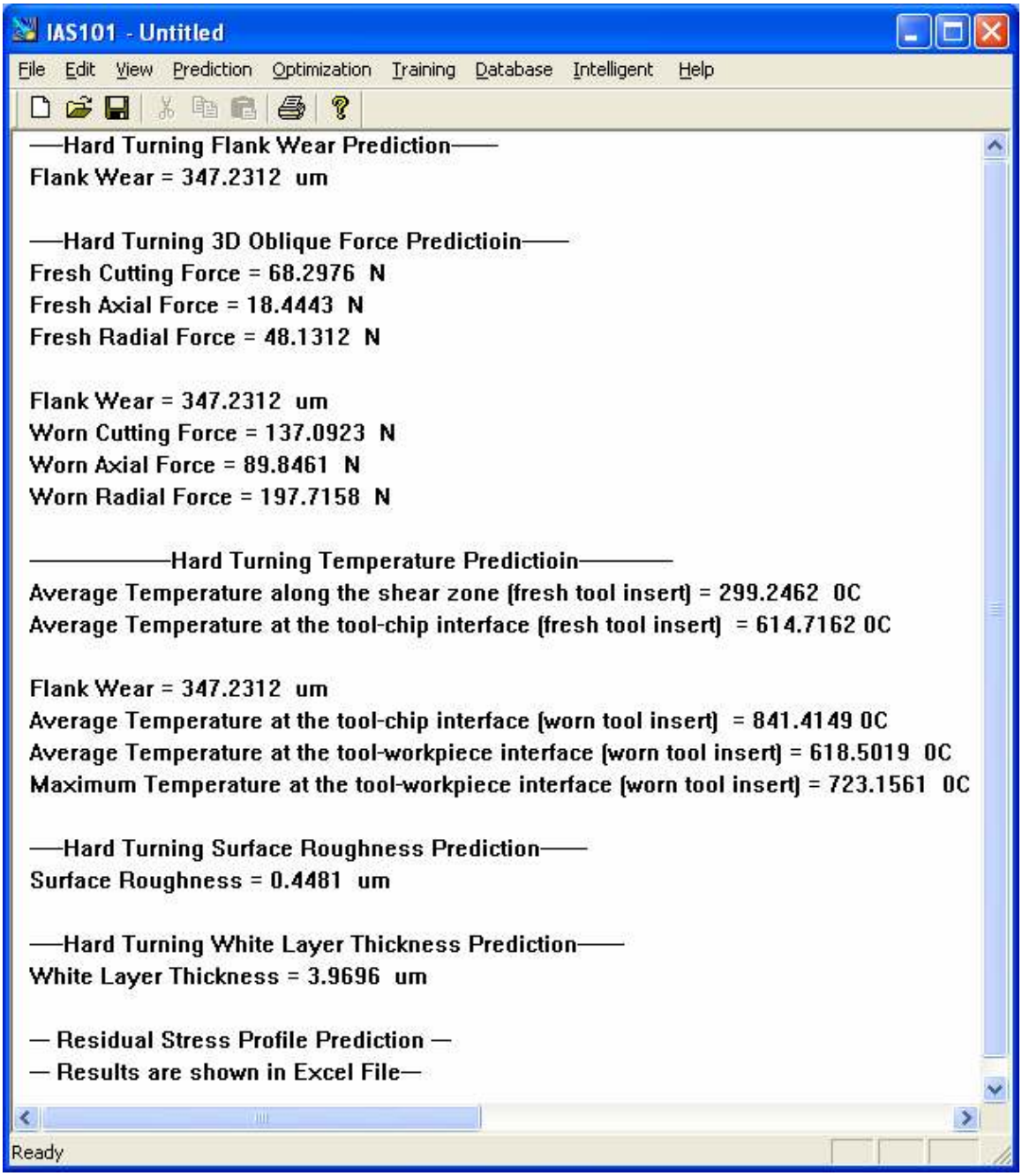


Figure 5-9 The output window for process prediction

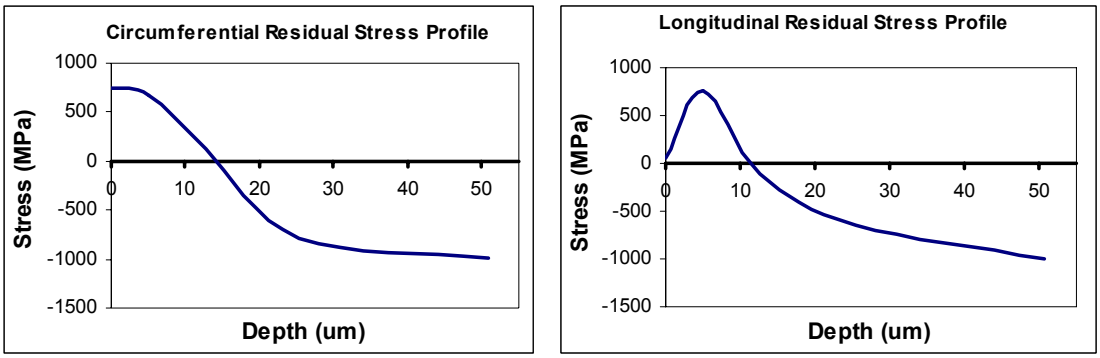


Figure 5-10 Residual stress profiles predicted from IAS101

### 5.2.2 Optimization Module

Input parameters for process optimization

There are two submenus under the Optimization Menu: Set Optimization Parameters and Optimize. When Set Optimization Parameters is selected, a dialog as shown in Figure 5-11 will pop up for users to enter the input parameters for process optimization.

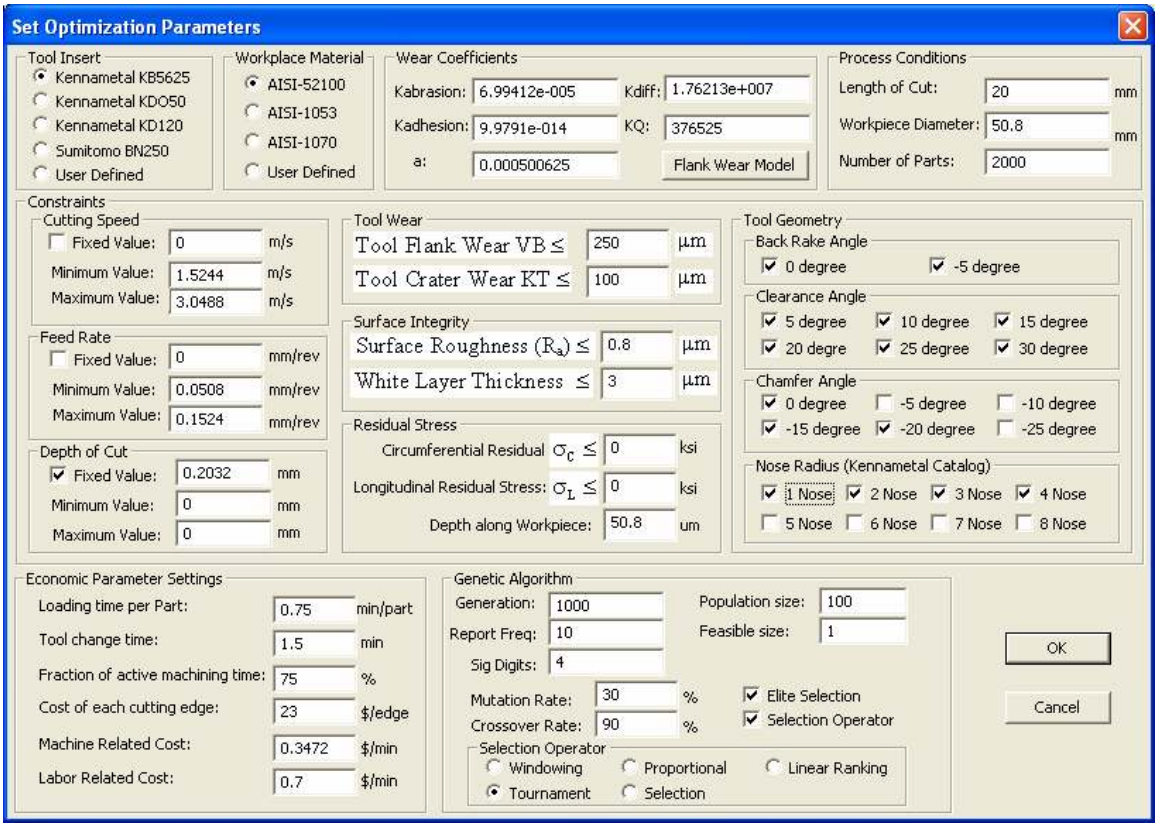


Figure 5-11 The dialog window to set optimization parameters for optimization module

The task of process planning and optimization is to design the tool geometry and optimize cutting conditions for given tool and workpiece materials in the current IAS101 system. Therefore cutting tool, workpiece material, the wear coefficients associated with this tool and workpiece combination should be specified as in the prediction module. Process conditions including length of cut, workpiece diameter should also be defined. The number of parts to be cut per insert can be fixed or can be a design variable determined based on the process objectives.

Cutting conditions including cutting speed, feed rate, and depth of cut can be fixed at certain values or can be selected as the design variables to be optimized. Lower bound and upper bound should be defined for each design variable. Similarly, tool geometry including tool nose radius, rake angle, chamfer angle, and clearance angle can be fixed at certain values or can be designed from available selections.

Other quality constraints including surface roughness, white layer thickness and residual stress profiles and practical constraints including maximum allowable tool flank wear and tool crater wear should be specified.

Process economic settings should be determined which are the basis for process planning and optimization. Those parameters include: loading time per part, tool change time, fraction of active machining time once loaded, cost of each cutting edge (some tool inserts have two cutting edges), machine related cost which is calculated based on the equipment cost and the associated investment loss and normalized in minutes, labor related cost which is calculated based on the average operator wage and the additional cost of non-salary benefits and normalized in minutes.

A Mixed Integer Evolutionary Algorithm as developed in Chapter 2 is embedded in IAS101 system as the optimization engine. MIEA related parameters should be entered. Default values are recommended for some of the parameter settings in Chapter 2. The algorithm parameters are defined as follows:

Generation: Total iteration numbers in finding the optimal solution

Population Size: The number of solutions in each generation

Feasible Size: The number of solutions enforced to be feasible in the initial

population, a value of "1" is recommended as its default setting

Report Freq: Report Frequency, how often the software will print out the result during the search (e.g. every 50 generations) so that the user can see the searching progress

Sig Digits: Significant Digits, the number of significant digits for each continuous variable

Mutation Rate: Mutation rate used in the genetic operator, 30% is recommended as its default value

Crossover Rate: Crossover rate used in the genetic operator, 90% is recommended as its default value

Selection Operator: Selection operator used in the algorithm, tournament selection with elite selection is set as its default setting.

The default settings for generation number and the population size are not given. The general guidelines for those two parameters are: for highly constrained problem, the population size should be set higher in order to distribute the initial population to the whole search space. And the generation number should be set according to the problem's difficulty degree.

Output parameters from optimization

After all the parameters for process optimization are defined in the "Set Optimization Parameters" window, the user can select Optimize for process optimization. First a dialog as shown in Figure 5-12 will pop up for users to select a process objective.

Currently only three objectives are included: Minimum cost per part, Maximum production rate or both of them based on a weighting function. However the system can be easily extended to integrate any process objectives, such as finest surface finish, longest tool life, and minimum white layer thickness.

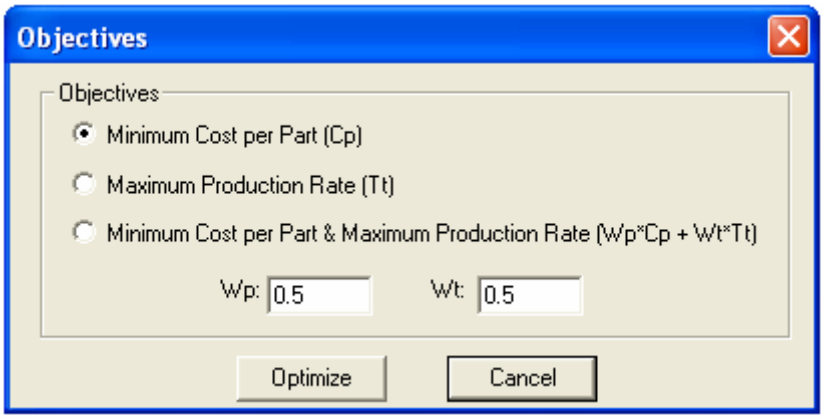


Figure 5-12 Dialog for process objective selection

The optimal cutting condition and tool geometry, number of part cut per insert, cost per part, cycle time per part, tool flank, surface roughness, and white layer thickness will be generated in the output window. An excel window will be automatically activated to display the circumferential and longitudinal residual stress profiles graphically at the end of simulation.

## 5.3 Conclusion and Discussion

An intelligent advisory system for hard turning process, named IAS101, has been developed with prediction and optimization functions. The developed system can help

predict the process variables and enable critical hard turning processes to run in optimal conditions based on specific objectives and practical constraints; ultimately it will greatly help the hard turning technology be a viable technology.

The developed Intelligent Advisory System offers a very good approach for hard turning process planning and optimization by integrating experimental, numerical and analytical knowledge into one system with user friendly interface. However current system is far from a comprehensive system, its functionality is partially implemented only. Additionally, the training module and the database module have not been integrated yet. Nevertheless, the current system could easily be extended to a more complete system once more knowledge and data are accumulated to predict hard turning process performance.

IAS101 has been rigorously evaluated by the ERC/NSM (the Engineering Research Center for Net Shape Manufacturing) research team of Ohio State University (Tapia *et al.* 2005) and the results are very reasonable.

# CHAPTER VI

# ACHIEVEMENTS AND RECOMMENDATION

## 6.1 Achievements

The objective of this dissertation is to enable critical hard turning processes to run in optimal conditions to ensure the economic and quality viability of the hard turning technology. Ultimately the goal is to help hard turning to be a successful alternative to grinding processes and to be widely adopted in industry. In order to achieve this goal, a scientific, systematic and reliable methodology is developed to guide the tool geometry design and to optimize the cutting conditions to achieve the specified process performance goals under the satisfactory surface integrity and any other practical constraints is developed. This section summarizes the achievements of this dissertation.

### 6.1.1 Summery and Conclusion

Background, motivation and objective of the focused research are introduced in Chapter 1. The characteristics of the hard turning process are summarized there. The optimization techniques which have been applied in the machining process optimization are reviewed. The underlying drawbacks about the existing optimization algorithms are discussed and the motivation for further research on extension and implementation of the

optimization algorithm are addressed. Efforts to design optimal tool geometry and cutting condition for machining processes are also briefly reviewed.

Chapter 2 and Chapter 3 are the major foundation of this dissertation. In Chapter 2, a general form of machining process optimization is mathematically formulated and its related terminologies are defined; then the proposed Mixed Integer Evolutionary Algorithm (MIEA) is elaborated in the areas of problem representation; selection scheme; genetic operators for integer, discrete, and continuous variables; constraint handling method; and population initialization. The improved algorithm has been successfully applied to twelve numerical cases and two machining problems. The best solutions found for twelve numerical cases are all very close to the known global optimum (except the test case G9) and are located within a very short computational time. The proposed constraint handling scheme outperforms most of the other methods reviewed by Michaelwicz (1996). It has also demonstrated higher performance and higher computational efficiency than the other optimization methods when applied to those two machining process problems.

In Chapter 3, hard turning process models - including the thermal model, 3-D oblique cutting force model, tool wear rate model and surface integrity models (surface roughness, white layer thickness, and residual stress profiles) - are addressed. Average temperatures along rake face and flank face are calculated considering the tool wear effects. 3-D oblique cutting forces are modeled by taking the modified Oxley's machining theory and the Waldorf's worn tool force model as its kernel. A unified approach in modeling the CBN tool flank wear rate developed by Huang is used to

estimate the tool flank wear progression in hard turning. Surface roughness is determined by feed rate and tool nose radius. Intelligent models for the white layer thickness and residual stress distribution are constructed from the experimental data based on Back Propagation Neural Networks. Some of the models are experimentally calibrated and verified in machining hardened AISI 1053 (hardness 58 - 60 HRC) using Kennametal KB5625 low CBN tools.

Based on the developed optimization algorithm in Chapter 2 and hard turning process models in Chapter 3, two hard turning process optimization cases are implemented in Chapter 4. The first case is to design the optimal tool geometry (back rake angle, chamfer angle, clearance angle and tool nose radius) and cutting conditions (cutting speed and federate) to achieve minimum cost per part and maximum production rate in outer diameter finish turning of hardened AISI 52100 under the constraints of the required surface integrity (including surface roughness, white layer thickness, and residual stress distribution), maximum allowable tool flank wear and available horsepower. The optimal results for this case showed its rationality by comparing with the other documented experimental and analytical work. The main purpose of the second case is to check and establish the validity of the developed methodology for hard turning process optimization by experiment. The objective is to optimize the finish hard turning of hardened AISI 1053 to achieve maximum material removal rate, minimum tool wear and best surface finish (considering surface roughness only) after turning 100 passes. The predicted optimal design is compared with the other eight non-optimal designs experimentally and distinguishes itself to be optimal not only in the simulation but also in

the experiment. Hence the reliability and validity of the proposed methodology for hard turning process planning and optimization are proved.

An intelligent advisory system for hard turning process, named IAS101, has been introduced in Chapter 5. It has a prediction module and an optimization module. The developed system offers a very useful tool for hard turning process planning and optimization by integrating experimental, numerical and analytical knowledge into one system with user friendly interface. It can help predict the process variables, and it enables critical hard turning processes to run in optimal conditions based on the specified objectives and the practical constraints; ultimately it will help the hard turning technology to be a viable technology.

Chapter 6 is a concluding section of this dissertation. First, a summery is outlined for each chapter in this dissertation. Then achievements of this dissertation are listed and recommendations to further improve state of the arts of the focused research are given.

### 6.1.2 Achievements

This dissertation provides a scientific, systematic and reliable methodology for hard turning process planning and optimization. The proposed methodology improves the state of the art in making tooling solution and process planning decisions for hard turning processes. Furthermore, the proposed methodology can be easily extended to today's complex manufacturing process planning and optimization. The main achievements in this dissertation are listed as follows:

On Optimization Algorithm (Chapter 2)

- Developed adaptive mutation and crossover operators in dealing with integer/discrete design variables to implement a one-gene-one-variable scheme for mixed-integer optimization problems in GA
- Developed a feasible superior and problem-independent constraint handling method in GA to drive search toward the optimal and feasible direction
- Proposed an $(\alpha, \mu)-$population initialization scheme to help distribute the initial population uniformly in the whole search space
- Implemented a systematic optimization algorithm (Mixed Integer Evolutionary Algorithm) based on GA which addresses the underlying drawbacks of GA in solving hard turning process optimization problems

On Hard Turning Process Models (Chapter 3)

- Implemented a 3-D oblique cutting force model under practical hard turning conditions to provide high fidelity process thermal and stress information
- Constructed intelligent models based on BPNN to take advantage of the experimental knowledge for white layer thickness and residual stress prediction

- Proposed a hierarchical modeling structure which consists of analytical models and BPNN models to predict white layer thickness and residual stress profiles
- Identified the machinability and material properties for hardened AISI 1053 steels experimentally

On Hard Turning Process Planning and Optimization (Chapter 4)

- Implemented an analytical approach to guide the tool geometry design and the cutting condition selection based on the specified objectives and the practical constraints
- Experimentally verified the developed methodology for hard turning process planning and optimization

On System Development and Integration (Chapter 5)

- Developed an Intelligent Advisory System for hard turning process with a user friendly interface; experimental, numerical and analytical knowledge are consolidated in one system with prediction and optimization functions

## 6.2 Recommendations for Future Work

The developed methodology and implemented system could be further improved. Recommendations for future work are given as follows:

*Probability and uncertainty*

The hard turning process, as well as the general machining process, is not a deterministic process but a process with certain probabilities and uncertainties. Such probability and uncertainty characteristics should be carefully addressed in the process models and integrated in process planning and optimization. For example, the prediction from a model can be an average value plus a certain degree of standard deviation instead of a deterministic value.

*Model improvement*

Hard turning process models provide indispensable process information for process planning and optimization. The selected/developed models have been integrated in the Intelligent Advisory System. The prediction capabilities of the Intelligent Advisory System (IAS101) have been rigorously evaluated by the ERC/NSM (the Engineering Research Center for Net Shape Manufacturing) research team of Ohio State University (Tapia *et al.* 2005). The future improvement for the process models can be given based on this evaluation:

The experimental results from Dawson (2002), Ramesh (2002), Huang (2002), Thiele (2002), and Chou (2004), (with total 36 experimental sets), are used to evaluate IAS101's capability to predict the cutting force. Average prediction errors from IAS101 for all 3D fresh and worn cutting forces are within 15%. Maximum errors up to 35% occur when small values of feed rate and depth of cut were used. The total cutting force consists of three components: force due to chip formation, force due to ploughing and force due to sliding (which is the force due to tool flank wear). However force due to ploughing is assumed to be negligible in this study.

A cutting tool with large nose radius and large negative chamfer angle is commonly used in hard turning, when feed rate and depth of cut are relatively small; the ploughing effect is rather pronounced and contributes a significant portion of the total cutting forces. The prediction accuracy could be further improved; the force components due to ploughing should be carefully addressed for those situations when small values of feed rate and depth of cut are used.

BPNN models for white layer formation and residual stress distribution were trained based on the limited experimental data. Unavoidably, those experimental data contained a large amount of noise. Overfitting is very likely to happen in the training process when one wants to train an over-sized neural network with a limited supply of data. The problem becomes even worse for data with a large amount of noise. The overfitting is that when the error on the training set has been minimized to a very small value, but the established model performs poorly on the unknown data (Mathwork 2002). A regulation technique should be integrated in the training process to improve the model's generation capability.

During the experimental verification for the proposed optimization scheme in Section 4.3, the measured surface roughness values greatly deviated from the model prediction and the variation of surface roughness with the progression of tool wear varied from case to case. A rough empirical model was reestablished in order for predicted values to match the measured results better. A comprehensive surface roughness model should be constructed which is able to compensate the effects for special cutting

condition and tool geometry in the hard turning and to account for its variation with the tool wear.

*Intelligent Advisory System*

In this study, all the accumulated knowledge was integrated to one system, which provides a very useful tool to make the tooling solutions and process planning decisions. However significant efforts should be further devoted to complete this system.

Currently, the system only has a prediction module and an optimization module, a training module and a database module should be further integrated to the system and to be linked together. Hence the system could not only serve for off-line optimization but also for on-line optimization. When more experimental data or practical data are available, they will be stored in the database. The training module will be automatically triggered whenever there is more data/knowledge available, and the prediction module will be updated. Process planning decisions will be made based on the updated prediction models. Such a system could also serve as an adaptive control system to achieve the best process performance for any particular hard turning process.

The functionality of the developed system is partially implemented; process models have not been available to all the commonly used tool inserts and workpiece material in hard turning application yet. More experiments/knowledge should be performed/accumulated in order to have a comprehensive advisory/expert system for practical hard turning applications and to eventually help hard turning technology to be a viable technology.

# APPENDIX A

# TEST CASES

## A.1 Twelve Numerical Cases (Michalewicz and Schoenauer 1996)

G1:

Minimize:

$$G1(X) = 5x_1 + 5x_2 + 5x_3 + 5x_4 - 5\sum_{i=1}^{4} x_i^2 - \sum_{i=5}^{13} x_i$$

Where: $0 \le x_i \le 1,\ i = 1,...,9;\ 0 \le x_i \le 100,\ i = 10,11,12;\ 0 \le x_{13} \le 1;$

$2x_1 + 2x_2 + x_{10} + x_{11} \le 10\ ;\ 2x_1 + 2x_3 + x_{10} + x_{12} \le 10\ ;$

$2x_2 + 2x_3 + x_{11} + x_{12} \le 10;\ -8x_1 + x_{10} \le 0;\ -8x_2 + x_{11} \le 0\ ;\ -8x_3 + x_{12} \le 0\ ;$

$-2x_4 - x_5 + x_{10} \le 0\ ;\ -2x_6 - x_7 + x_{11} \le 0\ ;\ -2x_8 - x_9 + x_{12} \le 0$

The problem has its global minimum at: $X^* = \{1,1,1,1,1,1,1,1,1,3,3,3,1\}$,

where $G1(X^*) = -15$.

**G2:**

Minimize:

$$G2(X) = x_1 + x_2 + x_3$$

Where: $100 \le x_1 \le 10000;\ 1000 \le x_i \le 10000,\ i = 2,3;\ 10 \le x_i \le 1000,\ i = 4,...8;$

$1 - 0.0025(x_4 + x_6) \ge 0;\ 1 - 0.0025(x_5 + x_7 - x_4) \ge 0;\ 1 - 0.01(x_8 - x_5) \ge 0;$

$x_1 x_6 - 833.33252 x_4 - 100 x_1 + 83333.333 \ge 0$;

$x_2 x_7 - 1250 x_5 - x_2 x_4 + 1250 x_4 \ge 0;\ x_3 x_8 - 1250000 - x_3 x_5 + 2500 x_5 \ge 0$

The problem has its global minimum at:

$X^* = \{579.3167, 1359.943, 5110.071, 182.0174, 295.5985, 217.9799, 286.4162, 395.5979\}$,

where $G2(X^*) = -7049.330923$.

**G3:**

Minimize:

$$G3(X) = (x_1 - 10)^2 + 5(x_2 - 12)^2 + x_3^4 + 3(x_4 - 11)^2 + 10 x_5^6 + 7 x_6^2 + x_7^4 - 4 x_6 x_7 - 10 x_6 - 8 x_7$$

Where: $-10 \le x_i \le 10,\ i = 1,...7;$

$127 - 2x_1^2 - 3x_2^4 - x_3 - 4x_4^2 - 5x_5 \ge 0;\ 282 - 7x_1 - 3x_2 - 10x_3^2 - x_4 + x_5 \ge 0;$

$196 - 23x_1 - x_2^2 - 6x_6^2 + 8x_7 \ge 0;\ -4x_1^2 - x_2^2 + 3x_1 x_2 - 2x_3^2 - 5x_6 + 11x_7 \ge 0$

The problem has its global minimum at:

$X^* = \{2.330499, 1.951372, -0.4775414, 4.365726, -0.6244870, 1.038131, 1.594227\}$,

where $G3(X^*) = 680.6300573$.

**G4:**

Minimize:

$$G4(X) = e^{x_1 x_2 x_3 x_4 x_5}$$

Where: $-2.3 \le x_i \le 2.3,\ i = 1,2;\ -3.2 \le x_i \le 3.2,\ i = 3,4,5;$

$$x_1^{\,2} + x_2^{\,2} + x_3^{\,2} + x_4^{\,2} + x_5^{\,2} = 10\,;\ x_2 x_3 - 5x_4 x_5 = 0;\ x_1^{\,3} + x_2^{\,3} = -1$$

The problem has its global minimum at:

$X^* = \{-1.717143, 1.595709, 1.827247, -0.7636413, -0.7636450\}$,

where $G4(X^*) = 0.0539498478$.

**G5:**

Minimize:

$$\begin{aligned} G5(X) = {} & x_1^{\,2} + x_2^{\,2} + x_1 x_2 - 14x_1 - 16x_2 + (x_3 - 10)^2 + 4(x_4 - 5)^2 + (x_5 - 3)^2 \\ & + 2(x_6 - 1)^2 + 5x_7^{\,2} + 7(x_8 - 11)^2 + 2(x_9 - 10)^2 + (x_{10} - 7)^2 + 45 \end{aligned}$$

Where: $-10 \le x_i \le 10,\ i = 1,\ldots 10;$

$$105 - 4x_1 - 5x_2 + 3x_7 - 9x_8 \ge 0\,;$$

$$-3(x_1 - 2)^2 - 4(x_2 - 3)^2 - 2x_3^{\,2} + 7x_4 + 120 \ge 0\,;\ -10x_1 + 8x_2 + 17x_7 - 2x_8 \ge 0;$$

$$-x_1^2 - 2(x_2 - 2)^2 + 2x_1x_2 - 14x_5 + 6x_6 \geq 0\,;\; 8x_1 - 2x_2 - 5x_9 + 2x_{10} + 12 \geq 0;$$

$$-5x_1^2 - 8x_2 - (x_3 - 6)^2 + 2x_4 + 40 \geq 0;$$

$$3x_1 - 6x_2 - 12(x_9 - 8)^2 + 7x_{10} \geq 0;$$

$$-0.5(x_1 - 8)^2 - 2(x_2 - 4)^2 - 3x_5^2 + x_6 + 30 \geq 0;$$

The problem has its global minimum at:

$$X^* = \{2.171996, 2.363683, 5.095984, 0.9906548,$$
$$1.430574, 1.321644, 9.828726, 8.280092, 8.375927\}'$$

where $G5(X^*) = 24.3062091$.

**G6:**

Maximize:

$$G6(X) = \left| \frac{\sum_{i=1}^{n} \cos^4(x_i) - 2\prod_{i=1}^{n} \cos^2(x_i)}{\sqrt{\sum_{i=1}^{n} i x_i^2}} \right|$$

Where: $0 < x_i < 10\,,\; i = 1, \ldots, n$

$$\prod_{i=1}^{n} x_i > 0.75\,;\; \sum_{i=1}^{n} x_i < 7.5n$$

The function G6's global maximum if unknown. For $n = 20$ (G6-1), the best solution found in this work is $G6(X^*) = 0.80361664$ with

$X^* = \{3.16043258, 3.12754512, 3.09359360, 3.06049466, 3.02768564, 2.99235296, 2.95944715, 2.92219949, 0.49483365, 0.48731905, 0.48034167, 0.47483969, 0.47307324, 0.46573946, 0.46269602, 0.45579949, 0.45373166, 0.44978923, 0.44504631, 0.44064420\}$

For $n = 50$ (G6-2), the best solution found in this work is $G6(X^*) = 0.83520228$ with

$X^* = \{6.28234386, 3.16757345, 3.15456867, 3.14324331, 3.12941480, 3.11366415, 3.10167003, 3.08602786, 3.07424927, 3.06255317, 3.04743624, 3.03712273, 3.02034664, 3.00651383, 3.00001884, 2.97560692, 2.96612120, 2.95461059, 2.93431211, 2.92233706, 0.49643144, 0.48006836, 0.49415991, 0.46941942, 0.47801661, 0.47702739, 0.47604510, 0.47386724, 0.47658002, 0.46413743, 0.47684807, 0.46653312, 0.47030780, 0.45434538, 0.45569429, 0.45161772, 0.45535612, 0.44744486, 0.45442498, 0.44980237, 0.44996986, 0.45574158, 0.44432029, 0.44588098, 0.43479106, 0.44538400, 0.45508292, 0.44191003, 0.44009739, 0.43020955\}$

**G7:**

Maximize:

$$G7(X) = \left(\sqrt{n}\right)^n \prod_{i=1}^{n} x_i$$

Where: $0 \le x_i \le 1,\ i = 1, \ldots, n;$

$$\sum_{i=1}^{n} x_i^2 = 1$$

n = 20 is used in this paper. The problem has its global maximum at: $X^* = \{\frac{1}{\sqrt{n}},...,\frac{1}{\sqrt{n}}\}$,

where $G7(X^*) = 1$.

**G8:**

Minimize:

$$G8(X) = 5.3578547x_3^{\ 2} + 0.8356891x_1x_5 + 37.293239x_1 - 40792.141$$

Where: $78 \le x_1 \le 102,\ 33 \le x_2 \le 45,\ 27 \le x_i \le 45,\ i = 3,4,5;$

$$0 \le 85.334407 + 0.0056858x_2x_5 + 0.0006262x_1x_4 - 0.0022053x_3x_5 \le 92;$$

$$90 \le 80.51249 + 0.0071317x_2x_5 + 0.0029955x_1x_2 + 0.0021813x_3^{\ 2} \le 110;$$

$$20 \le 9.300961 + 0.0047026x_3x_5 + 0.0012547x_1x_3 + 0.0019085x_3x_4 \le 25$$

The problem has its global minimum at: $X^* = \{78.0, 33.0, 29.995, 45.0, 36.776\}$,

where $G8(X^*) = -30665.5$.

**G9:**

Minimize:

$$G9(X) = 3x_1 + 0.000001x_1^{\ 3} + 2x_2 + 0.000002/3x_2^{\ 3}$$

Where: $0 \le x_i \le 1200,\ i = 1,2;$ $-0.55 \le x_i \le 0.55,\ i = 3,4;$

$$x_4 - x_3 + 0.55 \geq 0\,;\;\; x_3 - x_4 + 0.55 \geq 0\,;$$

$$1000\sin(-x_3 - 0.25) + 1000\sin(-x_4 - 0.25) + 894.8 - x_1 = 0\,;$$

$$1000\sin(x_3 - 0.25) + 1000\sin(x_3 - x_4 - 0.25) + 894.8 - x_2 = 0$$

$$1000\sin(x_4 - 0.25) + 1000\sin(x_4 - x_3 - 0.25) + 1294.8 = 0$$

The problem has its global minimum at:

$X^* = \{679.9453, 1026.067, 0.1188764, -0.3962336\}$ , where $G9(X^*) = 5126.4981$ .

**G10:**

Minimize:

$$G10(X) = (x_1 - 10)^3 + (x_2 - 20)^3$$

Where: $13 \leq x_1 \leq 100;\; 0 \leq x_2 \leq 100;$

$$(x_1 - 5)^2 + (x_2 - 5)^2 - 100 \geq 0;\;\; -(x_1 - 6)^2 - (x_2 - 5)^2 + 82.81 \geq 0\,;$$

The problem has its global minimum at: $X^* = \{14.095, 0.84296\}$ ,

where $G10(X^*) = -6961.81381$ .

**G11:**

Maximize:

$$G11(X) = \frac{\sin^3(2\pi x_1)\sin(2\pi x_2)}{x_1^3(x_1 + x_2)}$$

Where: $0 \le x_1 \le 10;\ 0 \le x_2 \le 10;$

$$x_1^2 - x_2 + 1 \le 0;\ 1 - x_1 + (x_2 - 4)^2 \le 0$$

The problem has its global maximum with $G11(X^*) = 0.095825$.

**G12:**

Minimize:

$$G12(X) = x_1^2 + (x_2 - 1)^2$$

Where: $-1 \le x_i \le 1,\ i = 1, 2;$

$$x_2 - x_1^2 = 0$$

The problem has its global minimum at: $X^* = \{\pm 0.70711, 0.5\}$,

where $G12(X^*) = -0.75000455$.

## A.2 A Unified Metal Cutting Problem (Jang D. Y. 1992)

Dimensional accuracy:

$$\delta = 100.66 f^{0.9707} d^{0.4905} V^{-0.2848} \tag{A-1}$$

Compressive surface residual stress:

$$\sigma_c = -2284.32 f^{0.7525} d^{-0.1797} V^{-0.3962} R^{-0.3828} \tag{A-2}$$

Maximum depth with compressive residual stress:

$$d_c = 0.1739 f^{0.67205} d^{-0.05849} V^{0.0909} R^{0.31652} \tag{A-3}$$

Peak to valley surface roughness:

$$h_{\max} = 124.3 f^2 / R \tag{A-4}$$

Flank wear rate caused by adhesion:

$$L_1 = 0.0792 \times 10^{-6} \times V (25 + 13 V L^{0.25})^{0.055} \tag{A-5}$$

Flank wear rate caused by diffusion:

$$L_2 = 0.137 \times 10^6 \times V \exp(-20000/(298 + 13VL^{0.25}))L^{-0.5} \quad \text{(A-6)}$$

Crater wear temperature:

$$T_c = 457.44V^{0.2761} f^{0.2874} d^{-0.0217} \quad \text{(A-7)}$$

Tool tensile stress:

$$\sigma_1 = 0.3875 f^{1.3466} V^{1.3610} \quad \text{(A-8)}$$

Plastic deformation temperature of the tool:

$$T_{pz} = 453.53V^{-0.036} f^{-0.0376} d^{0.0025} \quad \text{(A-9)}$$

## A.3 A Generalized Surface Grinding Problem (Lee 2000)

Surface Roughness:

$$R_a = R_0 {s_d}^x {a_d}^y \left(\frac{v_w}{v_s}\right)^z \left(\frac{s_t}{b_s}\right)^\gamma \quad \text{(A-10)}$$

$R_0$, x, y, z, $\gamma$ are determined from the experiment, where: $R_0 = 12.9$, $x = 0.54$, $y = 0.34$, $z = 0.38$, $\gamma = 0.43$

Grinding Force and Power:

$$P = F_t v_s \tag{A-11}$$

$$F_t = \mu_{ch} \frac{v_w a}{v_s} + \mu p_1 A \left( \frac{4 v_w}{d_s v_s} \right) (a d_s)^{1/2} \tag{A-12}$$

$$p_1 A = p_1 A_i + P_l l^c \tag{A-13}$$

$$p_1 A_i = P_0 - P_1 \ln(a_d) \tag{A-14}$$

$$l = \frac{v_s l_g}{2\pi d_s v_w} (a d_s)^{1/2} \tag{A-15}$$

$$l_g = (L_w + L_e) * n * \left( \frac{b_w + b_e}{s_t} \right) * N_d \tag{A-16}$$

Where: $P_l$, $c$ are 0.0143 and 2.86 respectively. $\mu$, $P_0$, $P_1$ are determined from the experiment, they are $\mu = 0.43$, $P_0 = 65600$, $P_1 = 10300$, $l$ is the sliding length.

Residual Stress:

$$\sigma_r = R_1 e^r \tag{A-17}$$

where: $e = \frac{F_t v_s}{v_w}$, $R_1$, $r$ are determined from the experiment, where: $R_1 = 6.8$, $r = 0.63$

G Ratio:

$$G = G_1 h_{eq}^{-g} \tag{A-18}$$

$G_1$, $g$ are determined from the experiment, where: $G_1 = 13.0$, $g = 0.90$

| Symbol | Definition |
|---|---|
| $a_d$ | Dressing depth, ( $\mu$m ) |
| $A$ | Fraction of flat area on the grinding wheel |
| $A_i$ | Initial fraction of flat area on the grinding wheel |
| $c$ | Constant |
| $F_t$ | Tangential grinding force, (N) |
| $g$ | Exponent for G-ratio model |
| $G_1$ | Constant for the G-ratio model |
| $h_{eq}$ | Equivalent chip thickness, ( $\mu m$ ) |
| $L$ | Maximum permissible wear land length |
| $l$ | Accumulated sliding length after dressing, (m) |
| $p_1$ | Constant for the contact stress |
| $P_0$, $P_1$ | Constants for the force model |

| | |
|---|---|
| $P_l$ | Constant |
| $r$ | Constant for the residual stress model |
| $R_0$ | Constant for the surface roughness model |
| $R_1$ | Constant for the residual stress model |
| $x$ , $y$ , $z$ | Exponent for the surface roughness model |
| $\delta$ | Exponent for the surface roughness model |
| $\gamma$ | Exponent for the surface roughness model |
| $\mu$ | Friction coefficient |
| $\mu_{ch}$ | Chip formation energy ($J/mm^3$) |

# APPENDIX B

## MODIFIED OXLEY'S MACHINING THEORY (OXLEY 1989)

Based on the geometric model in orthogonal cutting as shown in Figure B-1, the chip thickness $t_c$, length of shear zone $l$, shear velocity $V_s$ and chip velocity $V_{chip}$ can be obtained as in Equation (B-1), where shear angle $\phi$ will need to be determined iteratively as explained later, $t$ is the undeformed chip thickness, $\alpha$ is the effective rake angle, $V_c$ is the cutting speed.

$$\begin{aligned} t_c &= \frac{t\cos(\phi-\alpha)}{\sin\phi} \\ l &= \frac{t}{\sin\phi} \\ V_s &= V_c\frac{\cos\alpha}{\cos(\phi-\alpha)} \\ V_{chip} &= V_c\frac{\sin\phi}{\cos(\phi-\alpha)} \end{aligned} \tag{B-1}$$

The shear strain $\gamma_{AB}$, shear strain rate $\dot{\gamma}_{AB}$ and their effective strain $\varepsilon_{AB}$ and strain rate $\dot{\varepsilon}_{AB}$ along the shear zone AB is computed as in Equation (B-2), where strain rate constant $c$ will need to be determined iteratively as explained later.

$$\gamma_{AB} = \frac{1}{2}\frac{\cos\alpha}{\sin\phi\cos(\phi-\alpha)},\ \dot{\gamma}_{AB} = c\frac{V_s}{l}$$
$$\varepsilon_{AB} = \frac{\gamma_{AB}}{\sqrt{3}},\ \dot{\varepsilon}_{AB} = \frac{\dot{\gamma}_{AB}}{\sqrt{3}} \tag{B-2}$$

Temperature along the shear zone AB is estimated as

$$T_{AB} = T_0 + \eta\Delta T_{SZ} \tag{B-5}$$

The shear flow stress along *AB* can be calculated from the Johnson-Cook equation:

$$k_{AB} = \frac{\sigma_{AB}}{\sqrt{3}} = \frac{1}{\sqrt{3}}\left(A + B\varepsilon_{AB}^{n}\right)\left(1 + C\ln\frac{\dot{\varepsilon}_{AB}}{\dot{\varepsilon}_o}\right)\left(1 - \left(\frac{T_{AB} - T_r}{T_m - T_r}\right)^m\right) \tag{B-3}$$

Thus the shear force along *AB* can be obtained accordingly, where $w$ is width of cut.

$$F_S = k_{AB} l w \tag{B-4}$$

The angle between the resultant cutting force R and shear zone AB is given as below referring to (Huang 2002):

$$\theta = \tan^{-1}\left(1 + 2(\frac{\pi}{4} - \phi) - \frac{c\gamma_{AB} I}{k_{AB}}\right) \tag{B-6}$$

Based on the geometric model, the friction angle can be obtained as:

$$\beta = \theta + \alpha - \phi \tag{B-7}$$

Now referring to the cutting force circle as shown in Figure B-1, the resultant force $R$, friction force $F$ along the tool chip interface, normal force $N$ perpendicular to it, cutting force $F_C$ and thrusting force $F_Q$ all can be calculated with known shear force $F_S$ and force angles as:

$$\begin{aligned} R &= F_S / \cos\theta \\ F &= R / \sin\beta \\ N &= R / \cos\beta \\ F_C &= R\cos(\beta - \alpha) \\ F_Q &= R\sin(\beta - \alpha) \end{aligned} \tag{B-8}$$

With knowing $k_{AB}$, the normal stress on the tool face at B can be given by:

$$\sigma_N^{'} = k_{AB}\left(1 + \frac{\pi}{2} - 2\alpha - \frac{2c\gamma_{AB}I}{k_{AB}}\right) \tag{B-9}$$

By balancing the moment about point B, the tool chip contact length $h$ is calculated referring to (Huang 2002):

$$h = \frac{t\sin\theta}{\cos\beta\sin\phi}\left(1+\frac{\frac{c\gamma_{AB}I}{k_{AB}}}{3\left(1+2(\frac{\pi}{4}-\phi)-\frac{c\gamma_{AB}I}{k_{AB}}\right)}\right) \tag{B-10}$$

The stress distribution is assumed uniform along the tool-chip interface. The shear flow stress $\tau_{\text{int}}$, normal stress $\sigma_N$, strain rate $\dot{\gamma}_{\text{int}}$ and its effective strain rate $\dot{\varepsilon}_{\text{int}}$ at the tool-chip interface now can be calculated as below in Equation (B-11). Here the ratio $\delta$ of thickness of tool-chip interface plastic zone to chip thickness will need to be determined iteratively as explained later.

$$\begin{aligned}
\tau_{\text{int}} &= \frac{F}{hw} \\
\sigma_N &= \frac{N}{hw} \\
\dot{\gamma}_{\text{int}} &= \frac{V}{\delta t_2} \\
\dot{\varepsilon}_{\text{int}} &= \dot{\gamma}_{\text{int}} / \sqrt{3}
\end{aligned} \tag{B-11}$$

And the shear flow stress adjacent to the tool chip interface can also be calculated from the Johnson-Cook equation as (Huang 2002):

$$k_{\text{int}} = \frac{\sigma_{\text{int}}}{\sqrt{3}} = \frac{1}{\sqrt{3}}\,A\left(1+C\ln\frac{\dot{\varepsilon}_{\text{int}}}{\dot{\varepsilon}_o}\right)\left(1-\left(\frac{T_{\text{int}}-T_r}{T_m-T_r}\right)^m\right) \tag{B-12}$$

Where temperature $T_{\text{int}}$ at the tool-chip interface is calculated as in Equation (B-13):

$$T_{\text{int}} = T_0 + \Delta T_{sz} + \psi \Delta T_M \tag{B-13}$$

The relationships discussed above can not be utilized without knowing the shear angle $\phi$, strain rate constant C and the ratio of thickness of tool-chip interface plastic zone to chip thickness $\delta$. The shear angle $\phi$ is determined iteratively from $5^\circ$ to $45^\circ$ at the step size of $0.1^\circ$ until the calculated interface shear stress $\tau_{\text{int}}$ and the chip material shear flow stress $k_{\text{int}}$ is equal. The strain rate constant C is searched to satisfy: $\sigma_N = \sigma_N^{'}$. And the ratio of thickness of tool-chip interface plastic zone to chip thickness $\delta$ is determined by minimum force principle, the detail flow chart are shown in Figure B-2 (from Dawson 2002).

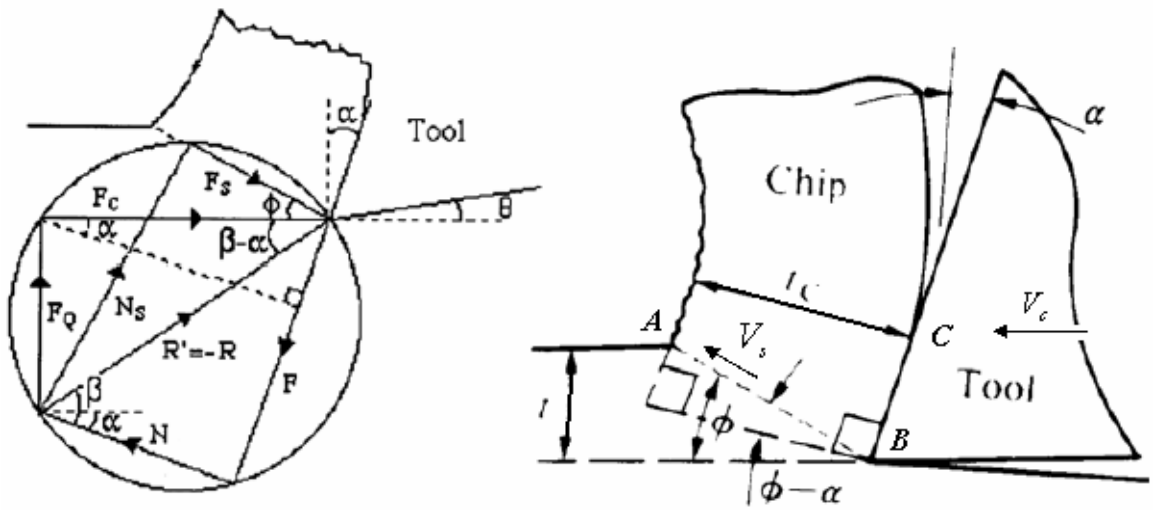


Figure B-1 Cutting force circle and geometric model in orthogonal cutting (Liang 2002)

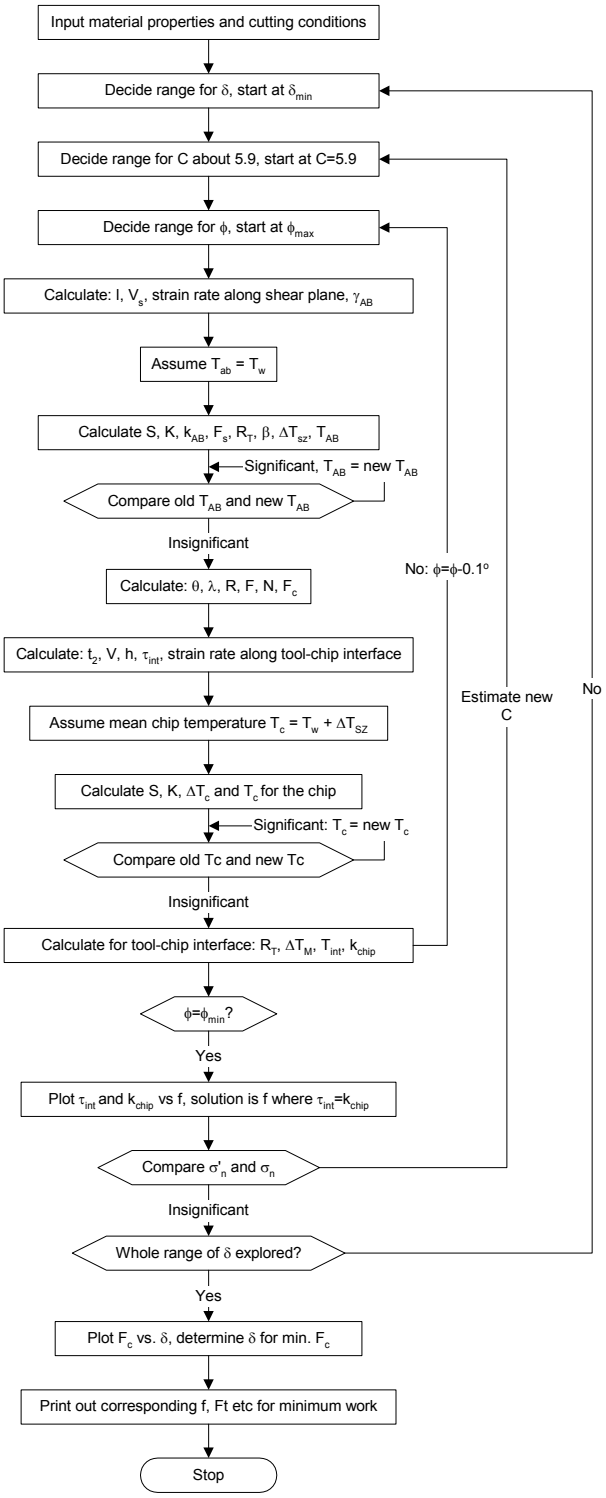


Figure B-2 Flow chart detailing the modified Oxley's method

# APPENDIX C

## WALDORF'S WEAR FORCE MODEL

## (ADOPTED FROM (HUANG 2002))

The force components due to flank wear in orthogonal cutting can be calculated as:

$$F_{CW} = w\int_0^{VB} \tau_w(x)dx\,,\ F_{QW} = w\int_0^{VB} \sigma_w(x)dx \tag{C-1}$$

To estimate the forces due to flank wear, the flank normal stresses $\sigma_w$ and shear stress $\tau_w$ must be properly modeled first. The results based on the slip-line field as proposed by Waldorf (Waldorf, 1996) and Waldorf el al. (Waldorf el al. 1998) are briefly reviewed here. For small flank wear length, there is only elastic contact between the tool flank and the workpiece. Due to the high temperature and stress on the flank of the tool, there is a critical flank wear length, $VB^*$, at which plastic flow is initiated at the front of the wear land. For this case, if $VB < VB^*$, purely elastic contact is present, but if $VB > VB^*$, plastic flow of the workpiece is present at the front edge of the wear land, the elastic contact will also be present at the back of the wear land.

Given shear flow stress $k$ and shear angle $\phi$, if only elastic contact exists between the tool flank face and the workpiece, the tool tip stresses $\sigma_w$ and $\tau_w$ can be modeled as:

$$\sigma_w(x) = \sigma_0 \left( \frac{VB - x}{VB} \right)^2 \quad \text{for} \quad 0 < x < VB$$

$$\tau_w(x) = \begin{cases} \tau_0, & \text{for } 0 < x < VB\left(1 - \sqrt{\frac{\tau_0}{\sigma_0}}\right) \\ \mu\sigma_w, & \text{for } VB\left(1 - \sqrt{\frac{\tau_0}{\sigma_0}}\right) < x < VB \end{cases} \tag{C-2}$$

Where:

$$\sigma_0 = k\left[1 + \frac{\pi}{2} - 2\rho - 2\phi + 2\gamma + \sin(2\gamma - 2\phi)\right], \quad \tau_0 = k\cos(2\gamma - 2\phi)$$
$$\gamma = \eta_p + \phi - \sin^{-1}(\sqrt{2}\sin(\rho)\sin(\eta_p)), \quad \eta_p = 0.5\cos^{-1}(m_p)$$

The variable $m_p$ is the friction factor at the cutting edge of the tool, and it is assumed to be unity due to the adhesive nature of contact at the tool cutting edge. The variable $\rho$ is the prow angle of the workpiece directly in front of the tool and can be taken as zero as suggested by Waldorf.

If $VB > VB^*$, the tool tip stress $\sigma_w$ and $\tau_w$ can be modeled as:

$$\sigma_w(x) = \begin{cases} \sigma_0, & \text{for } 0 < x < \left(VB - VB^*\right) \\ \sigma_0 \left( \dfrac{VB - x}{VB} \right)^2, & \text{for } \left(VB - VB^*\right) < x < VB \end{cases}$$

$$\tau_w(x) = \begin{cases} \tau_0, & \text{for } 0 < x < \left( VB - VB^* \sqrt{\dfrac{\tau_0}{\sigma_0}} \right) \\ \mu\sigma_w, & \text{for } \left( VB - VB^* \sqrt{\dfrac{\tau_0}{\sigma_0}} \right) < x < VB \end{cases} \qquad \text{(C-3)}$$

where:

$$\sigma_0 = k\left[1 + \frac{\pi}{2} - 2\rho + 2\eta_w + \sin(2\eta_w)\right], \quad \tau_0 = k\cos(2\eta_w), \quad \eta_w = 0.5\cos^{-1}(m_w)$$

The term $m_w$, which is the slip-line field angle for friction on the flank wear land, is similar to the friction factor at the tool cutting edge and is also assumed by Waldorf to be close to unity.

# REFERENCES


Abrao, A.M., Apinwall, D.K. and Wise, M.L.H. (1995); Tool Life and Workpiece Surface Integrity Evaluations When Machining Hardened AISI H13 and AISI E52100 Steels with Conventional Ceramic and PCBN Tool Materials; SME Technical Paper, MR95-159.

Abrao, A.M. and Aspinwall, D.K. (1996); The Surface Integrity of Turned and Ground Hardened Bearing Steel; Wear, Vol. 196, pp. 279-284.

Adams, J., Anschuetz, B. and Whitfield, G. (1991); Ceramic Cutting Tools; Engineered Materials Handbook: Ceramics and Glasses, Vol. 4, pp. 966-972.

Agha, S.R. and Liu, C.R. (2000); Experimental study on the performance of superfinish hard turned surfaces in rolling contact; Wear 244, pp. 52–59.

Akcan, S., Shah, S., Chaabra, P.N., Moylan, S.P., Chandrasekar, S., and Farris, T.N. (1999); Characteristics of White Layers Formed in Steels by Machining, ASME, MED-Vol. 10 pp. 789-795.

Amin, K. (1991); Toughness, Hardness, and Wear; Engineered Materials Handbook: Ceramics and Glasses; Vol. 4, pp. 599-609.

Archard, J.F. (1953); Contact and Rubbing of Flat Surfaces; J. of App. Physics., Vol. 24 pp. 981-988;

Armarego, E.J.A., Brown, R.H. (1967); The Machining of Metals; Englewood Cliffs, NJ, Prentice Hall.

Armarego, E.J.A., Smith, A.J.R., Wang, J. (1993); Constrained Optimization Strategies and CAM Software for Single Pass Peripheral Milling; Int. J. Prod. Res., Vol. 31(9), pp. 2139-2160.

Armarego, E.J.A., Smith, A.J.R., Wang, J. (1994); Computer-Aided Constrained Optimization Analyses and Strategies for Multipass Helical Tooth Milling Operations; Annals of the CIRP, Vol. 43, pp. 437-442.

Arsecularatne, J.A., Mathew, P. and Oxley, P.L.B. (1995); Prediction of Chip Flow Direction and Cutting Forces in Oblique Machining with Nose Radius Tools; Proc. Inst. Mech. Engrs., Vol. 209(B), pp 305–315

Arsecularatne, J.A., and Mathew, P. (2000); Oxley Modeling Approach - Its Applications and Future Directions; Machining Science and Technology, Vol. 4(3), pp.363-397.

Auschner, W. (1997); Stone Superfinishing of Hard-Turned Surfaces; Machining Technology Association of SME, Vol. 8(3) pp. 1-5.

Back, T. and Schutz, M. (1995); Evolution Strategies for Mixed-integer Optimization of Optical Multilayer Systems; Evolutionary Programming IV, Proceeding of the 4th Annual Conference on Evolutionary Programming, pp. 33-51

Barash, M.M. amd Schoech, W.J. (1971); A semi-analytical model of the residual stress zone in orthogonal machining; Advances in Machine Tool Design and Research, pp. 603-613

Back, T. (1996); Evolutionary Algorithms in Theory and Practice; Oxford Univesity Press; New York

Back, T., Eiben, A.E., Schoenauer, M. and Schwefel H.P. (1998); Lecture Notes in Computer Science; Amsterdam, Springer-Verlag, pp.231-240.

Bean, J.C. and Hadj-Alouane A.B. (1992); A Dual Genetic Algorithm for Bounded Integer Programs; Technical Report TR 92-53, Department of Industrial and Operation Engineering, The University of Michigan.

Boothroyd, G. (1963); Temperatures in Orthogonal Metal Cutting; Proc. Inst. Mech. Eng., Vol. 177, pp 789-802.

Boothroyd, G., Eagle, J.M. and Chisholm, A.W.J. (1967); Effect of Tool Flank Wear on the Temperatures Generated during Metal Cutting; Proceedings of 8th International Machine Tool Design and Research Conf., pp. 667-680.

Bouzakis, K.D., Michailidis, N., Vidakis, N., Efstathiou, K., Leyendecker, T., Erkens, G., Wenke, R., and Fuss, H.G. (2000); Optimization of the Cutting Edge Radius of PVD Coated Inserts in Milling Considering Film Fatigue Failure Mechanisms; Surface and Coating Technology, Vol. 133-134, pp. 501-507.

Chen, J.L. and Tsao, Y.C. (1993); Optimal Design of Machine Elements Usiing Genetic Algorithms; Journal of the Chinese Society of Mechanical Engineers, Vol. 14(2), pp. 193-199.

Chou, Y.K. (1994); Wear Mechanism of Cubic Boron Nitride Tools in Precision Turning of Hardened Steels; Ph.D. dissertation, Purdue University.

Cleghorn, W.L., Fu, J.F. and Fenton R.G. (1989); A General Method for Optimization Design of Gear Boxes through Nonlinear Programming; ASME Design and Automation Conference Proc. DE-VOL. 19(2), pp. 153-160.

Dasgupta D. and Michalewicz Z. (1997); Evolutionary Algorithm in Engineering Applications; Springer-Verlag Berlin Heigdelberg, New York.

Davis, L., (1991), Handbook of Genetic Algorithms; Van Nostrand Reinhold, New York.

Dowson, T. (2002); Machining Hardened Steel with Polycrystalline Cubic Boron Nitride Cutting Tools; Ph.D. Thesis, Georgia Institute of Technology.

Ermer, D.S. (1972); Optimization of the Constrained Machining Economics Problem by Geometric Programming; ASME Journal of Engineering for Industry; Vol. 94, pp. 1067-1070.

Ermer, D.S. and Patel, D.C. (1974); Maximization of the Production Rate with Constraints by Linear Programming and Sensitivity Analysis; Proc. NAMRC Vol. 2, pp. 436-449.

Ermer, D.S. and Kromodihardjo S. (1987); Optimization of Multipass Turning with Constraints; J. of Eng. for Ind., Transactions of the ASME, Vol. 103, pp. 462-468.

Ermer, D.S. (1997); A Century of Optimizing Machining Operations, Transactions of the ASME, Journal of Manufacturing Science and Engineering, Vol. 119, pp. 817-822.

Eshelman L.J. and Schaffer J.D. (1993); Real-coded Genetic Algorithm and Interval-Schemata; Proc. FOGA.

Eskicioglu, H., Nisli, M.S. and Kilic, E. (1985); An Application of Geometric Programming to Single-Pass Turning Operation; Proc. of Int'l. MTDR Conference, Birmingham, pp. 149-157.

Fischer, G.W., Wei Y. and Dontamsetti, S. (1989); Process-Controlled Machining of Gray Cast Iron; J. o f Mech. Working Tech., Vol. 20, pp. 45-57

Gen, M. and Cheng, R.W. (2000); Genetic Algorithm & Engineering Optimization; Wiley Series in Engineering Design and Automation, Hamid R. Parsaei, Series Editor.

Goldberg, D.E. (1989); Genetic Algorithm in search, Optimization and Machine Learning; Addison-Wesley, MA.

Goldberg, D.E. (1990); Real-Coded Genetic Algorithm, Virtual Alphabets and Blocking; University of Illinois at Urbana-Champaign, Technical Report No. 90001

Gonnet G. and Baeza R.Y. (1991); Handbook of Algorithms and Data Structures; 2nd edition, Addison-Wesley, Reading, MA.

Gopalakrishnak, B. and Al-Khayyal, F. (1991); Machine Parameter Selection for Turning with Constraints: An Analytical Approach Based on Geometric Programming; Int'l J. Prod. Research, Vol. 29, pp. 1897-1908.

Griffiths, B.J. and Furze D.C. (1987); Tribological Advantages of White Layers Produced by Machining; Transactions of the ASME: Journal of Tribology, Vol. 109, pp. 525-530.

Groover, M.P. (1975); Monte Carlo Simulation of the Machining Economics Problems; J. of Eng. for Ind., Trans., ASME, Vol. 97(3), pp 931-938.

Guo, Y.B. and Liu, C. R. (2002); 3D FEA Modeling of Hard Turning, Journal of Manufacturing Science and Engineering, Vol. 124 (May), pp. 198 -199

Hadj-Alouane, A.B. and Bean, J.C. (1992); A genetic algorithm for the multiple-choice integer program; Technical Report TR92-50, Department of Industrial and Operation Engineering, The University of Michigan.

Holland, J.H. (1975), Adaptation in Natural and Artificial Systems, Ann Arbor, University of Michigan Press.

Homaifar, A.S., Lai H.Y. and Qi X. (1994); Constrained Optimization via Genetic Algorithms; Simulation, Vol. 62, pp. 242-254.

Huang, Y. (2002); Predictive Modeling of Tool Wear Rate with Application to CBN Hard Turning; Ph.D. Thesis, Georgia Institute of Technology.

Huang, Y. and Liang, S.Y. (2003); Cutting Forces Modeling Considering the Effect of Tool Thermal Property-Application to CBN Hard Turning; Int. J. of Machine Tools and Manufacture, Vol. 43(3), pp. 307-315.

Huang, Y. and Liang, S.Y. (2004a); Modeling of CBN Tool Flank Wear Progression in Finish Hard Turning; ASME J. of Manufacturing Sci. and Eng., Vol. 126(1), pp 98-106.

Huang, Y. and Liang, S.Y. (2004b); Effect of Cutting Conditions on Tool Performance in CBN Hard Turning; Transactions of NAMRI/SME; Vol. 32, pp. 511-518.

Huang, Y. and Liang, S.Y. (2005); Modeling of Cutting Forces under Hard Turning Conditions Considering Tool Wear Effect; ASME J. of Manufacturing Sci. and Eng., Vol. 127(2), pp. 262-270.

Jang, Y.D. (1992); A unified Optimization model of a machining process for specified conditions of machined surface and process performance; Int. J. Prod. Res., Vol. 30(3), pp. 647 – 663.

Jha, N.K. and Hornik K. (1995); Integrated Computer-aided Optimal Design and Finite Element Analysis of a Plain Milling Cutter; Appl. Math. Modelling, Vol. 19, pp. 343-352

Joines, J.A. and Houck, C.R. (1994); On the Use of Non_Stationary Penalty Functions to Solve Nonlinear Constrained Optimization Problems With Gas; In Proceedings of the Evolutionary Computation Conference--Poster Sessions, part of the IEEE World Congress on Computational Intelligence, Orlando, pp. 579-584.

Kartalopoulos, S. (1996); Understanding Neural Networks and Fuzzy Logic, Basic Concepts and Applications, IEEE press.

Keane, A. (1994), Genetic Algorithms Digest, Vol. 8(16).

Kennametal, Inc. (1996), Kennametal Lathe Tooling Catalog 6000.

Konig W., Komanduri R., Tonshoff H.K. and Ackershott G. (1984); Machining of Hard Material; Annals of the CIRP, Vol. 33(2), pp. 417-427.

Konig W., Berktold A. and Koch K.F. (1993); Turning versus Grinding - A Comparison of Surface Integrity Aspects and Attainable Accuracies; Annals of the CIRP, Vol. 42(1), pp. 39-43.

Koziel, S and Michalewicz, Z. (1998); A Decoder-based Evolutionary Algorithm for Constrained Parameter Optimization Problems; Proceedings of the 5th Parallel Problem Solving from Nature.

Koziel, S. and Michalewicz, Z. (1999); Evolutionary Algorithms, Homomorphous Mappings, and Constrained Parameter Optimization; Evolutionary Computation, Vol. 7(1), pp. 19-44.

Ladd, S.R. (1995); Genetic Algorithm in C++, Hungry Minds Inc., 1995

Lee, C.W. (2000); Intelligent Modeling and Optimization of Grinding Process; Ph.D. thesis, Purdue University, West Lafayette

Lee, C.W. and Shin, Y.C. (2000); Evolutionary modeling and optimization of grinding processes; Int. J. Prod. Res., Vol. 38(12), pp. 2787-2813.

Lee, C.W., Choi, T. and Shin, Y.C. (2003); Intelligent Model-based Optimization of the Surface Grinding Process for Heat-treated 4140 Steel Alloys with Aluminum Oxide Grinding Wheels; Journal of Manufacturing Science and Engineering, Transactions of the ASME, Vol. 125(1), pp. 65-76.

Liang, S.Y. (2002); Lecture Notes: Machine Tool Analysis and Control; Georgia Institute of Technology, G.W. Woodruff School of Mechanical Engineering.

Liao, T.W. and Chen, L.J. (1994); A Neural Network Approach for Grinding Processes: Modeling and Optimization; International Journal of Machine Tools and Manufacture, Vol. 34(7), pp. 919-937.

Lin, Z.C., Lin Y.Y. and Liu, C.R. (1991); Effect of thermal load and mechanical load on the residual stress of a machined workpiece, Int. J. Mech. Sci., Vol. 33, pp. 263 -278.

Lin, C.Y. and Hajela, P. (1992); Genetic Algorithms in Optimzation Problems with Discrete and Integer Design Variables; Engineering Optimization, Vol. 19, pp. 309-327.

Liu, C.R. and Mittal S. (1998); Optimal Pre-stressing the Surface of a Component by Superfinish Hard Turning for Maximum Fatigue Life in Rolling Contact; Wear, Vol. 219, pp. 128-140.

Malkin S. (1976); Selection of Operating Parameters in Surface Grinding of Steels; Transactions of the SAME, Journal of Engineering for Industry, Vol. 98, pp. 56-62.

Mathworks (2002); MATLAB v6.5 Reference Manuals

Mayer, J.E. Jr. and Stauffer, D.J. (1974); Effects of the Tool Edge Hone and Chamfer on Wear Life, Trans. of NAMRI, pp. 5-15.

Michalewicz, Z. and Janikow, C. (1991); Handling Constraints in Genetic Algorithms; In Proceedings of the Fourth International Conference on Genetic Algorithms; Los Altos, CA, Morgan Kaufmann, Publishers, pp. 84-97.

Michalewicz, Z. and Attia, N. (1994); In Evolutionary Optimization of Constrained Problems; Proceedings of the 3rd Annual Conference on Evolutionary Programming, eds. A. V. Sebald and L. J. Fogel, River Edge, NJ, World Scientific Publishing, pp. 98-108.

Michalewicz, Z., (1995a), A Survey of Constraint Handling Techniques in Evolutionary Computation Methods; Proceedings of the 4th Annual Conference on Evolutionary Programming, MIT Press, Cambridge, MA, pp. 135-155.

Michalewicz, Z., (1995b), Genetic Algorithms, Numerical Optimization and Constraints; Proceedings of the 6th International Conference on Genetic Algorithms, Pittsburgh, pp. 151-158.

Michalewicz, Z., Nazhiyath G. (1995c); Genocop III: A co-evolutionary algorithm for numerical problems with nonlinear constraints; In D. B. Fogel (Ed.) Proceedings of the second IEEE international conference on Evolutionary Computation, IEEE Press, Piscataway, NJ, pp.647-651.

Michalewicz, Z. (1996); Genetic Algorithm + Data Structure = Evolution Programs; Third Revised and Extended Edition, Springer-Verlag Berlin Heigdelberg New York.

Michalewicz, Z. and Schoenauer, M. (1996); Evolutionary Algorithms for Constrained Parameter Optimization Problems, Evolutionary Computation, Vol. 4(1), pp. 1-32.

Milner, D.A. (1976); Use of Linear Programming for Machinability Data Optimization; ASME J. Mech. Design, Vol. 100, pp. 286-291.

Mittal, S. and Liu, C.R. (1998); A method of modeling residual stresses in superfinish hard turning, Wear 218, pp. 21-33.

Myung, H., Kim, J.H. and Fogel D. (1995); Preliminary investigation into a two-stage method of evolutionary optimization on constrained problems; Proceedings of the 4th Annual Conference on Evolutionary Programming, pp. 449-463, MIT Press.

Orvosh, D. and Davis, L. (1993); Shall We Repair? Genetic Algorithms, Combinatorial Optimization and Feasibility Constraints; In Proceedings of the Fifth International Conference on Genetic Algorithms, Los Altos, CA, Morgan Kaufmann Publishers, pp. 650.

Oxley, P.L.B. (1989); Mechanics of Machining, an Analytical Approach to Assessing Machinability; Ellis Horwood Limited, West Sussex, England.

Paredis, J. (1994); Co_evolutionary Constraint Satisfaction; In Proceedings of the 3rd Conference on Parallel Problem Solving from Nature; New York, Springer-Verlag; pg 46-55.

Phillips, D.T. and Beightler, C.S. (1970); Optimization in Toll Engineering Using Geometric Programming; AIIE Transcactions, Vol. 2(4), pp. 355

Phillipson, R.H. and Ravindran, A. (1978); Application of Goal Programming to Machinability Data Optimization; ASME J. Mech. Design, Vol. 100, pp. 286-291

Powell, D. and Skolnick, M.M. (1993); Using Genetic Algorithms in Engineering Design Optimization with Nonlinear Constraints; In Proceedings of the Fifth International Conference on Genetic Algorithms; Los Altos, CA, Morgan Kaufmann Publishers, pp. 421-430

Ramesh, A. (2002); Prediction of Process-Induced Micro-structural Changes and Residual Stresses in Orthogonal Hard Machining; Ph.D. Thesis, Georgia Institute of Technology.

Rangwala, S. and Dornfeld, D.A. (1989); Learning and Optimization of Machining Operations Using Computing Abilities of Neural Networks, IEEE Trans, Syst. Man Cybern. Vol. 19, pp. 299-314.

Rao, S.S. (1996); Engineering Optimization: Theory and Practice; 3rd edition, Reading, NY: John Wiley & Son.

Rech, J. and Moisan, A. (2003); Surface integrity in finish hard turning of case-hardened steels; International Journal of Machine Tools and Manufacture, Vol. 43(5), pp. 543-550.

Richardson J.T, Palmer, M.R., Liepins G. and Hilliard, M. (1989); Some Guidelines for Genetic Algorithms with Penalty Functions; In Proceedings of the Third International Conference on Genetic Algorithms, Los Altos, CA, Morgan Kaufmann Publishers, pp. 191-197.

Schoenauer, M. and Xanthakis, S. (1993); Constrained GA Optimization; In Proceedings of the Fifth International Conference on Genetic Algorithms, Los Altos, CA, Morgan Kaufmann Publishers, pp. 573-580.

Schwefel, H., (1981), Numerical Optimization of Computer Models; Wiley, Chilchester, Wes Sussex, England.

Schwefel, H., (1995); Evolution and Optimum Seeking; John Wiley & Sons Press, ISBN 0-471-57148-2.

Shahookar, K. and Mazumder, P. (1990); A Genetic Approach to Standard Cell Placement Using Meta-genetic Parameter Optimization; IEEE Transactions on Computer-Aided Design of Integrated Circuits and Systems, Vol. 9(5), pp. 500-511.

Shatla, M., Kerk, C. and Altan, T. (2001); Process Modeling in Machining Part 1: Determination of Flow Stress Data; Inter. J. Mach. Tools & Manuf., Vol. 41, pp. 1511 – 1534.

Shaw, M.C. (2002); Metal Cutting Principles; CBS Publishers & Distributors, reading

Shintani, K., Ueki, M. and Fujimura, Y. (1989); Optimum Tool Geometry of CBN Tool for Continuous Turning of Carburized Steel; Int. J. Mach. Tool & Manuf. Vol. 29(3), pp. 403-413

Smith, A. and Tate, D. (1993); Genetic Optimization using a Penalty Function; In Proceedings of the Fifth International Conference on Genetic Algorithms, Los Altos, CA, Morgan Kaufmann Publishers, pp. 499-503.

Stabler, G.V. (1951); The Fundamental Geometry of Cutting Tools, Proc. Inst. Mech. Eng., Vol. 165, pp. 14-21.

Strenkowski, J.S. and Wei, Y.M. (1997); Optimal Selection of Tooling and Cutting Conditions for End Milling Using Microgenetic Algorithms; Manufacturing Science and Technology, ASME, Vol. 2, pp. 253-260.

Sundaram, R.M. (1978); An application of Goal Programming Technique in Metal Cutting; Int'l. J. Prod. Research, Vol. 16 (5), pp. 375-382.

Tapia, P.E., Al-Zkeri I. and Altan T. (2005); Evaluation of the Georgia Tech's Computer Program for Predicting Hard Turning Variables; Report No. HPM–ERC/NSM-05-R-15

Taylor, F.W. (1907); On the art of the cutting metals; Trans. ASME Vol. 28, pp. 31-350.

Thiele, J.D. (1999); An investigation of surface generation mechanisms for finish hard turning of AISI 52100 steel; Georgia Institute of Technology, Master Thesis.

Tonshoff H.K., Arendt, C. and Ben A.R. (2000); Cutting Hardened Steel; Annals of the CIRP, Vol. 49 (2), pp. 1-19.

Tsai, P.F. (1986); An Optimization Algorithm and Economic Analysis for a Constrained Machining Model; Ph.D. Dissertation, West Virginia University

Waldorf, D.J. (1996); Shearing, Ploughing and Wear in Orthogonal Machining; Ph.D. Thesis, Univ. of Illinois at Urbana-Champaign.

Waldorf, D.J., DeVor, R.E. and Kapoor, S.G. (1998); A Slip-line Field for Ploughing during Orthogonal Cutting; ASME J. of Manuf. Sci and Eng., Vol. 120 (4), pp. 693-699.

Walvekar, A.G. and Lamber, B.K. (1970); An Application of Geometric Programming to Machining Variable Selection; Int'l J. Prod. Research, Vol. 8, pp. 241-245.

Wen, X.M., Tay, A.O.O. and Nee, A.Y.C. (1992); Micro-Computer-Based Optimization of the Surface Grinding Process; Journal of Materials Processing Technology, Vol. 29, pp. 75-90.

Wright A.H. (1991); Genetic Algorithm for Real Parameter Optimization, in Proc FOGA'91, pp. 205-218.

Wu, S.J. and Chow, P.T. (1995); Genetic Algorithms for Nonlinear Mixed Discrete-Integer Optimization Problems via Meta-Genetic Parameter Optimization; Engineering Optimization, Vol. 24, pp. 137-159.

Wu, S.W. and Matsumoto, Y. (1990); The effect of hardness on residual stresses in orthogonal machining of AISI 4340 steel, J. Eng. Ind., Vol. 112, pp. 245-252.

Xiao, G., Malkin, S. and Sanai, K. (1992); Intelligent Control of Cylindrical Plunge Grinding; Proceedings of the ACC, Chicago, IL, pp. 391-398.

Zhang, J.Y. and Liang, S.Y. (2005a); Evolutionary Optimization of Machining Processes; submitted to Journal of Intelligent Manufacturing, January 2005.

Zhang, J.Y. and Liang, S. Y. (2005b); Handling Constraints for Manufacturing Process Optimization Using Genetic Algorithm; International Journal of Computer Applications in Technology (IJCAT), in press

Zhang, J.Y., Liang, S.Y., Zhang, G.W. and Yen, D. (2005c); Modeling of Residual Stress Profile in Finish Hard Turning; Materials and Manufacturing Processes, in press, Vol. 20 (6).

# VITA

JingYing Zhang was born in Ningbo, Zhejiang, China in May, 1973. She received her B.S. degree in July 1995 and M.S. degree in June 1998 both in Mechanical Engineering from Huazhong University of Science and Technology (HUST), Wuhan. After she worked as a lecturer for one year in HUST, she went to Singapore and worked as a Manufacturing Engineer in Hewlett Packard for another two years. She started her Ph.D. program in January 2002 in the Georgia W. Woodruff School of Mechanical Engineering at Georgia Institute of Technology. She will receive her Ph.D. in August 2005.